Characterization of epigenetic changes in *Rana* [*Lithobates*] *catesbeiana* tissues during natural and induced thyroid hormone-dependent metamorphosis using mass spectrometry

By

Haley Noah Kuecks-Winger

A Thesis Submitted in Partial Fulfillment of the Requirements for the Degree of

MASTER OF SCIENCE

In the Department of Biochemistry and Microbiology

University of Victoria

We acknowledge and respect the lək^{w}əŋən peoples on whose traditional territory the University stands, and the Songhees, Esquimalt and W̱SÁNEĆ peoples whose historical relationships with the land continue to this day.

Supervisory Committee

Characterization of epigenetic changes in *Rana* [*Lithobates*] *catesbeiana* tissues during natural and induced thyroid hormone-dependent metamorphosis using mass spectrometry

By

Haley Noah Kuecks-Winger

Supervisory Committee

Dr. Caren C. Helbing, Supervisor
Department of Biochemistry and Microbiology

Dr. Anita Thambirajah, Departmental Member
Department of Biochemistry and Microbiology

Dr. Bob Chow, Outside Member
Department of Biology

Abstract

Thyroid hormone (TH) signaling is critical for proper development, growth and metabolism in all vertebrates. Amphibian metamorphosis is a TH-dependent developmental process that requires coordinated physical and biochemical changes to facilitate the transition from a tadpole to a frog. Metamorphosis involves extensive tissue-specific changes in the gene expression of differentiated tissues. *Rana catesbeiana* (American bullfrog) metamorphosis can be precociously induced by treatment with exogenous TH. However, metamorphosis is temperature-dependent and does not proceed at 5°C even in the presence of TH. Remarkably, a subsequent shift to permissive temperatures (24°C) results in an accelerated metamorphosis, implying that TH establishes a molecular memory at 5°C. Previous studies suggest that epigenetic processes, including histone variant incorporation and post-translational modifications, are involved in TH-signalling during natural metamorphosis and during temperature-modulated, TH-induced metamorphosis. Herein, we use mass spectrometry to characterize the histone composition of *R. catesbeiana* blood, liver, and tailfin during natural and temperature-modulated induced metamorphosis. The natural metamorphosis model identified tissue- and developmental stage-specific changes in histone abundance and PTMs. The temperature-modulated TH-induced metamorphic model demonstrated temperature- and tissue-specific changes in the abundance and PTMs of histones and other chromatin-binding proteins. To our knowledge, this represents the first unbiased analysis of the chromatin-associated proteins during amphibian metamorphosis. The findings presented herein expand our understanding of

putative epigenetic factors involved in regulating TH-dependent development, which has broad relevance to all vertebrate species due to the conserved nature of TH action.

Table of Contents

List of Tables

List of Figures

List of Abbreviations

ac	Acetylation
AGC	Automatic gain control
BCA	Bicinchoninic acid
BL	Blood
BLASTP	Basic local alignment search tool
CBP	CREB-binding protein
C/EBP	CCAAT/enhancer-binding protein
ChIP	Chromatin immunoprecipitation
CRF	Corticotropin releasing factor
Da	Dalton
DIT	Di-iodotyrosine
DNA	Deoxyribonucleic acid
DOT1L	Disruptor of telomeric silencing 1-like
EGFR	Epidermal growth factor receptor
FDR	False discovery rate
FTMS	Fourier transform mass spectrometry
FWHM	Full width at half maximum
HAT	Histone acetyltransferase
HCD	High-energy C-trap dissociation
HDAC	Histone deacetylase
HMG	High mobility group
HMGN	HMG nucleosomal-binding domain-containing protein
HMT	Histone methyltransferase
HPLC	High performance liquid chromatography
HPT	Hypothalamic-pituitary-thyroid
K	Lysine
LI	Liver
MAD	Median absolute deviation
MAPK	Mitogen-activated protein kinase
me	Methylation

me2	Dimethylation
me3	Trimethylation
MeCP2	Methyl-CpG binding protein
MIPS	Monoisotopic precursor selection
MIT	Mono-iodotyrosine
mRNA	Messenger ribonucleic acid
MS	Mass spectrometry
MS/MS	Tandem mass spectrometry
N-CoR	Nuclear co-repressor
NR	Nuclear receptor
phos	Phosphorylation
PI3K	Phosphatidylinositol-3-OH-kinase
ppm	Parts per million
PRMT1	Protein arginine methyltransferase 1
PTM	Post-translational modification
qPCR	Quantitative polymerase chain reaction
R	Arginine
RBC	Red blood cell
RFC	Relative fold change
RXR	Retinoic acid receptor
S	Serine
SCR	Steroid receptor coactivator
SDS-PAGE	Sodium dodecyl-sulfate polyacrylamide gel electrophoresis
SMRT	Silencing mediator for retinoid and thyroid hormone receptors
T_2	Diiodothyronine
T_3	Triiodothyronine
T_4	Thyroxine
TEAB	Triethylammonium bicarbonate
TF	Tailfin
TFA	Trifluoroacetic acid
TH	Thyroid hormone

thibz	Thyroid hormone-induced basic region leucine zipper
thrb	Thyroid hormone receptor beta
TK	Taylor Kollros
TMA	Trimethylacetic anhydride
TMS	Tricaine methanesulfonate
TMT	Tandem mass tag
TPO	Thyroid peroxidase
TR	Thyroid hormone receptor
TRE	Thyroid hormone response element
TRH	Thyrotropin-releasing hormone
TSH	Thyroid stimulating hormone

1.1. Introduction

1.2. Thyroid hormone

1.2.1. TH production and transport

Thyroid hormones (THs) are critical for the development, growth, and metabolism of all vertebrate species. THs are produced in the thyroid gland and their production is under the control of the hypothalamic-pituitary-thyroid axis (HPT) (Nussey and Whitehead, 2001). Environmental cues stimulate the hypothalamus to produce and secrete corticotropin releasing factor (CRF), or thyrotropin-releasing hormone (TRH) in mammals (De Groef et al., 2006; Zoeller et al., 2007). This triggers the pituitary gland to produce and secrete thyroid stimulating hormone (TSH), which in turn induces the production of TH in the follicular cells of the thyroid gland (Thambirajah et al., 2019; Zoeller et al., 2007).

The follicular cells of the thyroid gland actively take up iodide through sodium-iodide symporters and synthesize thyroglobulin. Iodide and thyroglobulin are required for TH production. Iodide is oxidized by thyroid peroxidase (TPO) to form iodine, which is then covalently attached to tyrosine residues on thyroglobulin (Nussey and Whitehead, 2001). A tyrosine residue can be singly iodinated at the 3 position or doubly iodinated at the 3 and 5 positions of the benzene ring, creating mono-iodotyrosine (MIT) and di-iodotyrosine (DIT), respectively (Giammanco et al., 2020; Nussey and Whitehead, 2001). TPO then catalyzes the coupling of two iodinated tyrosine residues. Coupling of a MIT with a DIT produces triiodothyronine (T_3), while the coupling of two

DITs produces thyroxine (T_4), which is the predominant TH secreted from the thyroid gland (Giammanco et al., 2020; Nussey and Whitehead, 2001). THs are released through lysosomal degradation of the thyroglobulin substrate and subsequent secretion from the follicular cells into the plasma (Nussey and Whitehead, 2001). THs repress production of CRF and TSH, thus establishing a negative feedback loop to regulate circulating TH levels (Zoeller et al., 2007).

THs are transported in the plasma by transport proteins such as transthyretin to peripheral tissues and are taken into cells via plasma membrane transporters (Zoeller et al., 2007). Once in the cell, T_4 can be converted to T_3 by type I and type II 5'-deiodinases (Bianco and Kim, 2006). T_4 has long been considered a pro-hormone that requires conversion to T_3. It has since been discovered that T_4 can exert direct biological effects, although it is approximately 5-fold less biologically active than T_3 (Maher et al., 2016). T_4 and T_3 were shown to elicit distinct tissue-specific changes in the transcriptomes of multiple *R. catesbeiana* tissues, suggesting that they play discrete biological roles (Jackman et al., 2022).

In contrast to type I and II deiodinases, type III deiodinases convert T_3 and T_4 to diiodothyronine (T_2) and reverse T_3, respectively, which were considered to be metabolically inactive (Bianco and Kim, 2006). More recently, biological roles have emerged for these THs, largely through non-genomic signalling pathways (Damiano et al., 2017; Lin et al., 2019).

The degree of conversion between TH types, in part dictated by the tissue-specific expression of deiodinases, and the genomic and non-genomic TH pathways, highlight the complexity of TH signalling (Giammanco et al., 2020; Maher et al., 2016).

1.2.2. TH signaling

TH acts predominantly through genomic signalling. In the nucleus, THs bind to TH receptors (TRs) TRα and TRβ, which are conserved among vertebrates. The TRs are members of the nuclear receptor (NRs) superfamily of transcription factors. NRs have a ligand binding domain and a zinc finger DNA binding domain that recognizes specific sequences within genomic DNA (Weikum et al., 2018). TRs typically form heterodimers with retinoic acid receptors (RXRs), which also belong to the NR superfamily (Brent, 2012). TRs are constitutively bound to TH response elements (TREs) in the promoter region of TH-controlled genes. In the absence of TH, TRs associate with co-repressor complexes that suppress expression of the TH-controlled gene. Upon TH binding to the TR, a conformational change occurs that results in the release of the co-repressor complex and allows binding of co-activator complexes and subsequent transcription of the TH-controlled gene (Glass and Rosenfeld, 2000). This is termed the dual function model as TRs can differentially repress and activate gene transcription based on TH binding (Figure 1). The co-repressor and co-activator complexes include histone-modifying enzymes and chromatin remodelers, which are discussed later in this section. It is important to note that this model does not sufficiently explain all TH action, as evidenced by genes that are negatively regulated by THs. Furthermore, the simplicity of this model is unlikely to account for the coordinated

tissue-specific changes in gene expression elicited by TH during developmental periods.

THs can also act through non-genomic pathways that do not involve binding to nuclear TRs. For example, THs can interact with plasma membrane integrin receptor αVβ3 to activate cellular signalling cascades that can include activation of mitogen-activated protein kinase (MAPK) pathways (Giammanco et al., 2020). Additionally, THs can bind truncated versions of TRs that lack the nuclear localization signals in the cytosol (Giammanco et al., 2020). In human fibroblasts, it was suggested that cytosolic TR signalling activated phosphatidylinositol-3-OH-kinase (PI3K) and led to increased translation of genes involved in cellular glucose metabolism (Moeller et al., 2005).

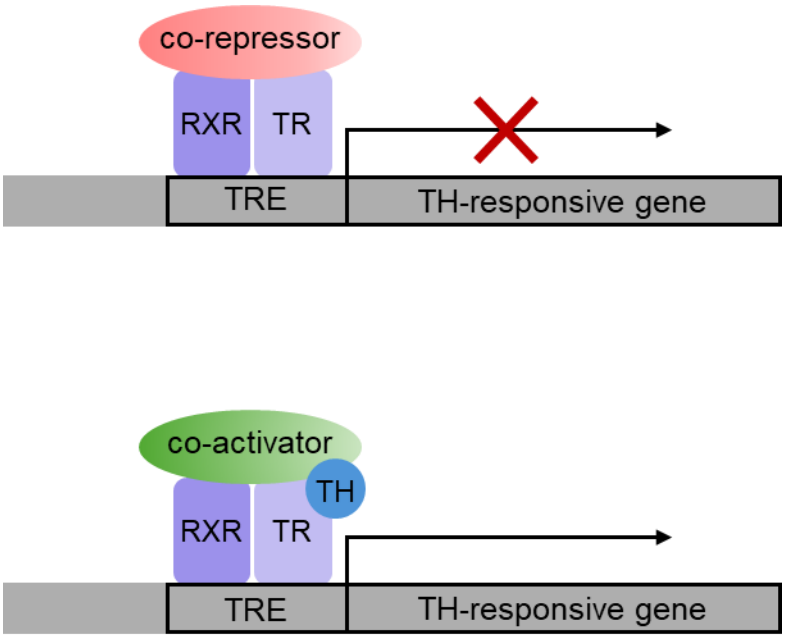

Figure 1. The dual function model. The thyroid hormone (TH) receptor (TR) forms a heterodimer with retinoic acid receptor (RXR) and is constitutively associated with the TH response element (TRE) in the regulatory region of TH-responsive genes. In the absence of TH, co-repressor complexes associate with the TR and repress transcription. TH enters the nucleus and binds to the TR, releasing the co-repressor complex and allowing a co-activator complex to bind, thus enabling transcription.

1.3. Amphibian metamorphosis

1.3.1. TH-dependent anuran metamorphosis

Perhaps the most striking example of a TH-dependent developmental process is anuran metamorphosis. TH-dependent metamorphosis involves whole-body remodeling wherein an aquatic tadpole becomes a (semi-)terrestrial frog. Metamorphic changes include the *de novo* development of limbs, lung development, intestinal remodelling, skin keratinization, immune system development, and many more (Shi, 2000). The work presented herein focuses on the blood, liver and tailfin, which are discussed later in this section.

Premetamorphic tadpoles are functionally athyroid and have virtually undetectable levels of circulating plasma TH (Poulson et al., 2023). The onset of TH production in the tadpole thyroid gland triggers the metamorphic process. Circulating TH levels increase during prometamorphosis, and maximal TH levels are reached at metamorphic climax after which THs decrease to suprabasal levels as metamorphosis completes (Figure 2) (Poulson et al., 2023). Over a century ago, it was discovered that precocious metamorphosis could be induced by feeding horse thyroid gland to premetamorphic tadpoles (Gudernatsch, 1912). The ability to induce metamorphosis by exogenous TH exposure or TH injection exemplifies the necessity of TH for amphibian metamorphosis and is a powerful experimental tool to control the precise timing of TH-dependent developmental programs. Furthermore, TH action is organ autonomous as premetamorphic tissue samples can be treated in culture with TH and elicit

transcriptional responses like those of natural metamorphosis (Hammond et al., 2016, 2015; Koide et al., 2022; Veldhoen et al., 2015).

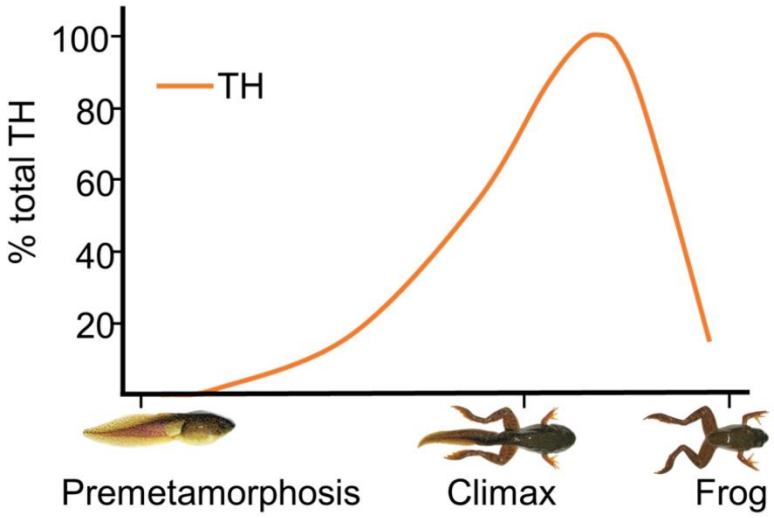

Figure 2. Serum levels of TH increase during *R. catesbeiana* metamorphosis. Adapted from Poulsen et al. (2023).

Tissue-specific physical and biochemical metamorphic changes must be tightly controlled and coordinated for a successful transition. Consequently, all tissues studied to undergo unique transcriptomic changes in response to TH, although the upregulation of certain TH-responsive transcripts, like TRβ (*thrb)* and TH-induced basic region leucine zipper (*thibz),* tend to be common among tissues (Jackman et al., 2022; Luehr et al., 2018; Row et al., 2016; Shi and Brown, 1993; Wang and Brown, 1993). It is not fully understood how the tissue-specific transcriptional responses to TH are established. TH-induced gene expression during metamorphosis is biphasic with an initial induction phase followed by an execution phase (Das et al., 2009; Koide et al., 2022; Shi and

Brown, 1993; Wang and Brown, 1993). *Thrb* and *thibz* are just two examples of TH direct response genes upregulated during the induction phase (Das et al., 2009; Koide et al., 2022; Shi and Brown, 1993; Wang and Brown, 1993). The biphasic model suggests that the expression of the direct response genes establishes the execution phase wherein a secondary wave of transcription occurs.

Amphibian metamorphosis has served as an invaluable model for the study of TH action. TH signaling is highly conserved in vertebrate species, and many discoveries about TH mechanisms have been made using amphibian systems (Grimaldi et al., 2013). In mammals, TH-dependent development begins *in utero* and is complicated by the presence of maternal THs (Buchholz, 2015; Grimaldi et al., 2013; Sachs and Buchholz, 2017). Amphibian metamorphosis is a post-embryonic TH-dependent developmental program, and tadpoles are naïve to THs prior to metamorphosis. Furthermore, there are remarkable similarities between amphibian metamorphosis and mammalian perinatal development, as both developmental processes require TH signaling and involve an aquatic (or amniotic) individual preparing for terrestrial life. Mammalian perinatal development and amphibian metamorphosis involve processes such as hemoglobin switching, induction of the urea cycle, apoptosis of embryonic/larval tissues, skin keratinization, lung development, and more (Buchholz, 2015; Sachs and Buchholz, 2017; Tata, 2006).

1.3.2. Amphibian blood during metamorphosis

Amphibian blood composition changes during metamorphosis. Serum protein content increases, white blood cell populations are altered, and a new population of red blood cells (RBCs) expressing adult hemoglobin is established (Davis, 2009; Shi, 2000).

RBCs are the major cellular component of blood, and an important part of metamorphosis is the switch from larval to adult hemoglobin. The low abundance of oxygen in water relative to air requires larval hemoglobin to have a greater affinity for oxygen than adult hemoglobin. A 1982 study purified newly differentiated RBCs from the blood of metamorphosing *R. catesbeiana* tadpoles and found that only adult hemoglobin was expressed, and that tadpole RBCs exclusively expressed larval hemoglobin (Dorn and Broyles, 1982). This suggested that the hemoglobin transition was achieved by the emergence of a new population of adult RBCs that replace larval RBCs. Later studies in *Xenopus* and *Ranid* species reconfirmed this hypothesis and additionally showed that the percentage of circulating larval and adult RBCs are inversely related, and that larval RBCs are selectively removed from circulation through apoptosis during metamorphosis (Hasebe et al., 1999; Mukhi et al., 2010; Tamori and Wakahara, 2000; Tamura et al., 2010; Wakahara and Yamaguchi, 2001; Weber et al., 1991, 1989). Amphibian RBCs are proliferative and only adult RBCs remain proliferative at metamorphic climax in *Rana ornativentris* (Yamaguchi et al., 2022).

1.3.3. Amphibian liver during metamorphosis

The liver is a major metabolic organ which must be reprogrammed to accommodate the metamorphic transition. The response to TH in the liver involves

increased transcription and translation, but notably does not involve substantial increases in DNA replication, indicating that the metamorphic changes are achieved through transcriptional reprogramming and not a new cell population (Litwack, 2012).

The most studied example of metamorphic liver reprogramming is the switch from ammonotelism to ureotelism. Normal metabolism generates nitrogenous waste that must be excreted from the body. In tadpoles, this waste is primarily excreted by the liver as ammonia, but by the end of metamorphosis, it is instead excreted as urea (Munro, 1953; Shi, 2000). The transition from ammonia to urea excretion is facilitated by the TH-dependent upregulation of urea cycle genes (Atkinson et al., 1996; Helbing et al., 1992; Shi, 2000).

1.3.4. Amphibian tailfin resorption during metamorphosis

The resorption of the tailfin is one of the most dramatic changes of amphibian metamorphosis. The tadpole tail is composed of multiple tissue types, including the notochord, muscle, skin, and connective tissue (Shi, 2000). The regression of the tailfin is a TH-dependent apoptotic process that is temporally and spatially coordinated and synchronized among the tissue types of the tailfin (Shi, 2000). In *R. catesbeiana* tadpoles, visible tail regression begins at metamorphic climax when THs have reached maximal levels and complete tail resorption marks the end of metamorphosis (Poulson et al., 2023).

1.3.5. Modulation of *R. catesbeiana* metamorphosis by temperature

R. catesbeiana tadpoles can overwinter, prolonging their larval stage until the conditions are more favourable for the high energy demands of metamorphosis (Viparina and Just, 1975; Wright et al., 1999). This evolutionary adaptation requires metamorphosis to be temperature sensitive.

In the 1960s, experiments with premetamorphic *R. grylio* tadpoles demonstrated that metamorphic progression (measured by tail resorption) slows as temperatures fall below 25°C and is completely inhibited at 5°C, even when tadpoles are injected with a high dose of TH that would rapidly trigger metamorphosis at warm temperatures (Frieden et al., 1965). A later study replicated these findings in *R. catesbeiana*, and further showed that cold temperature also abolished urea excretion in TH-injected tadpoles (Ashley et al., 1968). Remarkably, transferring the tadpoles to 25°C results in a rapid metamorphosis as measured by tail regression and urea excretion (Ashley et al., 1968; Frieden et al., 1965). This accelerated metamorphosis lacks the typical 2-day lag period which was observed following TH injection at warm temperatures, and was observed even after 80 days post injection, when all THs would have ostensibly been cleared from the body (Ashley et al., 1968; Frieden et al., 1965; Yamamoto et al., 1966). This phenomenon implies a molecular memory wherein exposure to TH primes a premetamorphic tadpole to undergo metamorphosis when temperatures become permissive.

It is not understood how cold temperature inhibits metamorphic progression or how TH molecular memory is established. TH can still enter cell nuclei and bind TRs at 4°C (Murata and Yamauchi, 2005), and activate the accumulation of some, but not all,

TH-dependent gene transcripts in a tissue-specific manner (Hammond et al., 2016; Hammond et al., 2015; Koide et al., 2022; Mochizuki et al., 2012a). The accelerated metamorphosis following a shift to permissive temperatures has been recapitulated at the transcriptomic level in the backskin, liver, and tailfin as there is a greater increase in transcript abundance of certain TH-responsive genes following a shift to permissive temperatures compared to tadpoles only held at metamorphically permissive temperatures (Hammond et al., 2016; Hammond et al., 2015; Koide et al., 2022). Transcriptomic studies have identified putative candidates for the establishment of molecular memory at cold temperatures by identifying transcripts that are upregulated following TH exposure at 5°C (Hammond et al., 2016; Hammond et al., 2015; Koide et al., 2022). The most common among all tissues studied is *thibz*, which is upregulated following TH treatment at 5°C in liver, brain, lung, back skin, and tailfin (Hammond et al., 2016; Hammond et al., 2015; Koide et al., 2022).

Treating tadpoles with TH at non-permissive temperatures (4-5°C) further separates the induction phase of TH action (Koide et al., 2022). Thus, the temperature sensitivity of *R. catesbeiana* can be used to elucidate the mechanisms of TH molecular memory as well as study the early actions of TH before the execution phase commences.

1.4. Chromatin regulation and TH-action

1.4.1. Chromatin structure

Chromatin is a regulated and highly dynamic complex of DNA and associated proteins within the nucleus of cells and is a critical modulator of the accessibility of

genetic material. Regulation of chromatin structure is an essential epigenetic mechanism as it allows for changes in gene expression without altering the DNA sequence. The accessible and typically transcriptionally active regions of chromatin are termed euchromatin. Conversely, heterochromatin describes condensed and inaccessible regions that are associated with silenced genomic regions. Beyond gene transcription, the regulation of chromatin structure is necessary for cellular functions such as DNA repair, chromosome segregation, and replication (Reyes et al., 2021).

The nucleosome is the fundamental repeat unit of chromatin. It is through nucleosome formation that DNA is compacted and organized (Figure 3). A nucleosome is composed of 147 base pairs of DNA wrapped 1.7 times around a histone protein octamer (Luger et al., 1997). Two copies of each core histone family (H2A, H2B, H3, and H4) form the histone core octamer through the interaction of an H3:H4 tetramer with two H2A:H2B dimers (Figure 3) (Luger et al., 1997). The DNA entering and exiting the nucleosome, also known as the linker DNA, may be bound by a linker histone such as H1 or H5. H5 is a linker histone which is specific to non-mammalian vertebrates such as birds, reptiles, and amphibians (Figure 3).

Histones are the major protein component of chromatin. Histones are highly basic proteins due to an abundance of lysine and arginine residues, and the positive charges enable histones to interact with the acidic phosphate groups on the DNA backbone. The core histones have a central globular histone fold domain flanked by N- and C-terminal tails (Figure 3) (Luger et al., 1997).

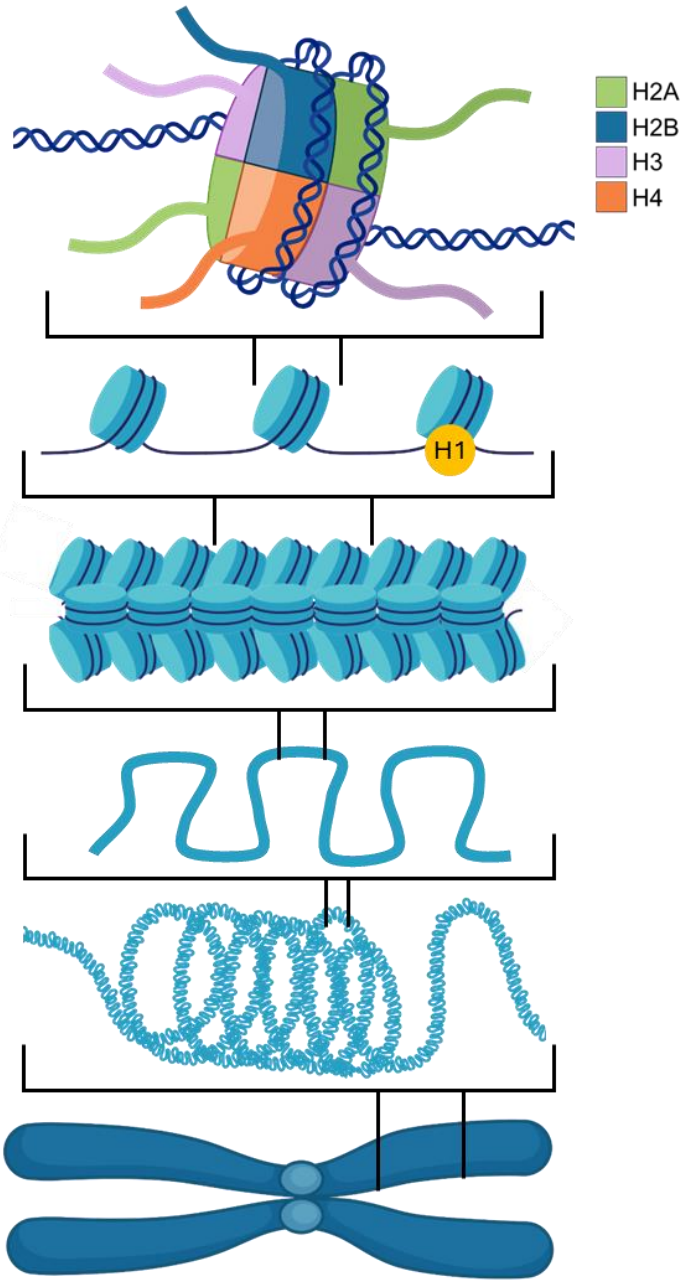

Figure 3. Representation of chromatin structure exemplified by mitotic chromosome compaction. Genomic DNA wraps around a histone protein octamer to form a nucleosome. The N-terminal histone tails protrude from the nucleosome and are common sites of post-translational modifications. Linker histones such as H1 can bind the linker DNA at the entry and exit of the nucleosome. Inter-nucleosomal interactions form higher order chromatin structures. Adapted from Jansen and Verstrepen (2011).

1.4.2. Histone variants

One way that chromatin conformation can be regulated is through the characteristics and composition of the histones in nucleosomes. Variant forms of the core histones and linker histones can be incorporated into nucleosomes in place of their canonical counterparts. The bulk of canonical histone translation occurs during the S-phase of the cell cycle to package replicating DNA (Talbert and Henikoff, 2021). These replication-dependent histones genes are typically found in gene clusters, which are multiple copies of a given histone (Singh et al., 2018). Some genes within a cluster encode histone isoforms with a high degree of sequence similarity, and the incorporation of these homomorphous isoforms can impart functional changes (Singh et al., 2018). Conversely, histone variants, also termed “replication-independent” histones, are expressed and incorporated into nucleosomes throughout the cell cycle in a regulated manner (Talbert and Henikoff, 2021). Replication-independent histone variants generally have greater sequence divergence from the canonical homomorphic isoforms and greater inter-species sequence variation (Talbert and Henikoff, 2021). The incorporation of heteromorphic histone variants or homomorphic isoforms into the nucleosome can alter nucleosomal stability by changing the interactions within the histone octamer or between the histone and DNA (Luger et al., 2012). Furthermore, histones are binding partners for many other nuclear factors and altering the histone composition of a nucleosome can attract or occlude factors such as chromatin remodelers, histone modifying enzymes, transcription factors, and transcriptional machinery.

1.4.3. Histone post-translational modifications

Histones can be modified with a diverse range of post-translational modifications (PTMs). Among the most well-characterized PTMs are methylation, acetylation and phosphorylation (Millán-Zambrano et al., 2022). The majority of known PTMs occur on the histone tails which are more accessible to nuclear factors. However, many PTMs within the globular histone fold domains have been identified, and typically affect histone-histone or histone-DNA interactions (Millán-Zambrano et al., 2022). As per the sequence divergence of histone variants, specific histone PTMs can attract or occlude binding of other nuclear factors. Additionally, the sequence differences between canonical histones and their isoforms or variants impart an additional layer of complexity as certain PTMs can be variant-specific (Joseph and Young, 2023). While a myriad of histone PTMs that have been identified, the work presented herein focuses on acetylation, methylation, and phosphorylation. The general characteristics of these PTMs are discussed below.

Histone acetylation involves the addition of one or more acetyl groups to the ε-amino group of a lysine residue through the action of histone acetyltransferases (HATs), and the acetyl groups can be removed by histone deacetylases (HDACs) that are part of co-activator or co-repressor complexes, respectively (Figure 1) (Bannister and Kouzarides, 2011). Histone acetylation is generally associated with transcriptional activation due to increased DNA accessibility as the addition of an acetyl group neutralizes the positive charge of lysine, which weakens the interaction between the lysine and the negatively charged DNA phosphate backbone (Bannister and Kouzarides, 2011; Zhang et al., 2021).

Histone lysine residues can be mono-, di-, or tri-methylated, as can arginine. Arginine dimethylation can occur symmetrically or asymmetrically, depending on which amine groups are methylated. Histone methylation is associated with transcriptional activation and repression, depending on which residue is methylated. For example, H3K27me3 is a marker of transcriptionally silent genomic regions while H3K36me3 marks actively transcribed gene body regions (Millán-Zambrano et al., 2022).

Histone phosphorylation can occur at serine, tyrosine, and threonine residues. Phosphorylation PTMs are deposited by histone kinases and removed by phosphatases (Bannister and Kouzarides, 2011). Phosphorylation adds negative charges to the histones; therefore, it is thought that phosphorylation may be associated with gene transcription due to increased DNA accessibility in a manner like histone acetylation (Bannister and Kouzarides, 2011; Millán-Zambrano et al., 2022).

1.4.4. Non-histone chromatin-associated proteins

Histones are the major protein component of chromatin, but there are many other non-histone proteins with critical roles in epigenetic regulation and chromatin structure. One important class of non-histone chromatin-associated proteins are the high mobility group (HMG) proteins, which are the most abundant nuclear proteins after histones in vertebrates (T. Starkova et al., 2023). HMG proteins can be grouped by their structures into HMGA, HMGB, and HMGN families that bind DNA through distinct domains (T. Starkova et al., 2023). HMGA proteins bind the minor groove of A/T-rich DNA through an AT-hook domain, HMGB proteins have a HMG box domain which facilitates binding with nucleosomal linker DNA, and HMGN proteins associate with the nucleosome through a

nucleosomal binding domain (NBD) (Postnikov and Bustin, 2016). HMGB and HMGN proteins do not bind DNA in a sequence-specific manner, but rather a structure-specific manner, and due to their binding sites, they can compete with linker histones (Nanduri et al., 2020; Postnikov and Bustin, 2016; T. Starkova et al., 2023; T. Y. Starkova et al., 2023). HMG proteins play critical roles in transcription, chromatin architecture, DNA repair, and replication (Nanduri et al., 2020; Postnikov and Bustin, 2016; T. Starkova et al., 2023; T. Y. Starkova et al., 2023).

Another important chromatin-binding protein is methyl-CpG binding protein 2 (MeCP2). MeCP2 is critical in neurological development and can serve to activate or repress gene transcription and influence chromatin structure through associations with linker DNA in place of linker histones (Ishibashi et al., 2008; Ortega-Alarcon et al., 2024; Thambirajah and Ausió, 2009). The transcriptional outcome imparted by MeCP2 is dependent on the chromatin context in which it is bound, for example DNA methylation, histone PTMs, and the recruitment of other regulatory factors (Ortega-Alarcon et al., 2024; Thambirajah and Ausió, 2009).

Like histones, non-histone chromatin-associated proteins, such as the ones discussed above, can be post-translationally modified. PTM state can alter chromatin binding, localization, and protein-protein interactions, thereby changing the functional outcome (Chikhirzhina et al., 2024; T. Starkova et al., 2023; Thambirajah and Ausió, 2009).

1.4.5. Chromatin regulation during TH signaling

Decades of research have demonstrated that histone PTMs and the regulation of chromatin structure are involved in TH signaling and TH-dependent amphibian metamorphosis. Many of the studies discussed below used *Xenopus* oocytes as a system to study transcription, chromatin structure and histone modifications in relation to TH. Researchers can inject the oocytes with mRNAs that will be translated into proteins of interest in the oocyte. Similarly, DNA can be injected into the oocyte nucleus and will become chromatinized. The oocyte system is therefore a powerful experimental tool, but it is important to note that it likely does not capture the full tissue-specific cellular contexts that are involved in amphibian metamorphosis.

Nuclear co-repressor (N-CoR) and silencing mediator for retinoid and thyroid hormone receptors (SMRT) are closely related transcriptional corepressors and both form HDAC-containing complexes (Li et al., 2000). Two studies using *X. laevis* as a model system revealed that the N-CoR/SMRT complex is recruited to the promoters of TH-controlled genes in the absence of T_3 and are released when T_3 is present and that there is a local increase in histone acetylation following the corepressor release (Sachs et al., 2002; Tomita et al., 2004). Furthermore, release of N-CoR/SMRT corresponded with increased transcription of the TH-controlled genes, and an overexpression of a dominant negative N-CoR, which blocks endogenous N-CoR binding, resulted in increased transcription of TH-dependent genes (Sachs et al., 2002; Tomita et al., 2004). These studies demonstrated that N-CoR/SMRT were critical for repression of TH-controlled genes and hinted at a role for HDACs. The importance of HDAC3 for effective TH-dependent repression has been demonstrated in *Xenopus* oocytes (Li et al., 2000).

A later study confirmed that the HDAC activity, most notably HDAC3, is required for TH-dependent gene repression in a human cell line (Ishizuka and Lazar, 2003). Interestingly, treatment of *X. laevis* tadpoles with trichostatin A, an HDAC inhibitor, leads to expression of TH-controlled genes in the absence of TH, but intriguingly trichostatin A also blocks metamorphic progression (Sachs et al., 2001b, 2001a). This suggests that while HDAC activity is important for effective transcriptional repression, HDACs must play a critical role during metamorphosis beyond repressing TH-dependent gene activation in the absence of TH. Transcriptional coactivator complexes HATs such as p300 and steroid receptor coactivator acetyltransferases (SRCs) are recruited to TRs in the presence of TH and that histone acetylation correlates with expression of TH-controlled genes (Havis et al., 2003; Paul et al., 2007; Paul and Shi, 2003). In premetamorphic *X. laevis* intestines, pan-acetylation of H3 and H4 increased at the TREs of TH-controlled genes following T_3 treatment (Matsuura et al., 2012b).

Histone methylation is also implicated in both the repression and activation of TH-mediated genes. In *Xenopus* oocytes it was determined that unliganded TR associates with the histone methyltransferase (HMT) SUV39H1 which specifically deposits the transcriptionally repressive histone PTMs H3K9me2 and H3K9me3 (Li et al., 2002; Weirich et al., 2021). SUV39H1 activity was required for repression of TH-responsive genes through its interaction with TR (Li et al., 2002). The repressive histone mark H3K27me3 decreased at the TRE of *thrb* and *thibz* in *X. tropicalis* intestine following T_3 treatment (Matsuura et al., 2012b). Methylation is also involved in transcriptional activation of TH-dependent genes. Protein arginine methyltransferase 1 (PRMT1) methylates H4R3, a PTM associated with transcription activation, and is

recruited to liganded TR through its complex with p300 and SRC3 (Shi et al., 2012). In *X. laevis* tadpoles, PRMT1 expression is increased following T_3 treatment and overexpression of PRMT1 increased TH-dependent gene activation and the rate of metamorphosis (Matsuda et al., 2009). H3K79me3 is associated with transcriptional activation and is enriched in the promoters of TH-dependent genes in natural and T_3-induced metamorphosis in *X. tropicalis* (Matsuura et al., 2012b). The methyltransferase disruptor of telomeric silencing 1-like (DOT1L) is the only known methyltransferase that methylates H3K79. TH induces the expression of DOT1L, and its overexpression increases TH-dependent gene activation, suggesting that DOT1L is an important factor in TH-mediated gene expression (Matsuura et al., 2012a; Wen et al., 2017). H3K4me3 and asymmetrical H3R17me2 have also been shown to be enriched at TREs upon T_3 treatment in *X. tropicalis* intestines (Matsuura et al., 2012b), and H3K36me2 and H3K36me3 are enriched at the *thrb* coding region in *R. catesbeiana* liver after 3 days of T_3 exposure (Mochizuki et al., 2012a).

Limited evidence suggests that histone phosphorylation is involved in TH-mediated gene expression. *R. catesbeiana* liver histones were analyzed following T_4 treatment and showed increased phosphorylation of H1 and H2A histones (Morris and Cole, 1980). Using the *Xenopus* oocyte system, phosphorylation of H3S10 was observed to be associated with TH-dependent gene expression (Li et al., 2002).

A 2011 study in *X. tropicalis* brain and tailfin demonstrated that histone acetylation and methylation PTMs at TREs following T_3 treatment is gene- and tissue-specific (Bilesimo et al., 2011). Pan-acetylation of H4 and H3K18ac were shown to increase at the TREs of *thrb* and *thibz* following T_3 treatment in both tissues, and

H3K9ac at the TRE of *thibz*, but not *thrb*, increased following T_3 treatment only in the tailfin. In both tissues, H3K4me2 increased following T_3 treatment at the *thibz* TRE but decreased at the *thrb* TRE. H3K27me3 decreased at the *thrb* TRE after T_3 treatment in both tissues, but a T_3-dependent decrease in this mark only occurred at the *thibz* TRE in the tailfin.

Chromatin remodeling is another mechanism involved in TH signaling. Studies in *Xenopus* oocytes noted that TR disrupts chromatin by nucleosome removal in a T_3-dependent manner (Hsia and Shi, 2002; Wong et al., 1997b). These findings have been recapitulated in *X. tropicalis* intestine, as histone occupancy was decreased at the TREs of TH-regulated genes following T_3 treatment and during natural metamorphosis (Matsuura et al., 2012b). Studies in the 1990s using *Xenopus* oocytes demonstrated that TRs can bind TREs that are within a nucleosome structure, but that the position of the TRE on the surface of the nucleosome (Wong et al., 1997; Wong et al., 1995). The ability of TRs to associate with a TRE within a nucleosome would likely be important for gene repression in the absence of TH, prior to the TH-induced nucleosome removal discussed above.

1.4.6. Cold temperature influences *R. catesbeiana* histones

Mochizuki *et al* (2012) conducted temperature exposures with *R. catesbeiana* tadpoles. Premetamorphic tadpoles were exposed to T_3 for 3 days at either 28°C or 4°C, after which the livers were dissected, and real-time quantitative polymerase chain reaction (qPCR) was used to analyze the expression of a variety of genes. Subsequent chromatin immunoprecipitation (ChIP) assays characterized H3 acetylation and

methylation PTMs in the coding regions of select genes. Transcript abundance of *thrb* increased significantly after T_3 treatment at 28°C, but not at 4°C. At 28°C, T_3 exposure resulted in no change in H3K36me1 and an increase in both H3K36me2 and H3K36me3 in the *thrb* coding region. T_3 treatment at 4°C altered these methylation patterns, as H3K36me1 decreased and the increase in H3K36me2 or H3K36me3 was abolished. A T_3-dependent decrease in H3K36me1 was also only observed at 4°C in the CCAAT/enhancer-binding protein 1 (C/EBP1) coding region; the transcription of which was upregulated in a TH-dependent manner at 28°C but not at 4°C. Lastly, the transcription of C/EBP2 was upregulated by cold temperature but was not affected by T_3 exposure. The cold temperature upregulation was accompanied by an increase in H3K9ac in the tadpoles at 4°C compared to those at 28°C, regardless of T_3 exposure.

Two studies published in 2019 used premetamorphic *R. catesbeiana* tadpoles to study the effects of temperature on liver histones (Ishihara et al., 2019; Ishihara and Yamauchi, 2019). In the first study, tadpoles were collected in the summer and in the winter and were immediately euthanized without acclimatization to laboratory conditions (Ishihara et al., 2019). A separate group of winter-collected tadpoles were maintained at 4°C for one week, and then a portion were subjected to a gradual increase in temperature to 21°C over three days. Histones from summer-collected tadpole liver homogenates had increased levels of H3K9ac compared to winter-collected tadpoles. Increased H3K9ac and pan-H4ac was observed in the experimentally warm-acclimated tadpoles compared to those held at 4°C. Protein levels of H2A.Z were higher in the summer-collected and the warm-acclimated animals compared to the winter-collected tadpoles and those maintained at 4°C.

The second study again used summer-collected tadpoles and acclimated them to 22°C for one week, then gradually decreased the temperature from 22°C to 4°C over 3 days (Ishihara and Yamauchi, 2019). ChIP assays on liver homogenates showed that H3K9ac and pan-H4ac were decreased in the cold-acclimated tadpoles compared to those maintained at 22°C. While global H3K9ac decreased at cold temperatures, this PTM increased in abundance at the *scd* gene, the expression of which was induced in the cold-acclimated tadpoles.

Together, these studies demonstrate that metamorphically non-permissive temperatures (*i.e.*, 4°C) alter the histone composition of *R. catesbeiana* liver, both with and without the influence of TH. The influence of temperature on *R. catesbeiana* histones in the presence and absence of TH has not been addressed using a non-targeted approach, or in multiple tissues. Furthermore, potential epigenetic components of the molecular memory model, wherein tadpoles treated with TH at non-permissive temperatures are then transferred to permissive temperatures, have not been investigated.

1.5. Hypothesis

I hypothesize that there are tissue-and stage-specific variations in the abundance of histone isoforms or variants and PTMs in the blood, liver, and tailfin of *R. catesbeiana* tadpoles undergoing natural metamorphosis. Additionally, I hypothesize that T_3 treatment at non-permissive (5°), permissive (24°C), and shifted (5°C→24°C) temperatures will result in distinct tissue-specific variations in histone isoform, variant, and PTM abundance.

1.6. Objectives

Overall objective: To further elucidate changes in histone and chromatin-associated protein abundance and PTMs that are potentially involved in TH signaling.

Specific objective 1: Analyze the histone composition of *R. catesbeiana* blood, liver, and tailfin at premetamorphosis, metamorphic climax, and of juvenile frogs using label-free tandem mass spectrometry.

Specific objective 2: Analyze the histone and chromatin-associated protein composition of *R. catesbeiana* blood, liver, and tailfin following T_3 injection under different temperature conditions using isobaric labeling tandem mass spectrometry.

To our knowledge, the work herein is the first unbiased analysis of amphibian histone variants and PTMs in multiple tissues over natural metamorphosis and following T_3 treatment at metamorphically non-permissive, permissive, and shifted (non-permissive → permissive) temperatures. The results presented herein offer insight into

potential epigenetic factors of TH-signaling, which has broad relevance to the health and development of vertebrate species.

2. Changes in histone abundance and post-translational modifications in *Rana catesbeiana* tissues during thyroid hormone-dependent metamorphosis.

2.1. Abstract

Amphibian metamorphosis is thyroid hormone (TH)-dependent and involves extensive changes in the gene expression profiles of differentiated tissues resulting in organismal remodeling. This likely involves changes in the epigenome, however this is poorly understood. We used tandem mass spectrometry (MS/MS) to investigate global variations in histone abundance and post-translational modifications (PTMs) during natural metamorphosis to identify putative epigenetic mediators of TH-mediated postembryonic development. Blood, liver, and tailfin from five *Rana (Lithobates) catesbeiana* (American bullfrog) individuals were collected from functionally athyroid premetamorphic tadpoles and from tadpoles at metamorphic climax (maximal TH levels). Only blood and liver were collected from five individual *R. catesbeiana* frogs (suprabasal TH levels), as the tailfin has been resorbed by this stage. Acid-extraction of nuclei enriched for basic proteins including histones and other chromatin-associated proteins. MS/MS data were queried against the *R. catesbeiana* proteome using open search parameters to capture modified histone peptides and stringent statistical evaluation was performed. The abundance of multiple histone variants and isoforms changed throughout metamorphosis, in particular H1 and H2A variants. We also identified putative changes in histone PTMs by analyzing the abundance of peptides carrying mass shifts corresponding to methylation, acetylation and phosphorylation. To

our knowledge, this is the first non-targeted analysis of histone isoform and variant abundance and PTMs during TH-mediated amphibian metamorphosis. Our findings broaden our understanding of the coordinated variations in histone abundance and PTMs that occur across all histone families to direct the tissue-specific transitions that are critical for TH-driven development in amphibians.

2.2. Introduction

Thyroid hormones (THs) are critical metabolic regulators of nearly every organ system in the body throughout life and particularly during development in all vertebrate species. Amphibian metamorphosis is one example of a TH-dependent postembryonic developmental process wherein an aquatic tadpole becomes a (semi-)terrestrial frog. Metamorphosis requires coordinated, whole-body remodeling that involves, but is not limited to, the replacement of larval red blood cells (RBCs) with adult RBCs, extensive metabolic reprogramming of the liver, and the resorption of the tadpole tailfin (Helbing et al., 2010; Shi, 2000; Tamori and Wakahara, 2000; Yamaguchi et al., 2022). The coordination of these diverse tissue fates and cellular mechanisms during metamorphosis is orchestrated in part by tightly controlled tissue-specific changes in gene expression (Jackman et al., 2022). Little is known about how THs elicit these diverse, tissue-specific changes in gene expression.

Premetamorphic tadpoles are functionally athyroid (Poulson et al., 2023). During prometamorphosis, the tadpole's thyroid gland produces TH predominantly as L-thyroxine (T_4) that can be converted to 3,5,3'-triiodothyronine (T_3) by deiodinase activity in target cells (Shi, 2000). Maximal TH levels are reached at metamorphic climax after

which the levels decrease to suprabasal levels in the juvenile frog (Poulson et al., 2023).

In the nucleus, THs regulate gene expression by binding to TH receptors (TRs), TRα and TRβ, that are constitutively bound to TH-response elements (TREs) in the regulatory regions of TH-controlled genes (Gilbert et al., 1996; Sachs et al., 2000). When not bound with TH, transcriptional co-repressor complexes associate with TRs. Subsequent TH binding results in a conformational change in the TR that permits a switch from co-repressor complexes to transcriptional co-activator complexes that associate with the liganded TR (Glass and Rosenfeld, 2000). These co-activator and co-repressor complexes contain chromatin remodeling proteins and histone modifying enzymes, implying that epigenetic processes are directly linked to TH-action (Shi et al., 2012).

Epigenetic processes regulate gene expression without changing the DNA sequences that encode the genome. DNA is organized and compacted within the nucleus of a cell by wrapping around histone proteins at regular intervals to form chromatin. Chromatin is a dynamic, pliable structure comprised of genomic DNA, histone proteins, and other chromatin-associated proteins, and is a pivotal functional organizer of DNA accessibility. Consequently, the regulation of chromatin structure is critical for vital cellular processes including DNA replication, repair, and gene transcription and silencing (Reyes et al., 2021). The modulation of chromatin structure is a major mechanism of epigenetic regulation (Reyes et al., 2021).

The fundamental repeat unit of chromatin is the nucleosome, wherein DNA wraps around a histone protein octamer composed of two monomers from each core histone family: H2A, H2B, H3 and H4 (Kornberg and Thomas, 1974; Luger et al., 1997; Oudet et al., 1975). The linker DNA that enters and exits the nucleosome may also be bound by linker histones (*i.e.*, H1 or H5) or other linker DNA-binding proteins. The bulk of histone translation occurs during the S-phase of the cell cycle to package newly replicated DNA. These “replication-dependent” histones are typically heteromorphous isoforms that have limited sequence divergence from canonical isoforms (West and Bonner, 1980). The organization of DNA within nucleosomes permits the condensation of nearly 2 meters of nuclear DNA through the formation of higher-order chromatin structures.

Variations in nucleosome composition can alter chromatin conformation, and thus, DNA accessibility and utilization ultimately affecting gene expression. One way in which chromatin organization can be altered includes the incorporation of histone variants into nucleosomes in place of their canonical counterparts, which can occur independently of replication (Talbert and Henikoff, 2021). Histone variants are typically non-allelic heteromorphous histones whose sequences diverge significantly from canonical forms. Replication-independent, histone variants are expressed during all stages of the cell cycle.

Post-translational modification (PTM) of histones can also alter chromatin structure both directly, by affecting proximal charges, and indirectly through the recruitment of chromatin modifying complexes. An increasing plethora of modifications are being identified and methylation, acetylation, and phosphorylation are among the

best studied (Millán-Zambrano et al., 2022). There are several other mechanisms by which chromatin structure can be modulated and they can work in concert with each other to encourage or occlude binding of other nuclear factors and complexes, including those involved in TH regulation (Bannister and Kouzarides, 2011; Henikoff and Smith, 2015; Talbert and Henikoff, 2017).

The importance of chromatin regulation during development is well established (Atlasi and Stunnenberg, 2017). Transcriptional regulation by THs involves the remodeling of chromatin associated with TH-responsive genes that are bound by TRs. In *Xenopus*, treatment with T_3 correlates with increased levels of H4 acetylation in premetamorphic tadpole intestine and tailfin (Sachs and Shi, 2000) and with decreased H3 trimethylation of lysine 27 (H3K27me3) at TH-regulated genes in the premetamorphic intestine (Matsuura et al., 2012b). Additionally, T_3 treatment results in an increase in H3K36me2 and H3K36me3 at the TH-responsive *thrb* gene in *R. catesbeiana* liver (Mochizuki et al., 2012a). These findings suggest that TH action may involve tissue-specific variations in histone composition. More research is required to explore the potential variations in histone dynamics occurring during TH-mediated metamorphosis in tissues with different fates.

Deciphering the variations in chromatin-bound histone isoforms, variants, and PTMs that occur during TH-mediated metamorphosis would uncover potential epigenetic mechanisms that are critical for this sensitive early developmental period. The mechanisms of TH signaling are highly conserved throughout vertebrates. Given that TH-dependent metamorphosis in amphibians parallels TH-mediated mammalian perinatal development, further study in this area is merited to expand our understanding

of coordinated and tissue-specific TH-mediated development (Grimaldi et al., 2013). Amphibians are uniquely poised for the study of TH-dependent development as metamorphosis in species such as *Rana (Lithobates) catesbeiana* begins with the induction of TH in functionally athyroid premetamorphic tadpoles. In contrast, any comparable studies of perinatal development in mammals are confounded by the presence of maternal THs.

In the present study, we examined global changes in histone proteins and associated inferred PTMs using tandem mass spectrometry (MS/MS) to characterize histone proteins in *R. catesbeiana* blood, liver, and tailfin throughout naturally occurring TH-mediated metamorphosis. *R. catesbeiana* is an ideal animal model to study TH action. The large size of the tadpoles negates the need to pool tissues from multiple individuals, and the widespread (invasive) population distribution allows for the use of wild-caught animals that capture natural variation. *R. catesbeiana* metamorphosis more closely resembles mammalian development as the aquatic tadpole develops into a terrestrial frog, whereas commonly used *Xenopus* species remain semi-aquatic as juveniles and adults.

Diploid nuclei were isolated from *R. catesbeiana* blood, liver, and tailfin of premetamorphic and metamorphic climax tadpoles, and from the blood and liver of recently metamorphosed (<1 year) juvenile frogs. Nuclei were acid extracted to enrich for basic proteins (including histones and DNA-binding proteins) and protein extracts were chemically modified with trimethylacetic anhydride (TMA) prior to trypsin digestion and MS/MS analysis (Kuchaříková et al., 2021). Histones have a high abundance of lysine and arginine residues and digestion with trypsin alone results in short peptides

that are not amenable to MS analysis (Kuchaříková et al., 2021; Lu et al., 2021). Lysine modification with anhydrides can achieve longer histone-derived tryptic peptides by blocking trypsin cleavage at anhydride-modified lysine residues (Lu et al., 2021). TMA was selected for the present study because it shows improved chromatographic retention and MS/MS analysis of histone-derived peptides compared to propionic anhydride, a commonly used anhydride (Kuchaříková et al., 2021).

MS/MS provides sufficient resolution to distinguish between peptides with even single amino acid sequence differences, thus allowing the identification of histone isoforms that have high sequence similarity. Further, MS/MS can detect potential PTMs on peptides by identifying mass shifts that correspond to the mass of known PTMs. This resolution can identify changes in histone isoform abundance and putative PTMs during *R. catesbeiana* metamorphosis in a tissue-specific manner. To our knowledge, this is the first comprehensive and untargeted MS/MS analysis of tissue-specific histone protein variations during amphibian metamorphosis.

2.3. Materials and methods

All chemicals and reagents were purchased from Sigma-Aldrich (Oakville, Ontario, Canada) unless indicated otherwise.

2.3.1. Animal care and handling.

R. catesbeiana tadpoles and juvenile frogs were caught in Victoria, British Columbia, Canada by Westwind Sealab Supplies and were housed at the University of Victoria Outdoor Aquatics Unit. Animals were separated by developmental stage and

held in 100-gallon (378.54 L) fiberglass covered tanks with recirculated dechlorinated municipal water at 15°C ±1°C, pH 6.8 and 96-98% dissolved oxygen. Animal handling was in accordance with the Canadian Council on Animal Care and the Animal Care Committee of the University of Victoria guidelines under the protocols #2019-025 and #AE-23-005.

2.3.2. Euthanasia and tissue collection.

The animals were visually assessed using Taylor Kollros (TK) staging (Taylor and Kollros, 1946) and animals were selected to represent premetamorphosis (TK stage 6-8; n = 5), metamorphic climax (TK stage 20; n = 5), and frogs (TK stage 25; n = 5) (Figure 4). Premetamorphic and metamorphic climax tadpoles were euthanized by immersion in 0.1% (w/v) tricaine methanesulfonate (TMS; Syndel Laboratories, BC, Canada) and 25 mM sodium bicarbonate solution followed by exsanguination. Frogs were euthanized by immersion in 1% (w/v) TMS and 25 mM sodium bicarbonate solution followed by double pithing. Blood and liver were collected from all animals, while tailfin was collected only from premetamorphic and metamorphic climax tadpoles (Figure 4). Liver and tailfin tissues were dissected, placed in Whirlpak bags, and flash frozen in liquid nitrogen before transfer and storage at -80°C. Blood samples were collected in 5 mL of blood storage buffer to prevent coagulation (20 mM Tris pH 7.5, 70 mM KCl, 10 mM EDTA). An equal volume of glycerol was added and gently mixed prior to storage at -80°C. Each tissue was analyzed (not pooled) to characterize the natural variation among biologically independent individuals.

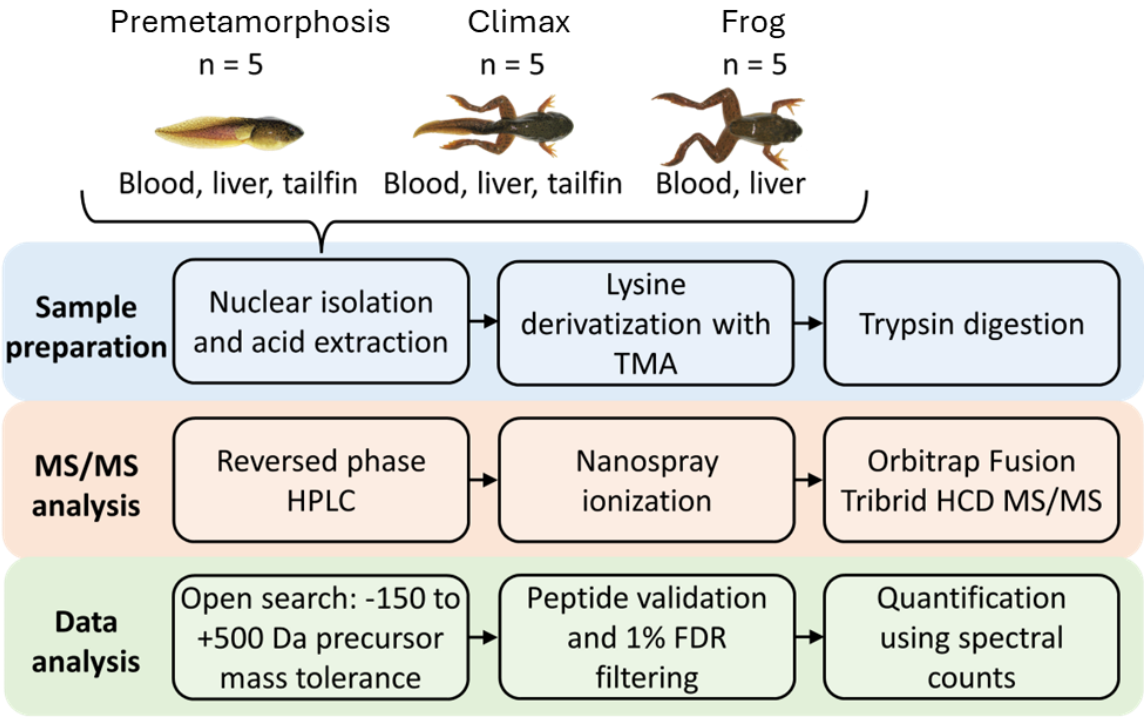

Figure 4. Experimental workflow from sample preparation to downstream data analysis. HPLC, high-performance liquid chromatography; HCD, high-energy collision dissociation; FDR, false discovery rate.

2.3.3. Liver and tailfin nuclei isolation.

Individual frozen liver and tailfin tissues were removed from storage at -80°C and placed into liquid nitrogen. The bagged tissues were removed from the liquid nitrogen, wrapped in paper towels and immediately shattered by hitting the covered tissue with a cold metal block. The shattered tissue was placed in 3 mL ice-cold nuclei isolation buffer (10 mM Tris-HCl pH 7.5, 250 mM sucrose, 3 mM $CaCl_2$, 0.1 mM dithiothreitol [DTT], 1 mM phenylmethylsulfonyl fluoride [PMSF], 5 mM sodium orthovanadate, 10 mM sodium fluoride, 1 mM phenylarsine oxide, and one protease inhibitor tablet [cOmplete mini EDTA-free Protease Inhibitor Cocktail, Catalog #11836170001] and one-half phosphatase inhibitor tablet [PhosSTOP, Catalog #4906837001] per 10 mL of isolation

buffer). Tissues were homogenized using a Heidolph polytron homogenizer (Heidolph Instruments, Schwabach, Germany). Triton X-100 (Catalog #T878) was added to the homogenate to a final concentration of 0.5% (v/v) and the homogenates were incubated on ice for 3 minutes. The homogenates were centrifuged at 4°C for 8 minutes at 2,200 x g. The supernatant was discarded, and the pellet was resuspended in 500 µL ice-cold nuclei isolation buffer to remove residual Triton X-100. The centrifugation step was repeated, the supernatant was discarded, and the pellet was resuspended in 300 µL ice-cold nuclei isolation buffer. The resuspended nuclei were transferred to 1.5 mL low retention microcentrifuge tubes (Catalog #3448; Thermo Scientific, Waltham, Massachusetts, USA), then stored frozen at -80°C.

2.3.4. Blood nuclei isolation.

Blood samples were thawed on ice and centrifuged at 1,500 xg at 4°C for 5 minutes and the supernatant containing the blood storage buffer and glycerol was discarded. Blood cell pellets were resuspended in 500 µL of ice-cold nuclei isolation buffer and centrifuged at 1,500 xg at 4°C for 2 minutes. The supernatant was discarded without disturbing the pellet. Pellets were gently resuspended in 1 mL of ice-cold nuclei isolation buffer and Triton X-100 was added to a final concentration of 0.2% (v/v). Resuspended pellets were incubated on ice for 3 minutes. The samples were centrifuged at 4°C for 5 minutes at 1,500 xg. The supernatant was discarded, and the pellet was resuspended in 300 µL of ice-cold nuclei isolation buffer. The centrifugation step was repeated and the supernatant was discarded. The nuclei pellet was resuspended in 100 µL ice-cold nuclei isolation buffer, transferred to a 1.5 mL low retention microcentrifuge tube and stored at -80°C.

2.3.5. Acid extraction and protein quantification.

Isolated nuclei were acid extracted to enrich for basic proteins such as histones and other acid-soluble proteins. Acid extractions were conducted as described previously (Sidoli et al., 2016) with some modifications. The frozen nuclei were thawed on ice and centrifuged at 16,000 xg at 4°C for 10 minutes. The supernatant was removed and the pellet was resuspended in 5 volumes of ice-cold 0.2 M H_2SO_4. Samples were shaken at full speed in a tube rack clamped to a Labline Titer Shaker (Model 4625, Melrose Park, Illinois, USA) at 4°C for 4 hours followed by centrifugation at 3,400 xg at 4°C for 5 minutes. The supernatant containing the acid-soluble proteins was transferred to a new low retention microcentrifuge tube. Ice-cold trichloroacetic acid (Catalog no. T0699) was added to a final concentration of 33% (v/v) and vortexed. The samples precipitated overnight at -20°C. The precipitate was collected by centrifugation at 10,000 xg at 4°C for 5 minutes. The supernatant was discarded, and the pellet was washed with 1 mL of ice-cold HPLC-grade acetone (Catalog no. A929-1, Fisher Chemical, Ottawa, Ontario, Canada) and centrifuged at 10,000 xg at 4°C for 2 minutes. The acetone wash was repeated twice more. Following the final wash, the supernatant was removed and the pellet was dried by vacuum concentrator (Savant SpeedVac SPD120, Thermo Scientific, Waltham, Massachusetts, USA) for 30 minutes at room temperature to remove residual acetone. The dried pellet was resuspended in 100 µL of ultrapure HPLC-grade water (Catalog no. 022934.K2, Thermo Scientific) and stored at -80°C. For each sample a 20 µL aliquot was taken for quantification and a 10 µL aliquot was taken for sodium dodecyl-sulfate polyacrylamide gel electrophoresis (SDS-PAGE) to confirm the integrity of the histone proteins. Protein quantification was performed

using a bicinchoninic acid (BCA) assay (Catalog no. 23252, Thermo Scientific) according to the manufacturer's instructions.

2.3.6. SDS-PAGE analysis of histones.

SDS-PAGE analyses were carried out as previously described (Rivera-Casas et al., 2017). Acid-extracted protein samples were added to 2X SDS-PAGE sample buffer (125 mM Tris-HCl pH 6.8, 4% SDS, 20% glycerol, 10% β-mercaptoethanol, 0.001% bromophenol blue) to a final composition of 1X sample buffer. 1 µg of protein sample was loaded per well of a 15% SDS-PAGE gel. Two µL Precision Plus Protein Dual Color Standard (Catalog no. 1610374, Bio-Rad, Hercules, California, USA) was loaded on each gel as a molecular weight marker. Electrophoresis was done using a Mini-Protean Tetra Cell system (Catalog no. 1658000, Bio-Rad) and VWR Power Source (250V model, VWR Chemicals, Mississauga, ON, Canada) at 250 V for 50 minutes in 1X SDS-PAGE Running Buffer (25 mM Tris, 192 mM glycine, 0.1% SDS). The gels were incubated overnight in Coomassie staining solution (0.03% Coomassie blue R250, 50% methanol,10% acetic acid) and shaken in destain solution (50% methanol, 10% acetic acid) until the background colour was removed. Staining and destaining were conducted at room temperature. After destaining, the gels were rinsed with deionized water, photographed and dried on a gel dryer (Model No. 583, Catalog no. 165-1745; Bio-Rad).

2.3.7. Protein TMA derivatization.

Acid extracted protein samples were chemically modified with TMA (Catalog no. AAB2298314; Thermo Scientific) as described previously (Kuchaříková et al., 2021).

Briefly, 18 µg per protein sample were dried in the SpeedVac at room temperature and resuspended in 18 µL 50% acetonitrile (ACN; HPLC LC-MS grade, Catalog #83640, VWR Chemicals, Mississauga, ON, Canada) diluted with ultrapure HPLC-grade water. Derivatization was performed one sample at a time by adding 1 µL ammonium hydroxide to the sample and immediately vortexing to attain pH ~8. 4.5 µL derivatization reagent (1 volume TMA to 3 volumes 100% ACN) and 1 µL ammonium hydroxide were then added and vortexed thoroughly after each addition. TMA is hygroscopic and exposure to air reduces its efficacy; therefore, fresh derivatization reagent was prepared every three samples. Following the first round of derivatization, samples were incubated for 5 hours and shaken at 1000 rpm at room temperature on a thermal mixer (Catalog #13687711; Thermo Scientific). A second round of derivatization was performed using the same volumes as above, followed by an overnight incubation with shaking at 1000 rpm at room temperature using a thermal mixer. The next day, the samples were dried by SpeedVac and resuspended in 18 µL 50% ACN. One round of microwave-assisted derivatization was done by performing the derivatization as described above followed by microwaving the samples for 1 minute. This was repeated for a total of three rounds of microwave-assisted derivatization (i.e., a total of three rounds of derivatization with each followed by a 1-minute microwave incubation). Samples were again dried in the SpeedVac, resuspended in 18 µL 50% ACN, and another three rounds of microwave-assisted derivatization were performed.

2.3.8. Trypsin digestion.

The samples were dried in the vacuum concentrator and resuspended in 80 µL 100 mM ammonium bicarbonate (Catalog no. A6141) and 0.6 µg of sequencing grade

modified trypsin (Catalog no. V5111; Promega, Madison, Wisconsin, USA). The samples were incubated on a thermal mixer at 1000 rpm for 4 hours at 37°C. To ensure complete digestion, another 0.6 µg trypsin was added per sample and incubated using a thermal mixer at 1000 rpm for 12 hours at 37°C.

2.3.9. Peptide TMA derivatization.

The digested peptides were dried down in the SpeedVac to approximately 5 µL and resuspended with 50% ACN to a final concentration of 0.6 µg/µL. Three rounds of microwave-assisted derivatization were performed and samples were dried and resuspended to 0.6 µg/µL as described above. A final three rounds of microwave-assisted derivatization were done and samples were dried completely in the SpeedVac at 40°C.

2.3.10. Preparing derivatized peptides for LC-MS/MS.

Peptide clean-up was performed using Pierce C-18 resin 100 µL pipette tips (Catalog #87784, Thermo Scientific, Waltham, Massachusetts, USA) according to the manufacturer's instructions. All solutions were made with ultrapure HPLC-grade water. Briefly, the samples were resuspended in 100 µL 0.35% trifluoroacetic acid (TFA, Catalog #T6508). The C-18 tip was first wet by aspirating then discarding 100 µL 50% ACN in ultrapure HPLC-grade water twice. The tip was then equilibrated by aspirating and discarding 100 µL 0.1% TFA twice. The sample was aspirated and dispensed 10 times to ensure complete binding. The tip was rinsed by aspirating and discarding 100 µL 0.1% TFA in 5% ACN. The sample was eluted by aspirating and dispensing 24 µL

0.1% formic acid (Catalog #F0507) in 75% ACN. The samples were dried completely in the SpeedVac at 40°C.

2.3.11. LC-MS/MS analysis.

LC-MS/MS analysis was performed at the University of Victoria Genome BC Proteomics Centre in British Columbia, Canada. The samples were resuspended to 0.5 µg/µL with 2% ACN and 0.1% formic acid. Approximately 2 µg per sample were separated by on-line reversed phase liquid chromatography using a Thermo Scientific EASY-nLC 1000 system, an Acclaim PepMap100 C18 reversed phase pre-column (100 µm I.D., 2 cm length, 5 µm, 100Å), and an AcclaimPepMap100 C-18 reversed phase nano-analytical column (75 µm I.D., 15 cm length, 3 µm, 100Å, Thermo Fisher Scientific, San Jose, California, USA) at a flow rate of 300 nL/min. This was coupled on-line with an Orbitrap Fusion Tribrid mass spectrometer (Thermo Fisher Scientific) with a Nanospray Flex NG source (Thermo Fisher Scientific). The MS1 scan range was set to 350-2000 m/z with a resolution of 60,000 full width at half maximum (FWHM) at 200 m/z. Data-dependent acquisition was scheduled at least every three seconds and the most intense ions with charge states 2-7 exceeding 50,000 counts were selected for higher energy collisional dissociation fragmentation. Comprehensive MS/MS details are presented in the appendix.

2.3.12. R. catesbeiana proteome.

The proteome used in the present study was the predicted proteins from the most current *R. catesbeiana* genome assembly (version 4, DOI https://doi.org/10.5281/zenodo.8125199).

2.3.13. Database search against the R. catesbeiana proteome.

Using MSFragger, experimental spectra were compared to theoretical spectra generated from the *in silico* tryptic digestion of the *R. catesbeiana* proteome (Kong et al., 2017). We allowed up to five missed cleavages to account for blocked tryptic cleavages at biologically modified and TMA-modified lysine residues. Open search settings included a precursor tolerance of -150-500 Da and a fragment tolerance of 20 ppm. The MSFragger localization-aware search was employed, which generated a series of mass-shifted ions in addition to the regular theoretical ion series for improved identification of modified peptides (Yu et al., 2020b).

2.3.14. Peptide validation and FDR filtering using Philosopher.

The peptide-spectrum matches (PSMs) identified by MSFragger were filtered to a 1% false discovery rate (FDR) at the peptide and protein levels using the Philosopher tools PeptideProphet and ProteinProphet, respectively (da Veiga Leprevost et al., 2020). The FDR was determined by a decoy approach using reversed protein sequences from the *R. catesbeiana* proteome.

2.3.15. Protein relative abundance analysis.

Peptide spectral counts (the number of PSMs identified for a given peptide sequence) were normalized according to the sum of all spectral counts in each sample. Peptides were then grouped by protein annotation to obtain a total spectral count for each protein. To be considered for statistical comparison between developmental stages, a protein had to be detected in ≥4/5 biological replicates of both developmental stages being compared or be detected in ≥4/5 biological replicates of one

developmental stage and have an original spectral count of zero (before imputation to 0.9) in ≥4/5 biological replicates in the other stage (Figure 5A). For a protein to be deemed “detected” in a biological replicate, there must be at least one PSM mapped to that protein.

2.3.16. Mass shift analysis.

Mass shift analyses were performed at the peptide-level and protein-level. To be considered for this analysis, a peptide or protein had to be detected in at least 4 out of 5 biological replicates of both stages being compared. The percentage of PSMs of the peptide or protein that had a mass shift within 0.01 Da of common PTMs were calculated: 14.0157 Da (methylation), 28.0313 Da (dimethylation), 42.047 (trimethylation), 42.0106 Da (acetylation), and 79.9663 Da (phosphorylation). A peptide or protein was considered for mass shift statistical analysis if the mass shift was detected either in ≥ 4/5 biological replicates in both conditions being compared, or in ≥ 4/5 biological replicates of one condition and not detected (prior to imputation to 0.9, see *Statistical analyses*) in ≥ 4/5 biological replicates of the other (Figure 5B).

By requiring detection or non-detection in ≥4/5 biological replicates ensure a robust stringency in our analyses. While only requiring ≥3/5 biological replicates would have been sufficient for statistical analysis, by using a more stringent approach, we can focus our analysis on the most robust changes in the dataset.

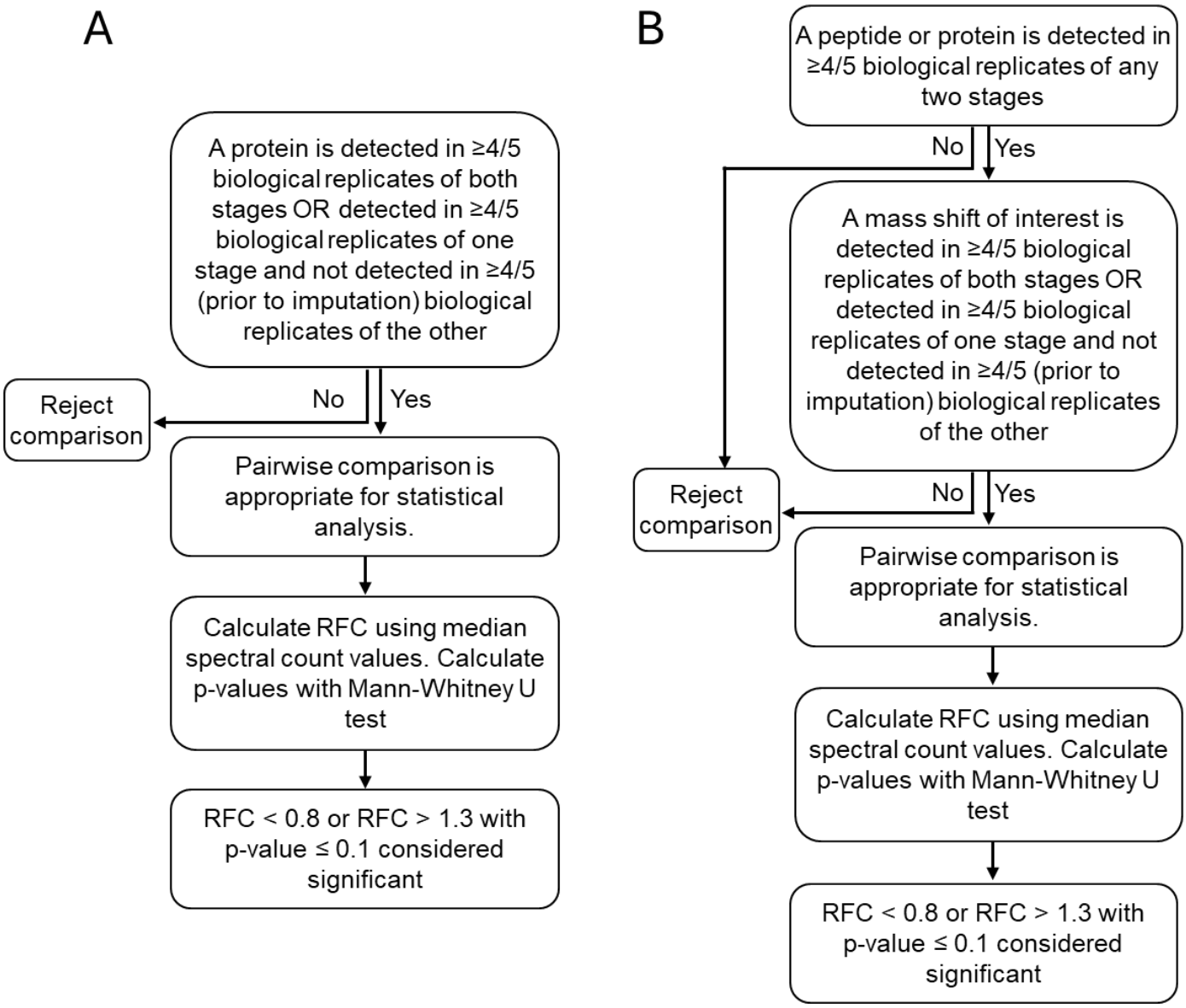

Figure 5. Decision tree for the analysis of **A)** protein differential abundance and **B)** mass shift abundance. RFC, relative fold change.

2.3.17. Statistical analyses.

Zero values were imputed as 0.9 to avoid “infinite” or artifactually large or small fold changes, wherein a zero value would otherwise be the numerator or denominator in a fold change calculation. Protein abundance fold changes were calculated between developmental stages using the median normalized spectral count values. The median percentage of PSMs of each peptide or protein that had a mass shift was used to calculate the fold change of the associated putative PTM. P-values were calculated using the non-parametric Mann-Whitney U test. P-values ≤0.1 and relative fold changes (RFC) less than 0.8 or greater than 1.3 were considered significant (Figure 5).

2.4. Results and discussion

To our knowledge, the present study is the first tissue-specific, non-targeted characterization of histone variations that occur during TH-dependent amphibian metamorphosis. The observed histone-based changes suggest potential epigenetic mechanistic targets that intersect with TH regulation of critical early developmental periods.

2.4.1. Conserved stoichiometry of intact histone proteins

All acid-extracted protein samples were run on 15% SDS-PAGE to assess the quality of the histone proteins. All samples had well-resolved histone protein bands that indicate that the isolated histones are intact without substantial degradation. Importantly, the equivalent stoichiometry among the core histones was conserved (see Figure 6 for representative samples) (Rivera-Casas et al., 2017).

2.4.2. Majority of acid-extracted proteins are chromatin-associated

We identified a median of 5,746 ± 412 (blood), 6,389 ± 1,112 (liver), and 7,376 ± 439 (tailfin) PSMs of which 88.7 ± 1.9%, 89.8 ± 2.1%, and 68.6 ± 3.4% were respectively mapped to histones in the *R. catesbeiana* proteome (Table 1). This suggests that the acid extraction successfully enriched the samples for histones.

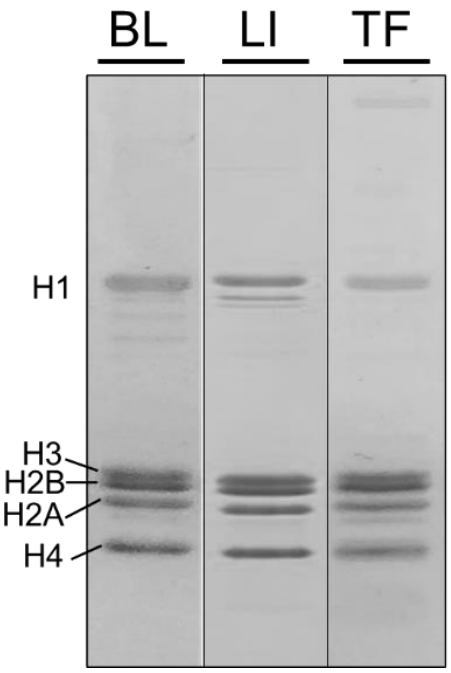

Figure 6. Representative SDS-PAGE of acid-extracted histones from premetamorphic tadpole blood (BL), liver (LI), and tailfin (TF).

Table 1. Peptide-spectrum matches (PSMs) across all tissues predominantly mapped to histone proteins in the *R. catesbeiana* proteome. Median values and associated median absolute deviations (MADs) were calculated for all samples within a tissue.

Median mapped PSMs			Median percentage of PSMs mapped to histones
Tissue	The *R. catesbeiana* proteome	Histones	
Blood	5,746 ± 412	5,062 ± 474	88.7 ± 1.9
Liver	6,389 ± 1,112	5,848 ± 1,066	89.8 ± 2.1
Tailfin	7,376 ± 439	5,073 ± 530	68.6 ± 3.4

2.4.3. Protein annotations

The *R. catesbeiana* proteome is not fully annotated, so to better identify putative histone (homomorphous) isoforms and variants, we aligned the *R. catesbeiana* histone protein sequences to the human proteome using BLASTP. We found multiple occurrences of *R. catesbeiana* histones in the proteome with distinct amino acid sequences that had identical human BLASTP annotations. These histones, herein referred to as subtypes, have been distinguished in the tables and text by roman numerals and the amino acid sequence alignments can be found in the supplementary materials (Supplementary figures S1-S20).

2.4.4. Changes in histone protein abundance

Histones from all major families (H1, H2A, H2B, H3, and H4) were detected in all tissues with the most isoforms found in the liver (Table 2). Most of the histones detected did not change significantly in abundance over the metamorphic stages studied,

suggesting that the overall histone composition does not change drastically during metamorphosis (Table 2). However, some notable histone proteins did differ in abundance during postembryonic development within a given tissue. The H1 histone family collectively exhibited the greatest overall significant changes during metamorphosis compared to the other core histone families (Table 2). H1 isoforms are associated with epigenetic reprogramming and embryonic development in mammalian cells (Izzo et al., 2017; Talbert and Henikoff, 2021). Given the similarities between mammalian and amphibian TH-dependent postembryonic development, the differential H1 abundance we observed during amphibian metamorphosis may be linked to epigenetic regulation that is necessary for development. The most replication-independent variants were unsurprisingly detected in the histone H2A family. The H2A family has the greatest number of documented variants having significant sequence divergence from canonical isoforms among all core histone families (Table 2) (Bönisch and Hake, 2012).

Table 2. Relative fold changes (RFCs) and median absolute deviations of histone proteins in *R. catesbeiana* blood, liver and tailfin at premetamorphosis (Premet), metamorphic climax (Climax), and juvenile frog (Frog) developmental stages. Distinct protein entries from the *R. catesbeiana* proteome with identical protein annotations are differentiated by roman numerals. All indicated fold changes are statistically significant (p-value ≤ 0.1). Blue fields indicate a relative increase in abundance, yellow fields indicate a relative decrease in abundance, and the intensity of the colour corresponds to the size of the fold change. Grey fields indicate conditions where the data did not pass detection criteria for statistical evaluation (See Figure 2A for more information). n.s., non-significant RFCs. *, indicates that one stage had ≥4/5 biological replicates with spectral counts of 0 that were imputed to 0.9 for statistical analysis.

Protein type	Isoform annotation	Blood			Liver			Tailfin
		Premet→ Climax	Premet→ Frog	Climax→ Frog	Premet→ Climax	Premet→ Frog	Climax→ Frog	Premet→ Climax
H1	H1.0	n.s.	3.2±0.08	1.7±0.2	n.s.	1.8±0.3	n.s.	2.4±0.2
	H1.3 (i)	n.s.	0.6±0.06	n.s.	n.s.	n.s.	n.s.	n.s.
	H1.3 (ii)	n.s.	n.s.	n.s.	n.s.	0.8±0.1	n.s.	n.s.
	H1.3 (iii)	n.s.	n.s.	n.s.	n.s.	n.s.	n.s.	n.s.
	H1.10 (i)	n.s.	n.s.	1.4±0.1	n.s.	0.5±0.2	0.5±0.1	n.s.
	H1.10 (ii)	n.s.	2.9±0.3	1.4±0.1	0.8±0.1	n.s.	n.s.	1.9±0.2
H2A	H2A type 1-A	n.s.	n.s.	n.s.	n.s.	n.s.	n.s.	n.s.
	H2A type 2-B	n.s.	n.s.	n.s.	n.s.	n.s.	n.s.	n.s.
	H2A type 2-C (i)	n.s.	n.s.	n.s.	n.s.	n.s.	n.s.	n.s.
	H2A type 2-C (ii)	n.s.	n.s.	n.s.	n.s.	4.6±0.9	n.s.	n.s.
	H2A.X	0.7±0.1	n.s.	n.s.	n.s.	n.s.	n.s.	n.s.
	H2A.Z-2	n.s.	n.s.	n.s.	n.s.	1.3±0.1	n.s.	n.s.
	Macro-H2A.1	0.8±0.05	n.s.	n.s.	n.s.			
	Macro-H2A.2	n.s.	n.s.	n.s.	n.s.	n.s.	1.5±0.2	n.s.
H2B	H2B type 1 (i)	n.s.	n.s.	n.s.	n.s.	n.s.	n.s.	n.s.
	H2B type 1 (ii)	n.s.	n.s.	n.s.	n.s.	n.s.	n.s.	n.s.
H3	H3.2 (i)	0.8±0.06	n.s.	n.s.	n.s.	n.s.	n.s.	n.s.
	H3.2 (ii)	n.s.	n.s.	n.s.	n.s.	n.s.	n.s.	n.s.
	H3.3 (i)	n.s.	n.s.	n.s.	n.s.	n.s.	n.s.	
	H3.3 (ii)							n.s.
	H3.3 (iii)				n.s.	n.s.	n.s.	
H4	H4 (i)	n.s.	n.s.	n.s.	n.s.	n.s.	n.s.	n.s.
	H4 (ii)		0.5±0.03*					
	H4 (iii)	0.5±0.2	0.6±0.2	n.s.	n.s.	n.s.	n.s.	
	H4 (iv)	n.s.	n.s.	n.s.	n.s.	0.5±0.1	n.s.	n.s.
	H4 (v)					n.s.		n.s.

Histone H1.0 is a replication-independent H1 variant that is associated with terminally differentiated tissues, and with nucleolar domains that are typically transcriptionally repressed (Mayor et al., 2015; Talbert and Henikoff, 2021). Protein abundance of H1.0 increased over the metamorphic stages in all three tissues (Table 2). In blood and liver, H1.0 levels increased from premetamorphosis to frog by 3.2-fold and 1.8-fold, respectively. H1.0 increased from premetamorphosis to metamorphic climax by 2.4-fold in the tailfin. The increase in H1.0 abundance may be reflective of the terminal differentiation of the blood and liver cells following TH-mediated metamorphosis, and of the tailfin prior to its eventual resorption following metamorphic climax. Interestingly, a 1995 study found that TH could drive gene transcription through the mouse H1.0 promoter in a monkey cell line (Bauer-Hofmann and Alonso, 1995). To our knowledge, TH-driven H1.0 expression has not been suggested elsewhere, but further work is warranted to explore a connection between TH and H1.0 abundance.

Human H1.3 is a replication-dependent H1 that is generally associated with heterochromatic regions (Talbert and Henikoff, 2021). H1.3 (i) and H1.3 (ii) differ only at position 70 which is an alanine in H1.3 (i) and a serine in H1.3 (ii) (Supplementary Figure S2). H1.3 (i) decreased by 0.6-fold from premetamorphosis to frog in the blood (Table 2). In the liver, H1.3 (ii) decreased 0.8-fold from premetamorphosis to frog (Table 2). The decrease in abundance of the replication-dependent H1.3 in the blood and liver occurs over the same developmental period as the increase in abundance of the variant H1.0 (Table 2). It is possible that there may be some complementary activities between H1.3 subtypes and H1.0.

H1.10 is replication-independent histone variant that is associated with RNA polymerase II-enriched regions (Mayor et al., 2015). In mouse primordial germ cells, H1.10 is temporarily lost from chromatin during epigenetic reprogramming (Izzo et al., 2017). H1.10 (i) increased 1.4-fold from metamorphic climax to frog in the blood. H1.10 (ii) abundance increased in the blood by 2.9-fold from premetamorphosis to frog and 1.4-fold from metamorphic climax to frog (Table 2). In the liver, H1.10 (i) decreased 0.5-fold in the liver from premetamorphosis and metamorphic climax to frog, and H1.10 (ii) decreased by 0.8-fold from premetamorphosis to metamorphic climax (Table 2). H1.10 (ii) increased 1.9-fold from premetamorphosis to metamorphic climax in the tailfin (Table 2). While H1.10 (i) and H1.10 (ii) both align to the same human H1.10 protein, they vary in sequence and H1.10 (i) lacks a considerable portion of the human H1.10 C-terminal sequence (Supplementary Figure S3). Further investigation will be required to verify the identities of these H1.10 subtypes in the *R. catesbeiana* proteome. Overall, H1.10 abundance increased in the blood and tailfin but decreased in the liver. These tissue-specific variations in H1.10 could be due to the distinct fates of these tissues during metamorphosis.

We did not observe any significant changes in abundance of the replication-dependent isoforms H2A type 1-A, H2A type 2-B, H2A type 2-C (i) in any tissue. However, H2A type 2-C (ii) relative abundance increased 4.6-fold in the frog liver compared to the premetamorphic tadpole liver (Table 2). H2A type 2-C (ii) differs from H2A type 2-C (i) by 2 amino acids, V52 and F129, which are A52 and S129 in H2A type 2-C (i) (Supplementary Figure S6). H2A type 2-C (*Hist2h2ac*) mRNA expression is induced through the epidermal growth factor receptor (EFGR) pathway in breast cancer

(Monteiro et al., 2017) and is involved in hepatocyte proliferation (Bhushan and Michalopoulos, 2020). Thus, the increase in H2A type 2-C abundance in the frog liver after metamorphosis could be indicative of increased hepatocyte division.

H2AX is implicated in DNA repair, chromosome inactivation, mitotic chromatin regulation, and stem cell development (Turinetto and Giachino, 2015). In human hematopoietic cell lines, H2AX expression is decreased following differentiation (Lal et al., 2009). We found H2AX abundance was 0.7-fold lower at metamorphic climax compared to premetamorphosis in blood (Table 2). It has been established that the switch from larval to adult hemoglobin in *R. catesbeiana* is achieved through the replacement of larval RBCs by a new population of adult RBCs (Dorn and Broyles, 1982; Yamaguchi et al., 2022). H2AX expression and its genomic localization in larval RBCs compared to adult RBCs may be an interesting topic for future research.

The replication-independent H2A variant H2A.Z is nearly universally found in eukaryotes and is critical for metazoan development and differentiation (Bönisch and Hake, 2012; Dijkwel and Tremethick, 2022). H2A.Z is involved in transcriptional activation and repression and influences nucleosome positioning and RNA polymerase II recruitment (Bönisch and Hake, 2012). H2A.Z can poise genes for activation and when incorporated with H3.3, can destabilize nucleosomes at promoter regions (Li et al., 2023). H2A.Z is also implicated in estrogen-regulated gene expression (Gévry et al., 2009; Martire and Banaszynski, 2020). Two H2A.Z paralogs in vertebrates, H2A.Z-1 and H2A.Z-2, have tissue-specific functions (Dijkwel and Tremethick, 2022). H2A.Z-2 abundance was 1.3-fold higher in frogs compared to premetamorphosis in the liver, but did not change in abundance in blood or tailfin (Table 2). The tissue-specific functions of

H2A.Z may be involved in TH-mediated metamorphosis. Furthermore, the known crosstalk between the thyroid and estrogen endocrine systems could involve H2A.Z, as has been previously reviewed (Thambirajah et al., 2022).

MacroH2A is associated with transcriptional repression, X chromosome inactivation, inhibition of cellular reprogramming in mouse cells, and the regulation developmental genes (Buschbeck et al., 2009; Chadwick et al., 2001; Gaspar-Maia et al., 2013). In the blood, macroH2A.1 isoform 4 decreased 0.8-fold from premetamorphosis to metamorphic climax. MacroH2A.2 increased by 1.5-fold in liver from metamorphic climax to frog (Table 2). The changes in abundance observed in the blood suggest that macroH2A.1 isoform 4 is less abundant during metamorphic climax when TH levels are maximal (Poulson et al., 2023), while macroH2A.2 levels in the liver are lower at metamorphic climax compared to frog. These tissue-specific changes in macroH2A isoform-specific abundance could be due in part to the temporal regulation of TH-mediated metamorphosis.

Human H3.2 is a replication-dependent histone, while H3.3 is a replication-independent variant (Talbert and Henikoff, 2021). Among the detected H3 proteins, we saw a 0.8-fold decrease in H3.2 (i) from premetamorphosis to metamorphic climax in blood. There is a single amino acid difference between H3.2 (i) and H3.2 (ii) at position 98, which is an alanine in H3.2 (i) and a serine in H3.2 (ii) (Supplementary Figure S13). We also observed tissue-specific detection of differently annotated H3.3 subtypes. H3.3 (i) was only detected in blood and liver, H3.3 (ii) was only detected in the tailfin, and H3.3 (iii) was only detected in the liver (Table 2). H3.3 (ii) is identical to the aligned human H3.3 sequence, while in comparison, H3.3 (i) has a longer C-terminal sequence

and H3.3 (iii) has a truncated N-terminus (Supplementary Figure S14). Tissue-specific H3 expression is known to occur in vertebrates as a 2015 study showed multiple H3.3-like histone proteins that were expressed in a tissue-specific manner in mice (Maehara et al., 2015).

We detected five proteins annotated as H4 across all tissues (Table 2). H4 (ii) has the greatest sequence divergence from human H4 while the other identified subtypes differ only by a few amino acids (Supplementary Figure S15). In blood, we observed a 0.5-fold decrease of H4 (ii) abundance from premetamorphosis to frog (Table 2). Also in blood, H4 (iii) decreased by 0.5-fold from premetamorphosis to metamorphic climax, and 0.6-fold from premetamorphosis to frog (Table 2). In liver, H4 (iv) decreased 0.5-fold from premetamorphosis to metamorphic climax (Table 2). Histone H4 has the fewest variants, with only one identified variant in humans (Talbert and Henikoff, 2021). However, it is possible that multiple subtypes exist within a histone isoform in *R. catesbeiana*. Further validation will be required to investigate whether these are true H4 variants or subtypes.

2.4.5. Identification of Putative PTMs at Protein and Peptide Levels.

To assess changes in putative PTMs, we calculated the proportion of peptides with mass shifts indicative of common histone PTMs: acetylation, methylation and phosphorylation (Table 3). The relative abundance of these mass shifts was compared between premetamorphosis tadpoles, metamorphic climax tadpoles, and juvenile frogs within blood, liver, and tailfin. These results are summarized at the peptide level (Table

3) and at the protein level (Table 4). Protein-level results were achieved by calculating the proportion of peptides mapped to a given protein with the mass shift of interest (Table 4).

Table 3. Relative fold changes (RFCs) and median absolute deviations of mass shifts associated with histone peptides in *R. catesbeiana* blood, liver and tailfin at premetamorphosis (premet), metamorphic climax (climax), and juvenile frog (Frog) developmental stages. ac, acetylation; me, methylation; me2, dimethylation; phos, phosphorylation. *, indicates that one stage had ≥4/5 biological replicates with spectral counts of 0 that were imputed to 0.9 for statistical analysis. See Table 2 legend for additional details.

Protein type	Annotation	Peptide	Mass shift	Blood			Liver			Tailfin
				Premet→ Climax	Premet→ Frog	Climax→ Frog	Premet→ Climax	Premet→ Frog	Climax→ Frog	Premet→ Climax
H1	H1.3 (i)	1-18	ac							1.3±0.08
	H1.3 (ii)	1-18	ac	1.5±0.2	n.s.	n.s.				
		1-31	me		2.9±0.3*	2.9±0.3*				
	H1.3 (iii)	1-18	me2		9.7±0.7*	9.7±0.7*		10.1±0.8*	10.1±0.8*	
		1-19	me2		5.1±0.2*	5.1±0.2*				
H2A	H2A type 2-C (i)	21-29	ac	2.3±0.5	n.s.	n.s.				
	H2AX	4-18	ac	0.03±0.3*						
H2B	H2B type 1 (ii)	46-56	me2	0.1±0.1*						
		51-61	ac	n.s.	n.s.	n.s.			n.s.	7.9±0.7*
H3	H3.2 (i)	9-17	ac	n.s.	n.s.	n.s.	0.6±0.1	n.s.	1.7±0.3	n.s.
		18-26	me2					4.1±1.0*	4.1±1.0*	
		27-36	me	n.s.	n.s.	0.7±0.07				n.s.
		73-83	me2	n.s.	2.5±0.4	1.9±0.3				n.s.
		84-115	phos				1.8±0.3	n.s.	0.3±0.2	
H4	H4 (i)	4-17	ac	n.s.	n.s.	0.7±0.04	n.s.	n.s.	n.s.	n.s.
		20-35	me2	n.s.	1.5±0.1	1.6±0.1	n.s.	n.s.	n.s.	n.s.
		24-35	ac	0.5±0.2*	2.3±0.2	4.3±0.2*				1.3±0.2*

Table 4. Relative fold changes (RFCs) and median absolute deviations of mass shifts of histone proteins in *R. catesbeiana* blood, liver and tailfin at premetamorphosis (premet), metamorphic climax (climax), and juvenile frog (Frog) stages. *, indicates that one stage had ≥4/5 biological replicates with spectral counts of 0 that were imputed to 0.9 for statistical analysis. **, to preserve the directional fold change, the imputed value for metamorphic climax was 0.1 instead of 0.9 as the median value of premetamorphic tadpoles was less than 0.9. See Table 2 legend for additional details.

Protein type	Annotation	Mass shift	Blood			Liver			Tailfin
			Premet→ Climax	Premet→ Frog	Climax→ Frog	Premet→ Climax	Premet→ Frog	Climax→ Frog	Premet→ Climax
H1	H1.3 (ii)	me	n.s.	2.2±0.3	n.s.	n.s.	n.s.	n.s.	
	H1.3 (ii)	me2		4.6±0.8					
	H1.3 (iii)	me2		3.0±0.4*	3.0±0.4*		2.4±0.1*	2.4±0.1*	
H2A	H2A type 2-C (i)	me	n.s.	n.s.	n.s.			1.7±0.4	
	H2AX	ac	0.0015±0.1**	n.s.	n.s.			n.s.	
H2B	H2B type 1 (ii)	me2	0.4±0.1*						n.s.
H3	H3.2 (i)	ac	n.s.	1.3±0.06	n.s.	n.s.	n.s.	n.s.	n.s.
		me3	0.6±0.05	n.s.	1.7±0.05	n.s.	n.s.	n.s.	n.s.
		phos						0.8±0.04	
H4	H4 (i)	ac	n.s.	n.s.	n.s.	n.s.	n.s.	0.7±0.1	n.s.
		me2	n.s.	1.7±0.2	n.s.	n.s.	n.s.	n.s.	0.8±0.02

2.4.5.1. Methylation

Histone methylation can include mono-, di-, or tri-methylation of lysine and arginine residues. Depending on the type of methylated residues and the specific region of genomic association, histone methylation can be associated with transcriptional activation or repression. For example, H3K27me3 is a marker of transcriptionally silent genomic regions and H3K36me3 marks actively transcribed regions (Millán-Zambrano et al., 2022).

H1 methylation has been generally associated with transcriptional repression and heterochromatin, which is refractory to expression (Andrés et al., 2020; Izzo and Schneider, 2016). In blood and liver, mass shifts corresponding to monomethylation and

dimethylation of H1.3 N-terminal peptides increased over metamorphosis (Table 3). Specifically, methylation mass shifts of peptide 1-31 of H1.3 (ii) were 2.9-fold more abundant in juvenile frogs compared to premetamorphosis or metamorphic climax in blood (Table 3). Dimethylation mass shifts of H1.3 (iii) peptide 1-18 were increased by more than 9-fold in frog compared to premetamorphosis and metamorphic climax in both the blood and the liver (Table 3). Dimethylation mass shifts of H1.3 (iii) peptide 1-19 were increased by 5.1-fold in frog blood compared to premetamorphosis and metamorphic climax. Similar trends were also detected at the protein level (Table 4). In addition, at the protein level, dimethylation mass shifts associated with H1.3 (ii) increased 4.6-fold from premetamorphosis to frog (Table 4). The overall increase in putative H1.3 methylation in frog compared to earlier stages in the blood and liver suggests that methylation marks may accumulate after metamorphosis completes. These changes in methylation could be associated with the regulation of gene expression.

H2A type 2-C showed a 1.7-fold increase in methylation mass shifts at the protein level in the frog liver compared to metamorphic climax (Table 4). In the blood, dimethylation mass shifts of the H2B type 1 (ii) peptide 46-56 decreased by 0.1-fold from premetamorphosis to metamorphic climax (Table 3), and a similar trend was seen at the protein level (Table 4). Overall, our results for the blood and liver suggest that dimethylation of H2B and monomethylation of H2A, respectively, are reduced at metamorphic climax compared to other metamorphic stages. These tissue-specific changes in H2A and H2B methylation mass shifts may be reduced under peak TH levels.

Studies in *Xenopus* and *Rana* have shown that transcriptional activation by TH involves tissue- and gene-specific methylation of multiple H3 residues (Bilesimo et al., 2011; Fu et al., 2019; Helbing et al., 2011; Li et al., 2002; Shi et al., 2012). Indeed, the fine-tuning of transcriptional activity has been associated with distinct methylation patterns in different genomic regions (i.e., gene bodies, promoters, enhancers, etc.) in eukaryotic model systems (Garcia et al., 2008; Millán-Zambrano et al., 2022). A 2012 study showed that T_3 treatment resulted in an increase in H3K36me2 and H3K36me3 in the coding region of the TH-responsive *thrb* gene in *R. catesbeiana* liver (Mochizuki et al., 2012b). In the blood, peptide 27-36 of H3.2 (i) decreased 0.7-fold in monomethylation mass shifts from metamorphic climax to frog (Table 3). Additionally, dimethylation mass shifts of the H3 peptide 73-83 increased 2.5-fold and 1.9-fold from premetamorphosis and metamorphic climax, respectively, to frog (Table 3). Lastly, at the protein level in blood, trimethylation mass shifts associated with H3.2 (i) decreased by 0.6-fold from premetamorphosis to metamorphic climax, then increased by 1.7-fold from metamorphic climax to frog (Table 4). This suggests a temporary reduction in global H3 trimethylation events at metamorphic climax. In the liver, there was a 4.1-fold increase of dimethylation mass shifts of H3.2 (i) peptide 18-26 from both premetamorphosis and metamorphic climax to frog (Table 3).

A well-studied H4 methylation event is the dimethylation of H4 lysine 20, which has been implicated in DNA repair and replication (Jørgensen et al., 2013). In the blood, we found that the H4 (i) peptide 20-35 had a 1.5-fold increase in dimethylation mass shifts from premetamorphosis to frog, and a 1.6-fold increase from metamorphic climax to frog (Table 3). A similar increase in dimethylation from premetamorphosis to frog was

seen at the protein level (Table 4). Localization of this dimethylation mass shift will be required to confirm which residue is being modified, but our data suggest that dimethylation of an N-terminal tail H4 peptide accumulates following metamorphosis in the blood.

2.4.5.2. Acetylation

Histone acetylation involves the addition of one or more acetyl groups to a histone lysine residue. The negatively charged acetyl group neutralizes the positive charge of lysine, thus weakening the interaction between the lysine-containing histone and the DNA. Hence, histone acetylation is generally associated with more open and transcriptionally active chromatin regions.

Acetylation of H1 has previously been associated with transcriptionally active genes (Izzo and Schneider, 2016). Acetylation mass shifts of peptide 1-18 of histone H1.3 (i) increased by 1.3-fold from premetamorphosis to metamorphic climax in tailfin (Table 3). Similarly, acetylation mass shifts of H1.3 (ii) peptide 1-18 increased 1.5-fold from premetamorphosis to metamorphic climax in the blood (Table 3). These increases in H1 acetylation at metamorphic climax when TH levels peak may be involved in TH-mediated gene expression.

Acetylation mass shifts of H2A type 2-C (i) peptide 21-29 increased by 2.3-fold from premetamorphosis to metamorphic climax in the blood (Table 3). It is important to note that this peptide also exists in the other replication-dependent H2A variants detected in the dataset and in H2A.Z-2. Consequently, we cannot distinguish which forms of H2A have increased acetylation mass shifts. Acetylation mass shifts of H2AX

peptide 4-18 decreased by 0.03-fold in blood over the same period (Table 3), which was also reflected at the protein level (Table 4). Overall, these data suggest that there are variations in the acetylation-state of H2A-family histones in the blood from premetamorphosis to metamorphic climax.

Acetylation of multiple lysine residues in the N-terminal tail of H2B is catalyzed by the histone acetyltransferase p300 and has been identified as a mark of active enhancers (Narita et al., 2023). In the tailfin, there was a 7.9-fold increase in acetylation mass shifts of H2B type 1-J (ii) peptide 51-61 (Table 3). It is important to note that the H2B type 1-J (ii) protein identified in the *R. catesbeiana* proteome has an extended N-terminal sequence, and the peptide 51-61 corresponds to the human N-terminal sequence (Supplementary figure S12). TRs bound by TH associate with co-activator complexes that can include the p300, thus H2B acetylation could be associated with TH-dependent activity at metamorphic climax (Paul et al., 2007).

Acetylation of H3 lysine residues is generally associated with transcriptional activation and has been implicated in TH-controlled gene expression in *Xenopus* (Præstholm et al., 2020). In the blood at the protein level, there is a 1.3-fold increase in acetylation mass shifts from premetamorphosis to frog (Table 4). In the liver, acetylation mass shifts of H3.2 (i) peptide 9-17 decreased 0.6-fold from premetamorphosis to metamorphic climax, then increased by 1.7-fold from metamorphic climax to frog (Table 3). This is suggestive of a temporary reduction in acetylation at metamorphic climax.

We found that acetylation mass shifts of H4 (i) peptides change significantly in blood and tailfin (Table 3). The H4 peptide 4-17 decreased 0.07-fold in acetylation mass

shifts from metamorphic climax to frog in the blood (Table 3). Acetylation of H4K16 is associated with chromatin disruption by weakening inter-nucleosomal interactions, thus it will be informative to determine which amino acid is being modified in this H4 peptide (Zhang et al., 2016). In the tailfin, H4 peptide 24-35 acetylation mass shifts increased 1.3-fold from premetamorphosis to metamorphic climax (Table 3). In the blood, acetylation mass shifts associated with the same peptide decreased 0.5-fold from premetamorphosis to metamorphic climax, followed by a 4.2-fold increase from metamorphic climax to frog (Table 3), again suggesting a temporary reduction of acetylation at metamorphic climax. In the liver at the protein level, acetylation mass shifts associated with H4 (i) decreased by 0.7-fold from metamorphic climax to frog (Table 4).

2.4.5.3. Phosphorylation

Histones can be phosphorylated by histone kinases at serine, tyrosine, and threonine residues, and removed by phosphatases [18]. TH treatment has been shown to induce changes in histone H3S10 phosphorylation in *Xenopus* oocytes (Li et al., 2002; Morris and Cole, 1980). Only one significant phosphorylation event was observed in the dataset. Histone H3.2 (i) peptide 84-115 in the liver had a 1.8-fold increase in phosphorylation mass shifts from premetamorphosis to metamorphic climax, which was followed by a 0.3-fold decrease from metamorphic climax to frog, which suggests a temporary increase in this phosphorylation event during metamorphic climax (Table 3). At the protein level, only a 0.8-fold decrease in phosphorylation mass shifts occurs from metamorphic climax to frog, indicating that there is likely other H3.2 (i) phosphorylation events that did not pass our filter for statistical analysis (Table 4). *In vitro* experiments

have shown that phosphorylation of H3T118 weakens the interaction between the nucleosome and DNA and increases nucleosome mobility, and is important for *Drosophila* development (Graves et al., 2016; North et al., 2011).

2.4.5.4. Hexose-annotated mass shifts in blood

One of the most abundant putative PTMs detected was a mass shift of 162.052 Da in the blood. While we cannot presently confirm the identity of this modification, a mass shift of 162.052 Da is consistent with the addition of a hexose group.

Glycosylation, specifically O-GlcNAcylation, of histone proteins has been identified on all canonical histones and some variants, and has been associated with DNA repair, transcriptional regulation, and crosstalk with other histone PTMs [66–68]. Changes in skin glycoconjugates during metamorphosis have been observed in *Ranid* species, but to our knowledge, there have not been any reports of glycosylation of histones during amphibian metamorphosis (Faszewski et al., 2008; Kaltenbach et al., 2004).

At the peptide level, there were changes in abundance of this mass shift associated with peptides of H1.0, H1.3 (i, ii, and iii), H2A type 2-C, H2AX, and H2B type 1-J (i and ii) (Table 5). At the protein level, there were also significant changes in abundance of this 162.052 mass shift associated with H4 (i) (Table 6). While these included increased and decreased fold changes across all comparisons analyzed, our results show an overall increase at the frog stage compared to earlier metamorphic stages (Tables 5 and 6).

Our data show that changes in this 162.052 Da mass shift occurs in nearly every histone family in the blood, suggesting that this putative PTM may play a global role in TH-mediated metamorphosis. Further investigation will be required for an in-depth characterization of this putative PTM.

Table 5. Relative fold changes (RFCs) and median absolute deviations of putative hexose mass shifts associated with histone H1 peptides in *R. catesbeiana* blood at premetamorphosis (premet), metamorphic climax (climax), and juvenile frog (Frog) developmental stages. *, indicates that one stage had ≥4/5 biological replicates with spectral counts of 0 that were imputed to 0.9 for statistical analysis. See Table 2 legend for additional details.

Protein type	Annotation	Peptide	Premet→ Climax	Premet→ Frog	Climax→ Frog
H1	H1.0	178-192	18.5±3.1*	10.1±1.9*	n.s.
		238-251		27.8±4.6*	27.8±4.6*
		257-267	37.0±9.3*	27.8±4.6*	n.s.
		303-312	n.s.	18.5±1.9*	18.5±1.9*
	H1.3 (i)	68-82	n.s.	1.7±0.2	1.7±0.3
	H1.3 (ii)	2-24			1.6±0.08
		2-25	n.s.	1.4±0.1	n.s.
		58-67	n.s.	1.6±0.2	n.s.
		110-122	n.s.	n.s.	1.5±0.2
		113-123	0.7±0	n.s.	n.s.
		124-133	12.3±0.8*		
		137-145	n.s.	0.4±0.05	n.s.
		155-164	n.s.	1.7±0.1	n.s.
		168-179	0.6±0.1	n.s.	n.s.
		172-180	n.s.	0.07±0.2*	0.07±0.07*
		200-209	n.s.	n.s.	1.3±0.1
		200-215		8.5±0.4*	
	H1.3 (iii)	2-20			0.2±0.03*
H2A	H2A type 2-C (i)	22-30	1.7±0.2	n.s.	n.s.
		120-131	n.s.	n.s.	1.4±0.2
	H2AX	121-135		15.9±1.3*	
H2B	H2B type 1 (i)	68-82	n.s.	n.s.	1.4±0.1
	H2B type 1 (ii)	47-57	n.s.	2.2±0.1	n.s.
		52-62	n.s.	1.8±0.2	n.s.

Table 6. Relative fold changes (RFCs) and median absolute deviations of putative hexose mass shifts associated with histone proteins in *R. catesbeiana* blood at premetamorphosis (premet), metamorphic climax (climax), and juvenile frog (Frog) developmental stages. See Table 2 legend for additional details.

Protein type	Annotation	Premet→ Climax	Premet→ Frog	Climax→ Frog
H1	H1.0	1.7±0.04	1.6±0.2	n.s.
	H1.3 (i)	n.s.	1.9±0.5	n.s.
	H1.3 (ii)	n.s.	1.3±0.1	n.s.
	H1.3 (iii)	n.s.	n.s.	0.6±0.05
H4	H4 (i)	n.s.	1.5±0.1	n.s.

2.5. Conclusion

To our knowledge, the present study is the first comprehensive characterization of the global variations in histone composition within multiple tissues during naturally occurring, TH-dependent amphibian metamorphosis. We have identified histone variants and putative PTMs that are significantly altered during this post-embryonic developmental period. We have provided a roadmap of novel and potentially coordinated changes in histone abundance and PTMs that may be associated with TH action during metamorphosis. Important next steps will be to understand where these changes are occurring within the genome and if they are associated with other epigenetic changes and transcriptional outcomes. Due to the conserved nature of TH-signaling in vertebrates and the similarities of amphibian metamorphosis to mammalian perinatal development, the broad relevance of the present study can serve as a foundation for future research into critical developmental periods in other vertebrates.

3. Changes in histone abundance and post-translational modifications in *Rana catesbeiana* tissues during temperature-mediated induced metamorphosis.

3.1. Abstract

Amphibian metamorphosis involves thyroid hormone (TH)-dependent postembryonic remodeling of differentiated tissues as a tadpole transforms into a frog. *Rana catesbeiana* (American bullfrog) metamorphosis can be precociously induced in premetamorphic tadpoles by treatment with exogenous TH. However, metamorphosis is temperature-dependent and does not occur at 5°C, even with TH treatment. Remarkably, exposure to TH at 5°C establishes a molecular memory that primes the tadpole for an accelerated metamorphosis when shifted to a permissive temperature (24°C). Previous research suggests that histone post-translational modifications (PTMs) and the incorporation of histone variants are altered upon cold temperature exposure in the presence and absence of TH. Herein, we use mass spectrometry to analyze the histone composition of premetamorphic *R. catesbeiana* blood, liver, and tailfin following TH injection at a permissive temperature (24°C), a non-permissive temperature (5°C), and a shifted condition (5→24°C). Using stringent selection criteria, we identified tissue- and temperature-specific changes in the abundance and putative PTMs of chromatin-binding proteins, including histones. Linker histone variant H1.0 abundance increased in all three tissues following TH treatment under permissive temperatures only. TH-dependent changes in the abundance of methyl-CpG binding protein 2 (MeCP2) and high mobility group (HMG) proteins were temperature- and tissue-specific. PTMs, including variations in H3K27 and H3K36 methylations in the liver, were differentially abundant following TH treatment under the different temperature conditions. We also

identified newly discovered HMGB2 methylation marks that exhibited temperature-specific changes in abundance following TH treatment. These observations suggest that epigenetic variations may contribute to early TH signaling events and to molecular memory.

3.2. Introduction

Thyroid hormones (THs) are critical regulators of development in vertebrate species. Anuran metamorphosis is a TH-dependent process that involves whole-body remodeling as an aquatic tadpole becomes a (semi-)terrestrial frog (Shi, 2000). In the premetamorphic tadpole, metamorphosis is initiated by the onset of TH production by the thyroid gland, and TH levels increase throughout metamorphosis and peak at metamorphic climax before declining as metamorphosis completes (Poulson et al., 2023). Metamorphosis can also be initiated by treatment with exogenous TH, which makes it an excellent model to study TH action. It is not fully understood how THs are able to elicit the tissue- and developmental stage-specific changes in gene expression required for a successful transition from tadpole to frog.

Rana (Lithobates) catesbeiana tadpole metamorphosis does not proceed at cold temperatures, which allows tadpoles to overwinter before metamorphosing under more favorable conditions (Wright et al., 1999). This phenomenon can be recapitulated in a lab setting, as tadpoles treated with TH at 25°C undergo metamorphosis, but metamorphosis will not proceed following TH treatment at 5°C (Frieden et al., 1965). Remarkably, a tadpole exposed to TH at 5°C retains a molecular memory of TH induction, as a shift to 25°C results in accelerated metamorphosis even after all THs

have been cleared from the body (Frieden et al., 1965; Yamamoto et al., 1966). TH treatment under cold temperatures has been used to study early TH-dependent metamorphic events as it separates the initiation of metamorphosis from the execution phase (Corrie et al., 2024; Field et al., 2024; Hammond et al., 2015; Koide et al., 2022).

TH is produced in the thyroid gland as L-thyroxine (T_4), which can be converted to 3,5,3'-triiodothyronine (T_3) by deiodinases in peripheral cells [1]. In the nucleus, T_3 and T_4 can bind to TH receptors (TRs) that are constitutively bound at regulatory regions of TH-responsive genes (Gilbert et al., 1996; Sachs et al., 2000). When not bound by TH, TRs associate with transcriptional co-repressor complexes (Sachs et al., 2000). TH binding induces conformational changes in TRs that permit associations with co-activator complexes, thereby allowing transcription of the proximal TH-dependent gene (Sachs et al., 2000). These complexes can include chromatin remodeling proteins and histone modifying enzymes, implicating epigenetic processes in TH action (Shi et al., 2012).

Chromatin is a complex of genomic DNA, histone proteins and other chromatin binding proteins, and controls the accessibility of the genomic DNA to nuclear factors. Regulation of chromatin structure is therefore essential for many processes including DNA replication, repair, and gene expression. Changing the accessibility of chromatin structure is an epigenetic process that modulates gene expression without altering genomic sequences.

The fundamental repeat unit of chromatin is the nucleosome, which is formed by DNA wrapping around a histone protein octamer that is composed of two monomers

from each core histone family: H2A, H2B, H3, and H4 (Kornberg and Thomas, 1974; Luger et al., 1997; Oudet et al., 1975). Linker DNA enters and exits the nucleosome and connects adjacent nucleosomes. Linker DNA can be bound by linker histones (i.e., H1 or H5) and other linker DNA-binding proteins (i.e., methyl-binding domain proteins, high mobility group (HMG) proteins, etc.). Most histones are produced during the S phase of cell replication to package nascent DNA and are commonly referred to as replication-dependent histones that constitute the major histone isoforms that have limited sequence variability between related family members. Also known as canonical histones, these 'packaging' histones can be replaced by histone variants, which are produced independently of replication and exhibit significant sequence variation from their canonical counterparts (Talbert and Henikoff, 2021). Post-translational modifications (PTMs) of histones can include, but are not limited to, methylation, acetylation, and phosphorylation (Millán-Zambrano et al., 2022). The incorporation of histone variants and the addition of PTMs can directly alter nucleosome conformation and/or facilitate or occlude the recruitment of *trans*-acting factors that can influence DNA accessibility. These are some of the mechanisms by which transcription, repression, replication, and other aspects of chromatin metabolism are regulated (Bannister and Kouzarides, 2011; Millán-Zambrano et al., 2022; Talbert and Henikoff, 2021).

Targeted co-immunoprecipitation studies have investigated histone variations during the arrest of *R. catesbeiana* metamorphosis in cold temperatures. In the tadpole liver, Mochizuki *et al.* showed that trimethylation of histone H3 lysine 36 (H3K36me3) at the TH-responsive gene *thrb* increases following T_3 treatment at 28°C, but not at 4°C (Mochizuki et al., 2012b). Two 2019 studies demonstrated that H3K9 and H4 acetylation

was higher in livers from *R. catesbeiana* tadpoles acclimated to 22°C compared to tadpoles at 4°C (Ishihara et al., 2019; Ishihara and Yamauchi, 2019). Additionally, the replication-independent variant H2A.Z was more abundant in the livers of tadpoles acclimated to 4°C compared to 21°C (Ishihara et al., 2019).

The blood, liver, and tailfin differentially respond to TH at cold temperatures compared to warmer temperatures and were chosen for the present study for their diverse metamorphic fates (Hammond et al., 2015; Mochizuki et al., 2012b; Murata and Yamauchi, 2005). In the blood, a new population of nucleated red blood cells (RBCs) are produced during metamorphosis that express adult hemoglobin while the larval hemoglobin-containing RBCs are removed from circulation (Dorn and Broyles, 1982; Yamaguchi et al., 2022). The liver is reprogrammed during metamorphosis, and most notably shifts from ammonia-excretion to urea-excretion, which requires the liver to produce enzymes required for the urea cycle (Helbing et al., 1992; Shi, 2000). Lastly, the tailfin is resorbed through apoptosis.

In the present study, we used tandem mass spectrometry (MS/MS) with tandem mass tag (TMT) labeling to characterize changes in the abundance and PTMs of histones and other chromatin-associated proteins in *R. catesbeiana* tadpole blood, liver, and tailfin following T_3 treatment under three different temperature conditions. In the metamorphically permissive and non-permissive temperature paradigms, premetamorphic tadpoles were exposed to T_3 at 24°C or 5°C, respectively. In the shifted temperature paradigm, tadpoles were exposed to T_3 at 5°C and then transferred to 24°C 24 hours later. The permissive temperature condition examines putative TH-associated chromatin-based changes under conditions that favor metamorphosis. The

non-permissive condition investigates early TH signaling events by uncoupling the initiation and execution phases of TH action, which may also be involved in establishing the cold-temperature molecular memory. The shifted condition mimics the accelerated metamorphosis observed following a return to permissive temperatures after the TH molecular memory has been established. The results presented herein broaden our understanding of early TH signaling events and the modulation of TH response by temperature.

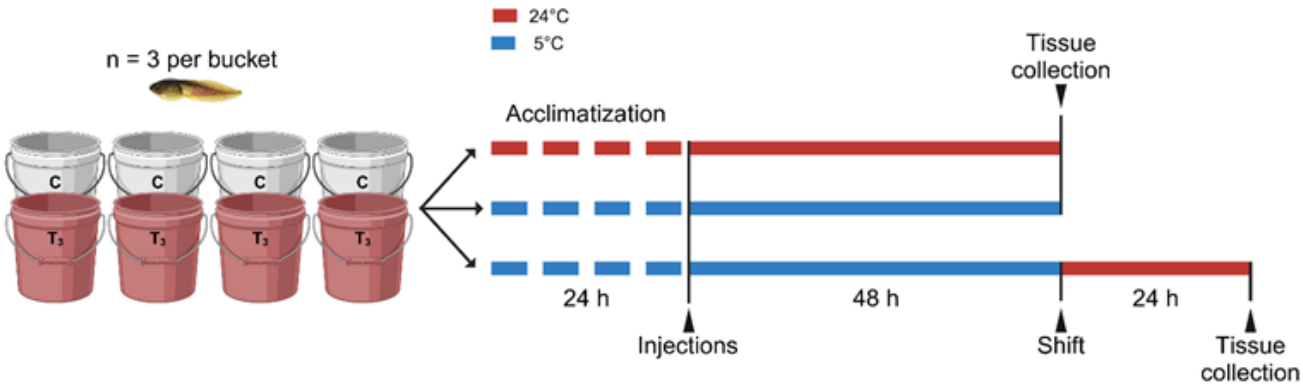

Figure 7. Experimental set up of the temperature shift experiment. Premetamorphic tadpoles were injected with either T_3 or a solvent control under one of three temperature conditions: permissive (24°C), non-permissive (5°C), and shifted (5°C followed by a shift to 24°C). Adapted from Corrie et al. 2024. Made in BioRender.

3.3. Materials and methods

3.3.1. Animal care and handling.

Premetamorphic *R. catesbeiana* tadpoles of uncharacterized sex were caught in Victoria, British Columbia, Canada by Westwind Sealab Supplies and were housed at the University of Victoria Outdoor Aquatics Unit in 100-gallon (378.54 L) fiberglass covered tanks with recirculated dechlorinated municipal water at 15°C ± 1°C, pH 6.8 and 96-98% dissolved oxygen. All animal handling was in accordance with the guidelines prescribed by the Canadian Council on Animal Care and the Animal Care Committee of the University of Victoria (protocols #2019-025 and #AE-23-005).

3.3.2. Experimental set up and temperature conditions.

The animals and experimental design used in the present study have been detailed in Corrie et al., 2024 as parallel, published studies (Corrie et al., 2024; Field et al., 2024). Briefly, we used three temperature paradigms: permissive (24°C throughout the experiment), non-permissive (5°C throughout the experiment), and shifted (5°C → 24°C, treated with TH at 5°C, then increased to 24°C) (Figure 7). Twelve tadpoles were used in each treatment (T_3 or vehicle control) per temperature condition. Three premetamorphic tadpoles were placed in 8 L of water (from the same source as the tadpole's home tank) in a 12 L high-density polyethylene bucket. Four buckets containing 3 tadpoles each were used per treatment. The buckets were held in temperature-controlled sea trays at 24 ± 1°C for the permissive condition or at 5 ± 0.6°C for the non-permissive and shift conditions. The temperature was checked daily, and all animals were monitored daily for general health (*i.e.*, swimming normally, alert, no signs

of disease) and were not fed throughout the experiment. Each bucket was equipped with an air stone to provide aeration and the pH and ammonia levels in all buckets were tested daily. Throughout all experiments, the pH remained at 6.8 and the ammonia levels were between 0.25-0.5 ppm.

Following a 24 h temperature acclimatization period, the tadpoles were injected intraperitoneally with either T_3 or a vehicle control (400 µM NaOH). The T_3-treated tadpoles were injected with 10 pmol T_3/g body weight. A 10 µM T_3 solution in 400 µM NaOH was used at 1 µL/g body weight and measured to the nearest 0.5 µL using a 50 µL Hamilton syringe and 26-gauge x ½" sterile needles. The control tadpoles were injected with 1 µL/g body weight 400 µM NaOH. The 10 µM T_3 solution was prepared from a 10^{-5} M T_3 stock solution (CAS #55–06-1; Alfa Aesar, Ward Hill, MA, US) that had been quantified at the University of Victoria-Genome British Columbia Proteomics Centre by liquid chromatography multiple reaction monitoring mass spectrometry to verify the T_3 concentration, as described in Corrie *et al.*, 2021 (Corrie et al., 2021).

Forty-eight hours after injection, tadpoles from the permissive and non-permissive temperature conditions were euthanized and the tissues were collected as outlined below. Euthanasia and dissections of the tadpoles in the non-permissive experiment were carried out in a cold room maintained between 4-5°C. The tadpoles in the shift experiment were transferred into new buckets with 24°C water 48 h after injection and were euthanized and dissected a further 24 h later.

3.3.3. Euthanasia and tissue collection.

Tadpoles were euthanized by immersion in 0.1% (w/v) tricaine methanesulfonate (TMS; Syndel Laboratories, BC, Canada) and 25 mM sodium bicarbonate solution followed by exsanguination. Blood samples were collected into 5 mL of blood storage buffer (20 mM Tris pH 7.5, 70 mM KCl, 10 mM EDTA) and an equal volume of glycerol was added and gently mixed prior to storage at -80°C. Liver and tailfin tissues were isolated and placed in Whirlpak bags and flash frozen in liquid nitrogen prior to storage at -80°C. The large size of *R. catesbeiana* tadpoles (~5-15 g) enabled the analysis of biologically independent individuals, negating the need to pool tissues to achieve a sufficient sample size. The use of wild-caught animals also captures natural population variation.

3.3.4. Biologically independent sample handling.

Five individuals per treatment condition in each temperature condition were used for analysis, resulting in a total of 30 samples per tissue type. These samples were randomized within their tissue type prior to processing.

3.3.5. Liver and tailfin nuclei isolation.

Individually bagged and frozen liver and tailfin tissues were removed from -80°C and placed in liquid nitrogen. Each packaged tissue was removed from the liquid nitrogen, wrapped in paper towel and shattered by striking it with a cold metal block. The shattered tissue was then placed into 3 mL of ice-cold nuclei isolation buffer (10 mM Tris-HCl pH 7.5, 250 mM sucrose, 3 mM $CaCl_2$, 0.1 mM dithiothreitol [DTT], 1 mM phenylmethylsulfonyl fluoride [PMSF], 5 mM sodium orthovanadate, 10 mM sodium

fluoride and 1 mM phenylarsine oxide, with one protease inhibitor tablet [cOmplete mini EDTA-free Protease Inhibitor Cocktail; Sigma-Aldrich, Oakville, Ontario, Canada. Catalog #11836170001] and one-half phosphatase inhibitor tablet [PhosSTOP; Catalog #4906837001; Sigma-Aldrich] per 10 mL of buffer). Tissues were homogenized using a Heidolph polytron homogenizer (Heidolph Instruments, Schwabach, Germany). The nuclei isolation buffer and all samples were kept on ice throughout the protocol. Lysis was then performed by adding Triton X-100 (Catalog #T878; Sigma-Aldrich) to a final concentration of 0.5% (v/v) in the nuclei isolation buffer. The homogenates were incubated for 3 min on ice, then centrifuged at 4°C for 8 min at 2,200 x g. The supernatant was discarded, and the pellet was resuspended in 500 µL nuclei isolation buffer before repeating the centrifugation as before. The supernatant was removed, and the pellet was resuspended in 300 µL nuclei isolation buffer. The resuspended nuclei were transferred to individual 1.5 mL low retention microcentrifuge tubes (Catalog #3448; Thermo Scientific, Waltham, Massachusetts, USA) and stored at -80°C.

3.3.6. Blood nuclei isolation.

The blood samples were thawed on ice and centrifuged at 4°C for 5 min at 1,500 x g. The supernatant, containing the blood storage buffer and glycerol, was removed and the pellet was gently resuspended in 500 µL nuclei isolation buffer using a glass rod. The samples were centrifuged at 4°C for 2 min at 1,500 x g. The supernatant was removed, and the pellets were resuspended in 1 mL nuclei isolation buffer and 0.2% (v/v) Triton X-100 (final concentration). The samples were incubated on ice for 3 min before centrifugation at 4°C for 5 min at 1,500 x g. The supernatants were discarded, and the pellets were rinsed by resuspension in 300 µL nuclei isolation buffer, and the

centrifugation was repeated. The supernatants were removed, and the pellets were resuspended in 100 µL nuclei isolation buffer. The isolated nuclei were transferred to individual 1.5 mL low retention microcentrifuge tubes and stored at -80°C.

3.3.7. Acid extraction and protein quantification.

The isolated nuclei were acid extracted to enrich the samples for highly basic proteins such as histones and other chromatin-associated proteins. Acid extractions were performed as described previously with some modifications (Sidoli et al., 2016). The nuclei samples were thawed on ice and kept on ice throughout the protocol unless stated otherwise, and all steps were completed in 1.5 mL low retention microcentrifuge tubes. All reagents were kept ice-cold. The thawed nuclei were centrifuged at 4°C for 10 min at 16,000 x g. The supernatant was removed, and the pellet was resuspended in 5 volumes 0.2 M H_2SO_4 (Catalog #71008-946; VWR Chemicals, Mississauga, ON, Canada) prepared in ultrapure HPLC-grade water (Catalog #022934.K2, Thermo Scientific). The samples were shaken at full speed in a tube rack clamped to a Labline Titer Shaker (Model 4625, Melrose Park, Illinois, USA) at 4°C for 4 h. The samples were centrifuged at 4°C for 5 min at 3,400 x g. The supernatant containing the acid-soluble proteins was transferred to a new microcentrifuge tube. Trichloroacetic acid (Catalog #T0699; Sigma-Aldrich) was added to a final concentration of 33% (v/v). The samples were incubated overnight at -20°C to precipitate the protein.

The samples were centrifuged at 4°C for 5 min at 10,000 x g to pellet the precipitated protein. The supernatants were discarded, and the pellets were washed with 1 mL HPLC-grade acetone (Catalog #A929-1, Fisher Chemical, Ottawa, Ontario,

Canada), centrifuged at 4°C for 2 min at 10,000 x g and the supernatant was removed. The acetone wash was repeated twice more. The final pellets were dried by vacuum concentrator (Savant SpeedVac SPD120, Thermo Scientific) at room temperature for 30 min to remove residual acetone. The dried pellets were resuspended in 100 µL ultrapure HPLC-grade water. For each sample, a 20 µL aliquot was taken for quantification and a 10 µL aliquot was taken for sodium dodecyl-sulfate polyacrylamide gel electrophoresis (SDS-PAGE). The samples were quantified by bicinchoninic acid (BCA) assay (Catalog #23252, Thermo Scientific) according to the manufacturer's instructions.

3.3.8. SDS-PAGE analysis of histones.

SDS-PAGE analyses were carried out as previously described (Rivera-Casas et al., 2017). Acid-extracted protein samples were combined with 2X SDS-PAGE sample buffer (125 mM Tris-HCl pH 6.8, 4% SDS, 20% glycerol, 10% β-mercaptoethanol, 0.001% bromophenol blue) to a final composition of 1X sample buffer. One µg of protein per sample was loaded per well of a 15% SDS-PAGE gel. Two µL Precision Plus Protein Dual Color Standard (Catalog #1610374, Bio-Rad, Hercules, California, USA) ladder was loaded on each gel. Electrophoresis was carried out at 250 V for 50 min in SDS-PAGE running buffer (25 mM Tris, 192 mM glycine, 0.1% SDS) in a Mini-Protean Tetra Cell system (Catalog #1658000, Bio-Rad) connected to a VWR Power Source (250V model, VWR Chemicals). The gels were shaken overnight in Coomassie staining solution (0.03% Coomassie blue R250, 50% methanol,10% acetic acid), then transferred to destain solution (50% methanol, 10% acetic acid) and shaken until the background color was removed. Staining and destaining were conducted at room

temperature. The gels were then rinsed with deionized water, photographed and dried using a gel drying apparatus (Model #583, Catalog #165-1745; Bio-Rad).

3.3.9. Protein-level TMT labeling and trypsin digestion.

Isobaric chemical tags have identical masses when intact but produce distinct product ions following fragmentation in MS/MS, therefore allowing tagged samples to be multiplexed prior to MS/MS analysis. Due to the high abundance of lysine and arginine residues in histones, digestion with trypsin results in short peptides that are not amenable to MS analysis (Guo et al., 2022). TMT labels modify lysine residues and can therefore be used before trypsin digestion to block cleavage and produce longer peptides (Guo et al., 2022).

The proteins were labeled with TMTpro™ 16plex labels (Catalog #A44522, ThermoFisher Scientific) at the protein level using the double labeling approach developed by Guo et al. (2022) (Guo et al., 2022). An aliquot containing 30 µg protein from each sample was dried in the SpeedVac at 40°C and resuspended to 1 µg/µL with 100 mM triethylammonium bicarbonate (TEAB) buffer (Catalog #90114, ThermoFisher Scientific). A pooled sample containing an equal amount of all samples was created, of which, a 30 µg aliquot was used in each multiplex as a quality control sample that could be compared between multiplexes. The TMT tags were resuspended at room temperature to 25 µg/µL with HPLC-grade acetonitrile (ACN; HPLC LC-MS grade, Catalog #83640, VWR Chemicals). The TMT tags were added to the samples in a 1:4 protein to tag ratio and incubated at room temperature for 1 h. A second volume of TMT labels were added to the samples followed by another 1 h incubation at room

temperature. The TMT labeling reaction was quenched by adding 10% hydroxylamine (Catalog #90115, ThermoFisher Scientific) to a final 1.2% and samples were incubated at room temperature for 15 min. The samples were combined into multiplexes of 16 (15 samples from of the same tissue type and the pooled control sample). Ten volumes of ice-cold HPLC-grade acetone were added, and the sample was incubated overnight at -20°C.

The multiplexed sample was centrifuged at 4°C for 20 min at 3,400 x g to pellet the precipitated protein. The supernatant was removed, and the pellet was washed with 2 mL ice-cold HPLC-grade acetone and then centrifuged at 4°C for 10 min at 3,400 x g. The supernatant was removed, and the pellet was washed with 200 µL ACN, then centrifuged at 4°C for 3 min at 3,400 x g. The ACN wash was repeated. The pellet was left to dry in the fume hood for 5 min to allow any residual ACN to evaporate.

The dried pellet was resuspended in 50 mM TEAB buffer to a final protein concentration of 0.5 µg/µL. Trypsin (Catalog #V5111; Promega, Madison, Wisconsin, USA) was added to the sample in a 1:40 enzyme to substrate ratio and the sample was incubated at 37°C for 4 h with shaking at 500 rpm on a Thermo Mixer (Catalog #13687711; Thermo Scientific). The samples were dried in the SpeedVac at 40°C.

3.3.10. Peptide clean up.

Peptide clean-up was performed with Pierce™ Peptide Desalting Spin Columns (Catalog #89852; Thermo Scientific) according to the manufacturer's instructions. Briefly, the samples were resuspended in 300 µL 0.1% trifluoroacetic acid (TFA, Catalog #T6508; Sigma-Aldrich) in ultrapure HPLC-grade water. The spin columns were

conditioned with two washes with 300 µL 100% ACN, centrifuged for 1 min at 5,000 x g in between washes and the flow-through was discarded. Two additional washes were then performed as above with 0.1% TFA in ultrapure water. The sample was added to the column and centrifuged at 3,000 x g for 1 min at 4°C and the flow-through was discarded. The column was washed three times with 300 µL 0.1% TFA, and centrifuged at 3,000 x g for 1 min at 4°C. The flow-through was discarded after each wash. The column was then washed twice with 0.1% TFA in 5% methanol, centrifuged at 3,000 x g for 1 min at 4°C and the flow-through was discarded after each wash. The peptides were eluted by washing the column twice with 300 µL 0.1% TFA in 50% ACN, centrifuged for 3,000 x g for 1 min at 4°C and the eluate was pooled into a new low-bind microcentrifuge tube after each wash. The eluate was dried in the SpeedVac at 40°C.

3.3.11. Liquid chromatography (LC)-MS/MS analysis.

LC-MS/MS analysis was performed at the University of Victoria-Genome B.C. Proteomics Centre. All reagents were HPLC-MS grade. The two multiplexed samples for each tissue were run in the same batch to maintain consistency for comparisons within a tissue. The dried peptides were resuspended to 0.5 µg/µL in 2% ACN and 0.1% formic acid. A 2 µL aliquot was separated by on-line reversed phase LC at 300 nL/min over a 134 min gradient. The LC was coupled to an Orbitrap Fusion Tribrid mass spectrometer (Thermo Fisher Scientific) with a nano-electrospray ion source (Nanospray Flex NG source, Thermo Fisher Scientific). Data-dependent acquisition was scheduled every 3 s at least and the most intense ions with charge states 2-7 exceeding 50,000 counts were selected for HCD (higher energy collisional dissociation) fragmentation. Full MS details can be found in the Supplementary Materials.

3.3.12. R. catesbeiana proteome.

The proteome used in the present study was the predicted proteins from the most current *R. catesbeiana* genome assembly (version 4, DOI https://doi.org/10.5281/zenodo.8125199).

3.3.13. Data analysis.

The *.raw data files were converted to *.mzMl format using MSConvert (ProteoWizard version 3.0.22088) with the default peak picking filters (Chambers et al., 2012). The *.mzML spectral files were imported in FragPipe (Version 22.0) and a database search against the *R. catesbeiana* proteome was performed using MSFragger (Kong et al., 2017). The *in silico* digestion of the *R. catesbeiana* proteome was performed with up to four missed cleavages to account for lysine residues being blocked by the TMT labels. Mass calibration and parameter optimization was performed, the precursor and fragment mass tolerances were set to ±20 ppm, and the variable modifications included methionine oxidation, lysine and arginine mono-, di-, and tri-methylation, lysine acetylation, and lysine TMT. The peptide-spectrum matches were filtered to a 1% false discovery rate at the peptide and protein level using Percolator and ProteinProphet (da Veiga Leprevost et al., 2020; The et al., 2016). PTM site localization was performed by PTMProphet (Shteynberg et al., 2019). Intensity quantification was performed using IonQuant and TMT signal integration was done with TMT-Integrator (Yu et al., 2020a). Unique and razor-assigned peptides were used for quantification. Razor peptide assignment employs an “Occam’s razor” approach wherein shared peptides are assigned to proteins such that the smallest number of proteins can explain all detected

peptides. Since TMT-labeling was performed at the protein level, it was critical to set TMT-Integrator to allow “under-labeled” peptides for quantification, as a typical TMT workflow involves labeling tryptic peptides such that the newly generated N-termini are TMT-labeled. A virtual reference in TMT-Integrator was used for relative quantification. TMT-Integrator was used to perform intensity-based quantification and median-centering normalization at the protein level. Site-specific quantification was used for acetylation, and mono-, di-, and tri-methylation mass shifts. The data analysis steps were performed separately for each tissue within every temperature condition.

3.3.14. Statistical analysis.

The relative fold changes (RFC) of protein and PTM abundance were calculated by comparing the median intensity between the control and T_3-treated samples within each temperature condition. P-values were calculated using non-parametric Mann-Whitney U test and p-values ≤ 0.1 and an RFC ≥ 1.05 or RFC ≤ 0.95 were deemed significant. We chose to include the results with RFC values close to 1 because the tissues contain asynchronous, mixed cell types, potentially with diverse chromatin composition, and the exposure time to T_3 is relatively short. The results herein present a range of putative epigenetic changes during early TH induction.

3.4. Results and discussion

3.4.1. Conserved stoichiometry of histone proteins.

All acid-extracted protein samples were assessed using 15% SDS-PAGE to ascertain the quality of the histone proteins. All samples had well-resolved histone bands and were present in the expected equivalent stoichiometry (Rivera-Casas et al., 2017). Figure 8 shows representative samples of each tissue type.

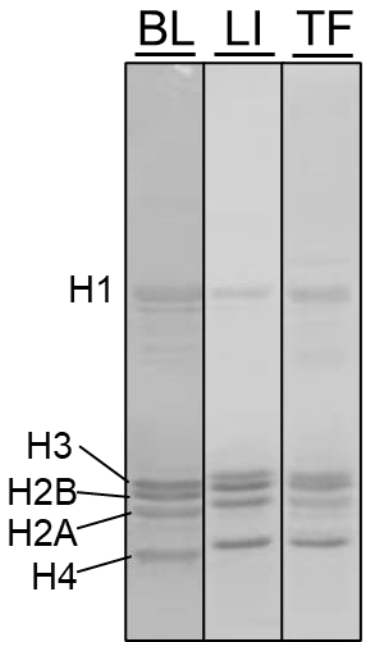

Figure 8. Representative SDS-PAGE of acid-extracted histones from control-treated tadpole blood (BL), liver (LI), and tailfin (TF) from the permissive temperature condition.

3.4.2. Acid-extraction enriched for histone proteins.

Overall, we identified 113 blood, 178 liver, and 192 tailfin proteins that mapped to the *R. catesbeiana* proteome (Table 7) within all temperature regimes. Only proteins

that were quantified in all samples of a given tissue were considered for statistical analysis, resulting in 73 blood, 109 liver, and 127 tailfin proteins that were evaluated for differential abundance (Table 7). We found that 98 ± 0.1%, 96 ± 0.5%, and 96 ± 0.3% of the combined signal from each multiplex was attributed to histone proteins in the blood, liver, and tailfin, respectively. These results suggest that the acid extraction successfully enriched the samples for highly basic proteins (Table 7).

Table 7. Proteins across all tissues predominantly mapped to histone proteins in the *R. catesbeiana* proteome. Median values and associated median absolute deviations (MADs) were calculated for all samples within a tissue.

Tissue	All proteins	All proteins consistently detected	Percent histones (%)
Blood	113	73	98 ± 0.1
Liver	178	109	96 ± 0.5
Tailfin	192	127	96 ± 0.3

3.4.3. Protein annotations.

As the *R. catesbeiana* proteome derived from version 4 of the genome assembly is not fully annotated, histone proteins and other chromatin-associated proteins of interest were aligned to the human proteome using BLASTP. These annotations were used in place of those from the *R. catesbeiana* proteome. In some instances, multiple proteins in the *R. catesbeiana* proteome aligned to the same human protein. These histones are herein distinguished by roman numerals. It has not been determined if these represent veritable histone subtypes found in *R. catesbeiana,* or if they are artefacts from the *in silico* translation of the genome into predicted protein products. The amino acid sequence alignments can be found in the supplementary materials (Supplementary figures S1-S20).

3.4.4. Tissue- and temperature-specific changes in the abundance histone and non-histone chromatin binding proteins following T_3 treatment.

For each protein that was consistently detected and quantified in all samples of a given tissue, the RFC was calculated by comparing the median intensity value of the control samples and T_3-treated samples. While many of the fold changes are modest, we sought to explore a broad range of potential chromatin-based changes. More information about the fold changes can be found in the Statistical Analysis section of the Materials and Methods.

Changes in histone and non-histone chromatin-associated protein abundance were observed in the blood, liver, and tailfin following T_3 treatment under the three temperature paradigms (Table 8). Each tissue had unique changes in protein abundance, and notably, we did not observe any changes in abundance that were common between the permissive and non-permissive paradigms of a given tissue (Table 8). These results suggest that chromatin-associated changes established following T_3 treatment are distinct under different temperature conditions and among tissues.

Under permissive temperatures, the liver had the greatest number of proteins change in abundance (Table 8). Furthermore, the liver was the only tissue with a significant change in histone abundance following T_3 treatment at the non-permissive temperature (Table 8), suggesting that the early, cold-temperature response to T_3 is distinct in the liver compared to the blood and tailfin.

Table 8. Relative fold changes (RFCs) and median absolute deviations of histone and non-histone chromatin-binding proteins in *R. catesbeiana* blood, liver and tailfin at following T_3 treatment under the permissive (24°C), non-permissive (5°C) and shifted (5→24°C) temperature regimes. Distinct protein entries from the *R. catesbeiana* proteome with identical protein annotations are differentiated by roman numerals. All indicated fold changes are statistically significant (p-value ≤ 0.1). Blue fields indicate a relative increase in abundance, yellow fields indicate a relative decrease in abundance, and grey fields indicate that the protein was not detected in at least one sample within that tissue. Non-significant RFCs are indicated by "n.s.".

Protein annotation	Blood			Liver			Tailfin		
	24°C	5°C	5→ 24°C	24°C	5°C	5→ 24°C	25°C	5°C	5→ 24°C
H1.0	1.2±0.06	n.s.	n.s.	1.2±0.05	n.s.	n.s.	1.3±0.1	n.s.	n.s.
H1.3 (i)	n.s.	n.s.	0.9±0.03	n.s.	n.s.	n.s.	n.s.	n.s.	n.s.
H1.3 (ii)	n.s.	n.s.	n.s.	n.s.	0.9±0.1	n.s.	n.s.	n.s.	n.s.
H1.3 (iii)	n.s.	n.s.	0.9±0.04	n.s.	0.9±0.05	n.s.	n.s.	n.s.	n.s.
macroH2A.1				0.9±0.03	n.s.	n.s.			
H2B type 1(ii)				1.1±0.01	n.s.	n.s.			
H3.2 (ii)	n.s.	n.s.	n.s.	0.9±0.1	n.s.	n.s.	n.s.	n.s.	n.s.
H3.3 (i)	n.s.	n.s.	n.s.	0.9±0.1	n.s.	n.s.	n.s.	n.s.	n.s.
MeCp2	0.9±0.04	n.s.	0.95±0.01	n.s.	n.s.	n.s.	1.2±0.01	n.s.	n.s.
HMGN3	n.s.	n.s.	n.s.	1.3±0.1	n.s.	n.s.	n.s.	n.s.	n.s.
HMGB2	n.s.	n.s.	n.s.	n.s.	0.7±0.1	n.s.	n.s.	n.s.	n.s.
HMGB3				n.s.	0.8±0.1	n.s.	n.s.	n.s.	n.s.

The H1 variant H1.0 can accumulate in terminally differentiated cells and associate with nucleolar domains (Mayor et al., 2015; Talbert and Henikoff, 2021). A 1995 study found that TH treatment resulted in gene transcription through the mouse H1.0 promoter in cell lines (Bauer-Hofmann and Alonso, 1995). In all three tissues under permissive temperature conditions, H1.0 increased in abundance following T_3 treatment by fold changes of 1.2 in blood and liver and 1.3 in the tailfin (Table 8). This was the only change in a chromatin-associated protein that was consistent across the three tissues, suggesting that an increase in H1.0 may be a result of TH induction under permissive temperatures. Further work is warranted to explore a connection between TH and H1.0 abundance.

H1.3 is a replication-dependent linker histone that is associated with heterochromatin (Talbert and Henikoff, 2021). Heterochromatin typically encompasses condensed chromatin regions that are refractory to transcription (Talbert and Henikoff, 2021). Two proteins annotated as H1.3 decreased in abundance by 0.9-fold in the blood under shifted temperatures, and by 0.9-fold in the liver and non-permissive condition (Table 8). These H1.3 subtypes differ from each other by approximately 10% of their amino acid sequences and some peptides cannot be ascribed to just one subtype, which may influence these results (Supplementary Figure S2). Overall, our data suggest that there is a temperature-specific decrease in H1.3 proteins in blood and liver following T_3 treatment. Considering the change in H1.0 abundance observed in all tissues only at permissive temperatures, more research is warranted to investigate the possible TH-driven changes in linker histone abundance.

Changes in the abundance of core histone proteins following T_3 treatment only occurred in the liver under permissive temperatures, wherein H2B type 1 increased by 1.1-fold, and H3.2, H3.3, and macroH2A.1 all decreased by 0.9-fold (Table 8). No significant changes in these proteins were observed in the liver under non-permissive or shifted temperature conditions, nor in the blood or tailfin (Table 8). This suggests that early TH signaling under non-permissive temperatures and the establishment of the molecular memory does not involve global changes in abundance of histones or chromatin-associated proteins in the blood, liver, or tailfin.

Methyl-CpG binding protein 2 (MeCP2) is a developmentally important chromatin-binding protein that binds methylated DNA and can serve to activate or repress gene transcription and influence chromatin structure through associations with

nucleosomes in place of linker histones (Ishibashi et al., 2008; Ortega-Alarcon et al., 2024; Thambirajah and Ausió, 2009). In the blood, MeCP2 decreased in abundance by 0.9-fold in permissive temperatures and by 0.95-fold in the shifted condition (Table 8). This was the only occurrence of a protein that changed in abundance in more than one temperature condition within a tissue, suggesting that reductions in MeCP2 may have a role in TH action in warm temperatures. MeCP2 increased in abundance by 1.2-fold in the tailfin only under permissive temperatures, indicating the tissue-specific differential expression of MeCP2 (Table 8).

High mobility group (HMG) proteins are chromatin-binding proteins involved in nuclear processes such as DNA repair, replication, and transcriptional regulation (Reeves, 2010). In the liver under non-permissive temperatures, HMG box proteins HMGB2 and HMGB3 decreased 0.7-fold and 0.8-fold, respectively, following T_3 treatment (Table 8). In mammals, both HMGB2 and HMGB3 are more abundant in stem cells and undifferentiated cells compared to other cell types and are typically associated with gene activation (Chikhirzhina et al., 2024; T. Starkova et al., 2023). HMG nucleosomal-binding domain-containing proteins (HMGN) are generally associated with transcriptional activation and can interact directly with liganded TRs *in vitro* (Amano et al., 2002; Reeves, 2010; T. Starkova et al., 2023). HMGN3 increased by 1.3-fold following T_3 treatment under permissive temperatures in the liver (Table 8). These results suggest that changes in the abundance of HMGB2 and HMGB3 may be involved in the early T_3 response at cold temperatures, while HMGN3 is potentially implicated in the T_3 response at permissive temperatures. Abundance changes in HMG proteins were

not detected in the blood or tailfin, again exemplifying the tissue-specific nature of these potential TH-driven chromatin-based changes.

3.4.5. Tissue- and temperature-specific changes in PTM abundance.

Histones and non-histone chromatin-binding proteins can be modified by PTMs that can affect DNA accessibility and nuclear factor binding. MS/MS can be used to identify the mass shifts caused by PTMs, which can be computationally localized to a particular amino acid. Temperature-specific PTM variations of histone and HMG proteins were observed in all three tissues following T_3 treatment (Table 9). The liver and tailfin, particularly under permissive conditions, had the most changes in PTM abundance while few were observed in the blood (Table 9). There were no PTM variations in common between the three tissues, highlighting the tissue-specific nature of TH action. Furthermore, there were no instances of a PTM increasing or decreasing in the same manner following T_3 treatment in more than one temperature condition, which emphasizes the importance of understanding the genomic contexts in which these changes are taking place.

3.4.5.1. H1 PTM variations.

H1 methylation is typically associated with transcriptional repression, and is posited to protect lysine residues from acetylation, which would otherwise lead to an increase in DNA accessibility (Andrés et al., 2020). In the liver under permissive temperatures, H1.3K108me2 increased by 1.2-fold following T_3 treatment (Table 9). Monomethylation of the equivalent lysine residue has been observed in mouse spleen;

however, functionality has not been ascribed to this PTM (Wiśniewski et al., 2007). Further investigation of this PTM and its putative modulation by TH is warranted.

Table 9. Relative fold changes (RFCs) and median absolute deviations of amino acid-localized PTMs histone and non-histone chromatin-binding proteins in *R. catesbeiana* blood, liver and tailfin at following T_3 treatment under the permissive (24°C), non-permissive (5°C) and shifted (5→24°C) temperature regimes. See Table 2 legend for full details. ac: acetylation; me: methylation; me2: dimethylation; me3: trimethylation.

Protein annotation	Residue	PTM	Blood			Liver			Tailfin		
			24°C	5°C	5→24°C	24°C	5°C	5→24°C	24°C	5°C	5→24°C
H1.3 (i)	K108	me2				1.2±0.1	n.s.	n.s.			
H3.2 (ii)	K18	ac	n.s.	n.s.	n.s.	n.s.	n.s.	0.9±0.02	n.s.	n.s.	1.1±0.1
	K23	ac	n.s.	n.s.	n.s.	n.s.	n.s.	n.s.	n.s.	n.s.	1.1±0.2
	K27	me2	n.s.	n.s.	n.s.	0.7±0.02	n.s.	n.s.	n.s.	n.s.	n.s.
	K27	me3	n.s.	n.s.	n.s.	0.8±0.06	n.s.	n.s.	n.s.	n.s.	n.s.
	K36	me2	n.s.	n.s.	n.s.	n.s.	n.s.	n.s.	n.s.	n.s.	1.1±0.05
	K36	me3	n.s.	n.s.	n.s.	0.9±0.07		n.s.	n.s.	n.s.	n.s.
	R40	me	n.s.	n.s.	n.s.	0.8±0.1	n.s.	n.s.	n.s.	1.1±0.04	n.s.
H4 (i)	K12	me3				n.s.	n.s.	1.1±0.02			
	K16	ac				n.s.	n.s.	1.1±0.01			
	K20	me2				1.1±0.07	n.s.	n.s.			
H4 (iii)	K20	me2	n.s.	n.s.	n.s.				0.5±0.1	n.s.	n.s.
H4 (vi)	K5	me3				n.s.	n.s.	n.s.	0.9±0.03	n.s.	n.s.
	K12	ac	n.s.	n.s.	n.s.				0.8±0.1	n.s.	n.s.
HMGB2	K123	me	n.s.	1.1±0.05	n.s.	n.s.	n.s.	n.s.	0.9±0.03	n.s.	n.s.
	K134	me3	n.s.	n.s.	n.s.	n.s.	0.8±0.08	n.s.			

3.4.5.2. H3 PTM variations.

Changes in the abundance of histone H3.2 PTMs were observed in the liver and tailfin, but not the blood. In the liver and tailfin, the PTMs established following T_3-treatment were distinct between the temperature paradigms. In the liver in permissive temperatures, there were decreases in H3.2K27me2, H3.2K27me3, and H3.2K36me3 of 0.7-fold, 0.8-fold, and 0.9-fold, respectively (Table 9). In the tailfin, there was a 1.1-fold increase in H3.2K36me2 (Table 9). H3K27me3 is a marker of facultative

heterochromatin, and both H3K27me3 and H3K27me2 are associated with transcriptionally repressed genomic regions (Laugesen et al., 2019; Millán-Zambrano et al., 2022). In contrast to H3K27 methylation, H3K36 di- and trimethylation are well characterized markers of actively transcribed genes (Millán-Zambrano et al., 2022). Taken together, these results indicate a potential TH-driven modulation of histone PTMs related to both transcriptional repression and activation under permissive temperatures. Identifying the genomic regions associated with these modified histones will help to uncover their possible roles in TH-mediated temperature-specific gene expression in the liver.

Histone acetylation is generally associated with transcriptional activation as the acetyl group neutralizes the negative charge of the lysine residue, thereby weakening the interaction between the histone and the DNA (Millán-Zambrano et al., 2022). In the liver under shifted temperatures, T_3 treatment resulted in a 0.9-fold decrease in H3.2K18ac (Table 9). In the tailfin under shifted temperatures, we observed a 1.1-fold increase in H3.2K18 and a 1.1-fold increase in K23 acetylation (Table 9). The abundance of a given histone PTM is governed by the balance of deposition and removal by histone modifying enzymes. Interestingly, H3K18 and H3K23 acetylation are deposited by the lysine acetyltransferase (KAT) p300/CREB-binding protein (CBP) (Henry et al., 2013), which is recruited to TH-responsive promoters through association with TH-liganded TRs (Paul et al., 2007). Conversely, lysine deacetylases (KDACs) associate with unliganded TRs (Jones et al., 2001), Further investigation could determine if the recruitment of KATs and KDACs to TRs corresponds with variations in these histone acetylation events. Changes in abundance in these PTMs were unique to

the shifted temperature paradigm of the liver and tailfin, suggesting that they may be involved in the accelerated response to T_3 under favourable conditions.

H3R40 monomethylation is involved in DNA binding by insertion into the minor groove (Armeev et al., 2021; Khan et al., 2023; Millan-Ariño et al., 2020). H3.2R40me1 decreased by 0.8-fold in the liver under permissive temperatures and increased by 1.1-fold in the tailfin at non-permissive temperatures (Table 9), suggesting that this PTM may be involved in TH action in a tissue- and temperature-specific manner.

3.4.5.3. H4 PTM variations.

There were three distinct H4 protein sequences detected in the present dataset. H4 (i) and H4 (iii) differ only by two amino acids in the N-terminal region (Supplementary Figure S15). H4 (vi) has an N-terminal sequence identical to that of human H4, but the rest of the sequence aligns to human H2B (Supplementary Figure S16). There were no peptides detected that span the H4-like sequence and the H2B-like sequence, suggesting that this sequence in the proteome is an artifactual combination of an H4 and H2B sequence. The PTMs identified on the N-terminus of this protein were therefore attributed to H4 (vi).

H4 PTM variations were observed in all three tissues. As with the previously discussed H3 acetylation, H4K12ac and H4K16ac are also deposited by p300/CBP (Henry et al., 2013). H4K12ac decreased in the tailfin following T_3 treatment under permissive temperatures (Table 9). H4K16ac increased by 1.1-fold in the liver under the shifted condition (Table 9). H4K16ac is associated with the disruption of higher-order chromatin structures by weakening inter-nucleosomal interactions (Zhang et al., 2016).

These data warrant further investigation into temperature- and tissue-specific p300/CBP recruitment following T_3 treatment.

H4K20me2 is associated with DNA replication and DNA repair (Kuo et al., 2012; Simonetta et al., 2018). Following T_3 treatment, H4K20me2 increased by 1.1-fold in permissive conditions in the liver, while in the tailfin, it decreased by 0.5-fold under the same temperature condition, suggesting tissue-specific regulation of this PTM (Table 9). We observed a 1.1-fold increase in H4K12me3 in the liver under shifted temperatures (Table 9). In tailfin, there was a 0.9-fold decrease in H4K5me3 under permissive temperatures (Table 9). Together, these results suggest tissue-specific regulation of histone H4 methylation following T_3 treatment under permissive and shifted temperature conditions.

3.4.5.4. HMG Protein PTM variations.

Methylation of high mobility group protein B2 (HMGB2) varied following T_3 treatment in the blood, liver, and tailfin. In the blood, HMGB2 K122me increased in the non-permissive temperature condition by 1.1-fold. In the liver under non-permissive conditions, there was a 0.8-fold decrease in HMGB2 K133me3, and in the tailfin under the permissive condition, HMGB2 K122me decreased by 0.9-fold (Table 9). These results suggest that HMGB2 methylation may be involved in early TH signaling under non-permissive temperatures in the blood and liver, but not in the tailfin. The HMGB2 sequence in the *R. catesbeiana* proteome lacks the N-terminal sequence of the human HMGB2 sequence, thus the human equivalent to bullfrog K122 is human K172 and bullfrog K133 is human K183 (Supplementary Figure S19). To our knowledge,

methylation of these human-equivalent (K172 and K133) HMGB2 sites has not been previously reported. Further study of these methylation events could uncover a novel HMGB2 function associated with TH-signaling.

3.5. Conclusion

To our knowledge, the work presented herein is the first non-targeted characterization of global changes of histones and non-histone chromatin-associated proteins during temperature-modulated T_3-induced amphibian metamorphosis. We identified histone PTMs and variants that are altered in a tissue- and temperature-specific manner. Further investigation of these proteins and PTMs, including determining their genomic localization, will be an important step in elucidating the involvement of epigenetic mechanisms in early TH-signaling and its temperature sensitivity.

The inhibition of metamorphosis at 5°C in the presence of TH separates the induction phase from the execution phase of TH-signaling, thereby creating an opportunity to investigate the early steps of TH action. Changes in the abundance and PTM of histone and chromatin-binding proteins that occur following T_3 treatment under non-permissive temperatures may be involved in early TH signaling events and the establishment of molecular memory. Under the non-permissive paradigm in the liver, we observed changes in the abundance of H1.3, HMGB2, HMGB3, and HMGB2 K133me3. There were also changes in abundance of HMGB2 K122me and H3.2R40me under the non-permissive paradigm in the blood and tailfin, respectively. These changes were only

observed at non-permissive temperatures, and their potential role in early TH signaling warrants further investigation.

While most fold changes presented herein are modest, we chose to include them due to the short TH exposure time, the potential for natural variation, and the use of tissues with mixed and asynchronous cell populations. Our findings broaden our understanding of potential epigenetic changes involved in the initial stages of TH signaling during metamorphosis and can inform future targeted inquiries of potential TH-driven epigenetic changes.

4. Conclusions and future directions

TH signaling is critical for the metabolism, growth and development of vertebrate species. Amphibian metamorphosis involves coordinated and tissue-specific TH-dependent developmental programs. Due to the conserved nature of TH signaling throughout vertebrates and the difficulties of studying mammalian development *in utero*, amphibian metamorphosis is a valuable model to study TH action and has led to many foundational discoveries. *R. catesbeiana* are a particularly exciting model species as cold temperature pauses metamorphosis and provides an opportunity to capture early responses to TH. These early TH-induced responses may also be involved in establishing the cold temperature molecular memory, which speaks to an intersection of environmental conditions and endocrine signaling.

Previous research has shown that epigenetic processes such as chromatin remodeling and histone modifications are involved in TH signaling during natural metamorphosis and TH-induced metamorphosis, as well as under different temperature conditions. These studies have used targeted methods such as ChIP which, while critical to understanding TH action, do not allow for novel discovery. Due to the diversity of tissue fates, the spatial and temporal regulation of gene expression, and the influence of environmental temperature, *R. catesbeiana* metamorphosis is uniquely positioned to study putative epigenetic factors of TH signaling. We therefore set out to perform the first unbiased MS/MS analysis of amphibian histones during natural and T_3-induced temperature-modulated metamorphosis.

This project required significant protocol development to isolate intact histones from amphibian tissues. Compared to mammalian nuclei, amphibian nuclei are significantly less stable and require buffers with different salt concentrations (Doyle et al., 1981), therefore previously published protocols for isolating mammalian cell nuclei for the purpose of histone analysis were not applicable. Further, performing bottom-up mass spectrometry of histone proteins has inherent complications. Due to the abundance of lysine and arginine residues in histone proteins, many peptides generated by trypsin cleavage are too small for effective MS analysis (Guo et al., 2022; Kuchaříková et al., 2021). One way to counteract this is to modify lysine residues prior to trypsin digestion to block cleavage at these sites, therefore producing longer peptides. In Chapter 1, this was done with TMA, while in Chapter 2 TMT tags were used upstream of protein digestion (Guo et al., 2022; Kuchaříková et al., 2021). Labeling the samples with TMT tags prior to trypsin digestion serves the dual purpose of blocking tryptic cleavage and allowing for sample multiplexing. Both methods have implications for downstream data analysis. For example, the addition of TMA modifications can significantly alter the actual retention time of a peptide compared to its theoretical retention time, which can impede the data analysis software. Labeling with TMT upstream of protein digestion means that only peptides with successfully labeled lysine residues can be quantified. Overall, the TMT labeling approach used in Chapter 2 offers advantages over the TMA method in Chapter 1. First, the ability to multiplex the samples allows for improved relative quantification and quantification of lower abundance peptides. Second, we can achieve amino acid-specific PTM localization through the TMT-Integrator software, which was not possible with the methodology used

in Chapter 1. However, to truly compare the two methods to assess their relative accuracy they would have to be applied to samples containing known amounts of histone proteins.

In Chapter 1, we observed tissue- and developmental stage-specific changes in histone abundance and PTMs during natural metamorphosis. We found changes in the abundance of the replication-independent histone variants H1.0, H1.10, H2AX,H2A.Z-2, and macroH2A (Table 2). These variants have identified roles in epigenetic regulation, but their potential involvement in TH-mediated development has not been explored. Additionally, we identified variations in the methylation, acetylation, and phosphorylation of peptides mapped to proteins in all five histone families (Table 3). Further work will be required to attempt to localize these PTMs to a single amino acid. Overall, our findings support the hypothesis that there are changes in the histone composition of *R. catesbeiana* tadpole tissues during natural metamorphosis. Further, most of the changes that we observed were specific to a tissue and/or developmental period. The distinct histone profiles of *R. catesbeiana* tissues throughout metamorphosis may be involved in THs ability to establish tissue-specific changes in gene expression required for a successful metamorphosis.

In Chapter 2, we used different temperature conditions to probe early TH action. The temperature-modulated T_3-induction experiment uncovered tissue- and temperature-specific variations in the abundance and PTM-state of histones and other chromatin-binding proteins. Changes that occurred following T_3 treatment under permissive temperatures were not observed to under non-permissive temperatures, suggesting that the epigenetic landscape induced by TH is temperature-specific (Table

8, Table 9). Changes in histone and non-histone chromatin-associated proteins following T_3 treatment at non-permissive temperatures may be involved early TH action and the establishment of molecular memory. Under cold temperature following T_3 treatment, we found an increase in HMGB2 K122me in the blood, decreases in H1.3, HMGB2 and HMGB3 protein levels and HMGB2 K133me in the liver, and an increase in H3R40me in the tailfin (Table 8, Table 9). Together, these results suggest that the early actions of TH at 5°C are tissue-specific. Overall, our findings support our hypothesis that there are temperature- and tissue-specific changes in histone and non-histone chromatin-associated proteins following T_3-treatment.

While the experiments conducted in Chapter 1 and Chapter 2 both assess the influence of TH, they represent two distinct scenarios, therefore it is not necessarily expected that the results will align. The metamorphosis model of Chapter 1 uses animals that have naturally been triggered to undergo metamorphosis through activation of the HPT axis, resulting in the secretion of T_4 into the blood stream and into target tissues. It is understood that there is crosstalk between TH and other developmental hormones, in part through common production pathways involving the hypothalamus and pituitary gland (Thambirajah et al., 2022). Additional hormonal influences may be present in the natural metamorphosis model that are not factors in the T_3-injected tadpoles studied in Chapter 2 due to the lack of HPT activation. Furthermore, the T_3-injected tadpoles were euthanized only 48 h post-injection in the permissive and non-permissive temperature regimes to study early TH action. Changes in histone abundance or PTMs observed in the natural metamorphosis model may take longer to be established, and therefore are not detected after only 48 h.

Interestingly, we observed an increase in abundance of H1.0 during natural metamorphosis and following T_3 injection at permissive temperatures in all three tissues (Table 2, Table 8). These results suggest that an increase in H1.0 may be involved in TH signaling during metamorphosis, which has not been previously reported. This is strongly supported by the fact that this change in abundance was observed in both experiments, as they represent distinct scenarios as discussed above. T_3 has been previously shown to induce transcription through the mouse H1.0 promoter in cell lines, which further supports a role for H1.0 in TH action among other vertebrates. Further study into the relationship between H1.0 and TH is warranted.

To begin to fully elucidate the epigenetic factors involved in TH signaling, it will be imperative to use targeted approaches such as ChIP sequencing to determine the genomic location of the changes in histone abundance and PTMs. Further, pairing ChIP assays with transcriptomics will assess if the epigenetic changes are associated with the modulation of transcription of TH-regulated genes. The ability to conduct ChIP experiments relies on the availability of an antibody specific to a histone variant or PTM, which is not always possible due to the high degree of sequence similarity between histone forms. This hinders the ability to directly assess the genomic localization of certain epigenetic marks in tissues. An alternative approach would be to use CRISPR-directed ChIP, wherein the CRISPR/Cas9 system can be engineered to associate with genomic regions of interest (e.g., TH-mediated gene regions) (Fujita and Fujii, 2013). ChIP is subsequently performed with an antibody against the enzymatically inactive Cas9 (Fujita and Fujii, 2013). The proteins associated with chromatin in this region can

then be analyzed by MS, negating any need for histone-specific antibodies (Fujita and Fujii, 2013).

One important future avenue for the work presented herein is to assess epigenetic effects of endocrine disrupting chemicals (EDCs). Amphibian species are particularly sensitive to perturbation by EDCs due to their reliance on proper TH signaling for a successful metamorphosis. Transcriptomic studies have used tadpoles as a model for studying perturbations by potential EDCs (Abbott and Helbing, 2021; Corrie et al., 2021; Veldhoen et al., 2006). Assessing changes in histone and non-histone chromatin-associated protein abundance and PTMs following exposure to a putative EDC could help discover novel EDCs and probe their modes of action. Given the conserved nature of TH signaling throughout vertebrate species, and the vast number of environmental contaminants with unknown impacts, this avenue of research could have large implications for human health.

The results presented herein expand our knowledge of putative epigenetic factors involved in TH-mediated development and provide a foundation for future studies to potentially uncover novel aspect TH signaling. Given the importance of TH signaling, it is critical to improve our understanding of its mode of action to better recognize means of disruption during disease or upon exposure to EDCs.

5. References

Abbott, E.A., Helbing, C.C., 2021. Sucralose affects thyroid hormone signaling in American bullfrog [*Rana* (*Lithobates*) *catesbeiana*] tadpoles. Arch. Environ. Contam. Toxicol. 80, 735–744. https://doi.org/10.1007/s00244-021-00838-y

Amano, T., Leu, K., Yoshizato, K., Shi, Y.-B., 2002. Thyroid hormone regulation of a transcriptional coactivator in *Xenopus laevis*: Implication for a role in postembryonic tissue remodeling. Dev. Dyn. 223, 526–535. https://doi.org/10.1002/dvdy.10075

Andrés, M., García-Gomis, D., Ponte, I., Suau, P., Roque, A., 2020. Histone H1 post-translational modifications: Update and future perspectives. Int. J. Mol. Sci. 21, 5941. https://doi.org/10.3390/ijms21165941

Armeev, G.A., Kniazeva, A.S., Komarova, G.A., Kirpichnikov, M.P., Shaytan, A.K., 2021. Histone dynamics mediate DNA unwrapping and sliding in nucleosomes. Nat. Commun. 12, 2387. https://doi.org/10.1038/s41467-021-22636-9

Ashley, H., Katti, P., Frieden, E., 1968. Urea excretion in the bullfrog tadpole: Effect of temperature, metamorphosis, and thyroid hormones. Dev. Biol. 17, 293–307. https://doi.org/10.1016/0012-1606(68)90066-3

Atkinson, B.G., Helbing, C., Chen, Y., 1996. 15 - Reprogramming of genes expressed in amphibian liver during metamorphosis, in: Gilbert, L.I., Tata, J.R., Atkinson, Burr G. (Eds.), Metamorphosis, Cell Biology. Academic Press, San Diego, pp. 539–566. https://doi.org/10.1016/B978-012283245-1/50017-8

Atlasi, Y., Stunnenberg, H.G., 2017. The interplay of epigenetic marks during stem cell differentiation and development. Nat. Rev. Genet. 18, 643–658. https://doi.org/10.1038/nrg.2017.57

Bannister, A.J., Kouzarides, T., 2011. Regulation of chromatin by histone modifications. Cell Res. 21, 381–395. https://doi.org/10.1038/cr.2011.22

Bauer-Hofmann, R., Alonso, A., 1995. Thyroid hormone receptors bind to the promoter of the mouse histone H1(0) gene and modulate its transcription. Nucleic Acids Res. 23, 5034–5040.

Bhushan, B., Michalopoulos, G.K., 2020. Role of epidermal growth factor receptor in liver injury and lipid metabolism: Emerging new roles for an old receptor. Chem. Biol. Interact. 324, 109090. https://doi.org/10.1016/j.cbi.2020.109090

Bianco, A.C., Kim, B.W., 2006. Deiodinases: implications of the local control of thyroid hormone action. J. Clin. Invest. 116, 2571–2579. https://doi.org/10.1172/JCI29812

Bilesimo, P., Jolivet, P., Alfama, G., Buisine, N., Mevel, S.L., Havis, E., Demeneix, B.A., Sachs, L.M., 2011. Specific histone lysine 4 methylation patterns define TR-binding capacity and differentiate direct T3 responses. Mol. Endocrinol. 25, 225–237. https://doi.org/10.1210/me.2010-0269

Bönisch, C., Hake, S.B., 2012. Histone H2A variants in nucleosomes and chromatin: more or less stable? Nucleic Acids Res. 40, 10719–10741. https://doi.org/10.1093/nar/gks865

Brent, G.A., 2012. Mechanisms of thyroid hormone action. J. Clin. Invest. 122, 3035–3043. https://doi.org/10.1172/JCI60047

Buchholz, D.R., 2015. More similar than you think: Frog metamorphosis as a model of human perinatal endocrinology. Dev. Biol., Modeling Human Development and Disease in Xenopus 408, 188–195. https://doi.org/10.1016/j.ydbio.2015.02.018

Buschbeck, M., Uribesalgo, I., Wibowo, I., Rué, P., Martin, D., Gutierrez, A., Morey, L., Guigó, R., López-Schier, H., Di Croce, L., 2009. The histone variant macroH2A is an epigenetic regulator of key developmental genes. Nat. Struct. Mol. Biol. 16, 1074–1079. https://doi.org/10.1038/nsmb.1665

Chadwick, B.P., Valley, C.M., Willard, H.F., 2001. Histone variant macroH2A contains two distinct macrochromatin domains capable of directing macroH2A to the inactive X chromosome. Nucleic Acids Res. 29, 2699–2705. https://doi.org/10.1093/nar/29.13.2699

Chambers, M.C., Maclean, B., Burke, R., Amodei, D., Ruderman, D.L., Neumann, S., Gatto, L., Fischer, B., Pratt, B., Egertson, J., Hoff, K., Kessner, D., Tasman, N., Shulman, N., Frewen, B., Baker, T.A., Brusniak, M.-Y., Paulse, C., Creasy, D., Flashner, L., Kani, K., Moulding, C., Seymour, S.L., Nuwaysir, L.M., Lefebvre, B., Kuhlmann, F., Roark, J., Rainer, P., Detlev, S., Hemenway, T., Huhmer, A., Langridge, J., Connolly, B., Chadick, T., Holly, K., Eckels, J., Deutsch, E.W., Moritz, R.L., Katz, J.E., Agus, D.B., MacCoss, M., Tabb, D.L., Mallick, P., 2012. A cross-platform toolkit for mass spectrometry and proteomics. Nat. Biotechnol. 30, 918–920. https://doi.org/10.1038/nbt.2377

Chikhirzhina, E., Tsimokha, A., Tomilin, A.N., Polyanichko, A., 2024. Structure and functions of HMGB3 protein. Int. J. Mol. Sci. 25, 7656. https://doi.org/10.3390/ijms25147656

Corrie, L.M., Kempe, M.N., Blajkevitch, O., Shang, D., Helbing, C.C., 2021. Dioctyl sodium sulfosuccinate as a potential endocrine disruptor of thyroid hormone activity in American bullfrog, *Rana* (*Lithobates*) *catesbeiana*, tadpoles. Arch. Environ. Contam. Toxicol. 80, 726–734.

Corrie, L.M., Kuecks-Winger, H., Ebrahimikondori, H., Birol, I., Helbing, C.C., 2024. Transcriptomic profiling of *Rana* [*Lithobates*] *catesbeiana* back skin during natural and thyroid hormone-induced metamorphosis under different temperature regimes with particular emphasis on innate immune system components. Comp. Biochem. Physiol. Part D Genomics Proteomics 50, 101238–101238. https://doi.org/10.1016/j.cbd.2024.101238

da Veiga Leprevost, F., Haynes, S.E., Avtonomov, D.M., Chang, H.-Y., Shanmugam, A.K., Mellacheruvu, D., Kong, A.T., Nesvizhskii, A.I., 2020. Philosopher: a versatile toolkit for shotgun proteomics data analysis. Nat. Methods 17, 869–870. https://doi.org/10.1038/s41592-020-0912-y

Damiano, F., Rochira, A., Gnoni, A., Siculella, L., 2017. Action of thyroid hormones, T3 and T2, on hepatic fatty acids: Differences in metabolic effects and molecular mechanisms. Int. J. Mol. Sci. 18, 744. https://doi.org/10.3390/ijms18040744

Das, B., Heimeier, R.A., Buchholz, D.R., Shi, Y.-B., 2009. Identification of direct thyroid hormone response genes reveals the earliest gene regulation programs during frog metamorphosis. J. Biol. Chem. 284, 34167–34178.

Davis, A.K., 2009. Metamorphosis-related changes in leukocyte profiles of larval bullfrogs (*Rana catesbeiana*). Comp. Clin. Pathol. 18, 181–186. https://doi.org/10.1007/s00580-008-0773-8

De Groef, B., Van der Geyten, S., Darras, V.M., Kühn, E.R., 2006. Role of corticotropin-releasing hormone as a thyrotropin-releasing factor in non-mammalian vertebrates. Gen. Comp. Endocrinol., Novel Functions of the Corticotropin-Releasing Factor System 146, 62–68. https://doi.org/10.1016/j.ygcen.2005.10.014

Dijkwel, Y., Tremethick, D.J., 2022. The role of the histone variant H2A.Z in metazoan development. J. Dev. Biol. 10, 28. https://doi.org/10.3390/jdb10030028

Dorn, A.R., Broyles, R.H., 1982. Erythrocyte differentiation during the metamorphic hemoglobin switch of *Rana catesbeiana*. Proc. Natl. Acad. Sci. 79, 5592–5596. https://doi.org/10.1073/pnas.79.18.5592

Doyle, M.J., Price, M.P., Frieden, E., 1981. Stabilization of amphibian and mammalian liver nuclei by zinc and other metal ions. Comp. Biochem. Physiol. Part C Comp. Pharmacol. 68, 115–120. https://doi.org/10.1016/0306-4492(81)90004-6

Faszewski, E.E., Tyrell, A., Guin, S., Kaltenbach, J.C., 2008. Metamorphic changes in localization of sugars in skin of the leopard frog, Rana pipiens. J. Morphol. 269, 998–1007. https://doi.org/10.1002/jmor.10639

Field, E.M., Corrie, L.M., Kuecks-Winger, H.N., Helbing, C.C., 2024. Utilization of temperature-mediated activation of thyroid hormone-induced molecular memory to evaluate early signaling events in the olfactory epithelium of *Rana [Lithobates] catesbeiana* tadpoles. Comp. Biochem. Physiol. Part D Genomics Proteomics 49, 101189. https://doi.org/10.1016/j.cbd.2024.101189

Frieden, E., Wahlborg, A., Howard, E., 1965. Temperature control of the response of tadpoles to triiodothyronine. Nature 205, 1173–1176. https://doi.org/10.1038/2051173a0

Fu, L., Yin, J., Shi, Y.-B., 2019. Involvement of epigenetic modifications in thyroid hormone-dependent formation of adult intestinal stem cells during amphibian metamorphosis. Gen. Comp. Endocrinol. 271, 91–96. https://doi.org/10.1016/j.ygcen.2018.11.012

Fujita, T., Fujii, H., 2013. Efficient isolation of specific genomic regions and identification of associated proteins by engineered DNA-binding molecule-mediated chromatin immunoprecipitation (enChIP) using CRISPR. Biochem. Biophys. Res. Commun. 439, 132–136. https://doi.org/10.1016/j.bbrc.2013.08.013

Garcia, B.A., Thomas, C.E., Kelleher, N.L., Mizzen, C.A., 2008. Tissue-specific expression and post-translational modification of histone H3 variants. J. Proteome Res. 7, 4225–4236. https://doi.org/10.1021/pr800044q

Gaspar-Maia, A., Qadeer, Z.A., Hasson, D., Ratnakumar, K., Adrian Leu, N., Leroy, G., Liu, S., Costanzi, C., Valle-Garcia, D., Schaniel, C., Lemischka, I., Garcia, B., Pehrson, J.R., Bernstein, E., 2013. MacroH2A histone variants act as a barrier upon reprogramming towards pluripotency. Nat. Commun. 4, 1565. https://doi.org/10.1038/ncomms2582

Gévry, N., Hardy, S., Jacques, P.-É., Laflamme, L., Svotelis, A., Robert, F., Gaudreau, L., 2009. Histone H2A.Z is essential for estrogen receptor signaling. Genes Dev. 23, 1522–1533. https://doi.org/10.1101/gad.1787109

Giammanco, M., Di Liegro, C.M., Schiera, G., Di Liegro, I., 2020. Genomic and non-genomic mechanisms of action of thyroid hormones and their catabolite 3,5-diiodo-L-thyronine in mammals. Int. J. Mol. Sci. 21, 4140. https://doi.org/10.3390/ijms21114140

Gilbert, L.I., Tata, J.R., Atkinson, B.G., 1996. Metamorphosis: postembryonic reprogramming of gene expression in amphibian and insect cells, Cell biology. San Diego.

Glass, C.K., Rosenfeld, M.G., 2000. The coregulator exchange in transcriptional functions of nuclear receptors. Genes Dev. 14, 121–141. https://doi.org/10.1101/gad.14.2.121

Graves, H.K., Wang, P., Lagarde, M., Chen, Z., Tyler, J.K., 2016. Mutations that prevent or mimic persistent post-translational modifications of the histone H3 globular domain cause lethality and growth defects in *Drosophila*. Epigenetics Chromatin 9, 9. https://doi.org/10.1186/s13072-016-0059-3

Grimaldi, A., Buisine, N., Miller, T., Shi, Y.-B., Sachs, L.M., 2013. Mechanisms of thyroid hormone receptor action during development: Lessons from amphibian studies. Biochim. Biophys. Acta BBA - Gen. Subj., Thyroid hormone signalling 1830, 3882–3892. https://doi.org/10.1016/j.bbagen.2012.04.020

Gudernatsch, J.F., 1912. Feeding experiments on tadpoles. Arch. Für Entwicklungsmechanik Org. 35, 457–483. https://doi.org/10.1007/BF02277051

Guo, Y., Yu, D., Cupp-Sutton, K.A., Liu, X., Wu, S., 2022. Optimization of protein-level tandem mass tag (TMT) labeling conditions in complex samples with top-down

proteomics. Anal. Chim. Acta 1221, 340037–340037. https://doi.org/10.1016/j.aca.2022.340037

Hammond, S.A., Jackman, K.W., Partovi, S.H., Veldhoen, N., Helbing, C.C., 2016. Identification of organ-autonomous constituents of the molecular memory conferred by thyroid hormone exposure in cold temperature-arrested metamorphosing *Rana* (*Lithobates*) *catesbeiana* tadpoles. Comp. Biochem. Physiol. Part D Genomics Proteomics 17, 58–65. https://doi.org/10.1016/j.cbd.2016.01.002

Hammond, S.A., Veldhoen, N., Helbing, C.C., 2015. Influence of temperature on thyroid hormone signaling and endocrine disruptor action in *Rana* (*Lithobates*) *catesbeiana* tadpoles. Gen. Comp. Endocrinol. 219, 6–15. https://doi.org/10.1016/j.ygcen.2014.12.001

Hasebe, T., Oshima, H., Kawamura, K., Kikuyama, S., 1999. Rapid and selective removal of larval erythrocytes from systemic circulation during metamorphosis of the bullfrog, Rana catesbeiana. Dev. Growth Differ. 41, 639–643. https://doi.org/10.1046/j.1440-169x.1999.00461.x

Havis, E., Sachs, L.M., Demeneix, B.A., 2003. Metamorphic T3-response genes have specific co-regulator requirements. EMBO Rep. 4, 883–888. https://doi.org/10.1038/sj.embor.embor908

Helbing, C., Gergely, G., Atkinson, B.G., 1992. Sequential up-regulation of thyroid hormone β receptor, ornithine transcarbamylase, and carbamyl phosphate synthetase mRNAs in the liver of *Rana catesbeiana* tadpoles during

spontaneous and thyroid hormone-induced metamorphosis. Dev. Genet. 13, 289–301. https://doi.org/10.1002/dvg.1020130406

Helbing, C.C., Maher, S.K., Han, J., Gunderson, M.P., Borchers, C., 2010. Peering into molecular mechanisms of action with frogSCOPE. Gen. Comp. Endocrinol., Amphibian Endocrinology 2010 168, 190–198. https://doi.org/10.1016/j.ygcen.2010.01.012

Helbing, C.C., Wagner, M.J., Pettem, K., Johnston, J., Heimeier, R.A., Veldhoen, N., Jirik, F.R., Shi, Y.-B., Browder, L.W., 2011. Modulation of thyroid hormone-dependent gene expression in *Xenopus laevis* by INhibitor of Growth (ING) proteins. PLoS ONE 6, e28658. https://doi.org/10.1371/journal.pone.0028658

Henikoff, S., Smith, M.M., 2015. Histone variants and epigenetics. Cold Spring Harb. Perspect. Biol. 7, a019364. https://doi.org/10.1101/cshperspect.a019364

Henry, R.A., Kuo, Y.-M., Andrews, A.J., 2013. Differences in specificity and selectivity between CBP and p300 acetylation of histone H3 and H3/H4. Biochemistry 52, 5746–5759. https://doi.org/10.1021/bi400684q

Hsia, S.-C.V., Shi, Y.-B., 2002. Chromatin disruption and histone acetylation in regulation of the human immunodeficiency virus type 1 long terminal repeat by thyroid hormone receptor. Mol. Cell. Biol. 22, 4043–4052. https://doi.org/10.1128/MCB.22.12.4043-4052.2002

Ishibashi, T., Thambirajah, A.A., Ausió, J., 2008. MeCP2 preferentially binds to methylated linker DNA in the absence of the terminal tail of histone H3 and independently of histone acetylation. FEBS Lett. 582, 1157–1162. https://doi.org/10.1016/j.febslet.2008.03.005

Ishihara, A., Sapon, M.A., Yamauchi, K., 2019. Seasonal acclimatization and thermal acclimation induce global histone epigenetic changes in liver of bullfrog (*Lithobates catesbeianus*) tadpole. Comp. Biochem. Physiol. A. Mol. Integr. Physiol. 230, 39–48. https://doi.org/10.1016/j.cbpa.2018.12.014

Ishihara, A., Yamauchi, K., 2019. Analysis of global and gene-specific acetylation of histones in the liver of American bullfrog (*Rana catesbeiana*) tadpoles acclimated to low temperature. J. Therm. Biol. 84, 488–495. https://doi.org/10.1016/j.jtherbio.2019.08.002

Ishizuka, T., Lazar, M.A., 2003. The N-CoR/histone deacetylase 3 complex is required for repression by thyroid hormone receptor. Mol. Cell. Biol. 23, 5122–5131. https://doi.org/10.1128/mcb.23.15.5122-5131.2003

Izzo, A., Schneider, R., 2016. The role of linker histone H1 modifications in the regulation of gene expression and chromatin dynamics. Biochim. Biophys. Acta BBA - Gene Regul. Mech., Histone H1 in gene expression and development 1859, 486–495. https://doi.org/10.1016/j.bbagrm.2015.09.003

Izzo, A., Ziegler-Birling, C., Hill, P.W.S., Brondani, L., Hajkova, P., Torres-Padilla, M.-E., Schneider, R., 2017. Dynamic changes in H1 subtype composition during epigenetic reprogramming. J. Cell Biol. 216, 3017–3028. https://doi.org/10.1083/jcb.201611012

Jackman, S.H., Evans, E.P., Kuecks-Winger, H.N., Corrie, L.M., Imbery, J.J., Miliano, R.C., Robert, B.J., Thompson, V.C., Thambirajah, A.A., Lesperance, M.L., Pyle, G.G., van Aggelen, G., Helbing, C.C., 2022. Comparison of transcriptome responses of the liver, tail fin, and olfactory epithelium of *Rana* [*Lithobates*]

catesbeiana tadpoles disrupted by thyroid hormones and estrogen. Aquat. Toxicol. 253, 106344. https://doi.org/10.1016/j.aquatox.2022.106344

Jansen, A., Verstrepen, K.J., 2011. Nucleosome positioning in *Saccharomyces cerevisiae*. Microbiol. Mol. Biol. Rev. MMBR 75, 301–320. https://doi.org/10.1128/MMBR.00046-10

Jones, P.L., Sachs, L.M., Rouse, N., Wade, P.A., Shi, Y.-B., 2001. Multiple N-CoR complexes contain distinct histone deacetylases. J. Biol. Chem. 276, 8807–8811. https://doi.org/10.1074/jbc.C000879200

Jørgensen, S., Schotta, G., Sørensen, C.S., 2013. Histone H4 Lysine 20 methylation: key player in epigenetic regulation of genomic integrity. Nucleic Acids Res. 41, 2797–2806. https://doi.org/10.1093/nar/gkt012

Joseph, F.M., Young, N.L., 2023. Histone variant-specific post-translational modifications. Semin. Cell Dev. Biol., Special Issue: Histone variants by Frédéric Berger 135, 73–84. https://doi.org/10.1016/j.semcdb.2022.02.012

Kaltenbach, J.C., Faszewski, E.E., Nytch, K.E., Potter, C.H., Shanthakumar, N., Fakin, A., 2004. Glycoconjugate localization in larval and adult skin of the bullfrog, Rana catesbeiana: A lectin histochemical study. J. Morphol. 261, 184–195. https://doi.org/10.1002/jmor.10237

Khan, T., Iftikhar, F., Akhlaq, R., Musharraf, S.G., Ali, A., 2023. Acidotic and hypoxic tumor microenvironment induces changes to histone acetylation and methylation in oral squamous cell carcinoma. Biomed. Chromatogr. 37, e5616. https://doi.org/10.1002/bmc.5616

Koide, E.M., Abbott, E.A., Helbing, C.C., 2022. Uncovering early thyroid hormone signalling events through temperature-mediated activation of molecular memory in the cultured bullfrog tadpole tail fin. Gen. Comp. Endocrinol. 323–324, 114047. https://doi.org/10.1016/j.ygcen.2022.114047

Kong, A.T., Leprevost, F.V., Avtonomov, D.M., Mellacheruvu, D., Nesvizhskii, A.I., 2017. MSFragger: ultrafast and comprehensive peptide identification in mass spectrometry–based proteomics. Nat. Methods 14, 513–520. https://doi.org/10.1038/nmeth.4256

Kornberg, R.D., Thomas, J.O., 1974. Chromatin structure: Oligomers of the histones. Sci. Am. Assoc. Adv. Sci. 184, 865–868. https://doi.org/10.1126/science.184.4139.865

Kuchaříková, H., Dobrovolná, P., Lochmanová, G., Zdráhal, Z., 2021. Trimethylacetic anhydride–based derivatization facilitates quantification of histone marks at the MS1 level. Mol. Cell. Proteomics 20, 100114. https://doi.org/10.1016/j.mcpro.2021.100114

Kuo, A.J., Song, J., Cheung, P., Ishibe-Murakami, S., Yamazoe, S., Chen, J.K., Patel, D.J., Gozani, O., 2012. The BAH domain of ORC1 links H4K20me2 to DNA replication licensing and Meier–Gorlin syndrome. Nature 484, 115–119. https://doi.org/10.1038/nature10956

Lal, A., Pan, Y., Navarro, F., Dykxhoorn, D.M., Moreau, L., Meire, E., Bentwich, Z., Lieberman, J., Chowdhury, D., 2009. miR-24–mediated downregulation of H2AX suppresses DNA repair in terminally differentiated blood cells. Nat. Struct. Mol. Biol. 16, 492–498. https://doi.org/10.1038/nsmb.1589

Laugesen, A., Højfeldt, J.W., Helin, K., 2019. Molecular mechanisms directing PRC2 recruitment and H3K27 methylation. Mol. Cell 74, 8–18. https://doi.org/10.1016/j.molcel.2019.03.011

Li, J., Lin, Q., Yoon, H.-G., Huang, Z.-Q., Strahl, B.D., Allis, C.D., Wong, J., 2002. Involvement of histone methylation and phosphorylation in regulation of transcription by thyroid hormone receptor. Mol. Cell. Biol. 22, 5688–5697. https://doi.org/10.1128/mcb.22.16.5688-5697.2002

Li, J., O'Malley, B.W., Wong, J., 2000. p300 requires its histone acetyltransferase activity and SRC-1 interaction domain to facilitate thyroid hormone receptor activation in chromatin. Mol. Cell. Biol. 20, 2031–2042.

Li, S., Wei, T., Panchenko, A.R., 2023. Histone variant H2A.Z modulates nucleosome dynamics to promote DNA accessibility. Nat. Commun. 14, 769. https://doi.org/10.1038/s41467-023-36465-5

Lin, H.-Y., Tang, H.-Y., Leinung, M., Mousa, S.A., Hercbergs, A., Davis, P.J., 2019. Action of reverse T3 on cancer cells. Endocr. Res. 44, 148–152. https://doi.org/10.1080/07435800.2019.1600536

Litwack, G., 2012. Biochemical actions of hormones V1. Elsevier.

Lu, C., Coradin, M., Porter, E.G., Garcia, B.A., 2021. Accelerating the field of epigenetic histone modification through mass spectrometry–based approaches. Mol. Cell. Proteomics 20, 100006. https://doi.org/10.1074/mcp.r120.002257

Luehr, T.C., Koide, E.M., Wang, X., Han, J., Borchers, C.H., Helbing, C.C., 2018. Metabolomic insights into the effects of thyroid hormone on *Rana* [*Lithobates*] *catesbeiana* metamorphosis using whole-body matrix assisted laser

desorption/ionization-mass spectrometry imaging (MALDI-MSI). Gen. Comp. Endocrinol. 265, 237–245. https://doi.org/10.1016/j.ygcen.2018.02.012

Luger, K., Dechassa, M.L., Tremethick, D.J., 2012. New insights into nucleosome and chromatin structure: an ordered state or a disordered affair? Nat. Rev. Mol. Cell Biol. 13, 436–447. https://doi.org/10.1038/nrm3382

Luger, K., Mäder, A.W., Richmond, R.K., Sargent, D.F., Richmond, T.J., 1997. Crystal structure of the nucleosome core particle at 2.8 A resolution. Nature 389, 251–260. https://doi.org/10.1038/38444

Maehara, K., Harada, A., Sato, Y., Matsumoto, M., Nakayama, K.I., Kimura, H., Ohkawa, Y., 2015. Tissue-specific expression of histone H3 variants diversified after species separation. Epigenetics Chromatin 8, 35. https://doi.org/10.1186/s13072-015-0027-3

Maher, S.K., Wojnarowicz, P., Ichu, T.-A., Veldhoen, N., Lu, L., Lesperance, M., Propper, C.R., Helbing, C.C., 2016. Rethinking the biological relationships of the thyroid hormones, l-thyroxine and 3,5,3′-triiodothyronine. Comp. Biochem. Physiol. Part D Genomics Proteomics 18, 44–53. https://doi.org/10.1016/j.cbd.2016.04.002

Martire, S., Banaszynski, L.A., 2020. The roles of histone variants in fine-tuning chromatin organization and function. Nat. Rev. Mol. Cell Biol. 21, 522–541. https://doi.org/10.1038/s41580-020-0262-8

Matsuda, H., Paul, B.D., Choi, C.Y., Hasebe, T., Shi, Y.-B., 2009. Novel functions of protein arginine methyltransferase 1 in thyroid hormone receptor-mediated transcription and in the regulation of metamorphic rate in *Xenopus laevis*. Mol. Cell. Biol. 29, 745–757. https://doi.org/10.1128/MCB.00827-08

Matsuura, K., Fujimoto, K., Das, B., Fu, L., Lu, C.D., Shi, Y.-B., 2012a. Histone H3K79 methyltransferase Dot1L is directly activated by thyroid hormone receptor during *Xenopus* metamorphosis 2, 25. https://doi.org/10.1186/2045-3701-2-25

Matsuura, K., Fujimoto, K., Fu, L., Shi, Y.-B., 2012b. Liganded thyroid hormone receptor induces nucleosome removal and histone modifications to activate transcription during larval intestinal cell death and adult stem cell development. Endocrinology 153, 961–972. https://doi.org/10.1210/en.2011-1736

Mayor, R., Izquierdo-Bouldstridge, A., Millán-Ariño, L., Bustillos, A., Sampaio, C., Luque, N., Jordan, A., 2015. Genome distribution of replication-independent histone H1 variants shows H1.0 associated with nucleolar domains and H1X associated with RNA polymerase II-enriched regions. J. Biol. Chem. 290, 7474–7491. https://doi.org/10.1074/jbc.M114.617324

Millan-Ariño, L., Yuan, Z.-F., Oomen, M.E., Brandenburg, S., Chernobrovkin, A., Salignon, J., Körner, L., Zubarev, R.A., Garcia, B.A., Riedel, C.G., 2020. Histone purification combined with high-resolution mass spectrometry to examine histone post-translational modifications and histone variants in *Caenorhabditis elegans*. Curr. Protoc. Protein Sci. 102. https://doi.org/10.1002/cpps.114

Millán-Zambrano, G., Burton, A., Bannister, A.J., Schneider, R., 2022. Histone post-translational modifications — cause and consequence of genome function. Nat. Rev. Genet. 23, 563–580. https://doi.org/10.1038/s41576-022-00468-7

Mochizuki, K., Goda, T., Yamauchi, K., 2012a. Gene expression profile in the liver of *Rana catesbeiana* tadpoles exposed to low temperature in the presence of

thyroid hormone. Biochem. Biophys. Res. Commun. 420, 845–850. https://doi.org/10.1016/j.bbrc.2012.03.085

Mochizuki, K., Goda, T., Yamauchi, K., 2012b. Gene expression profile in the liver of *Rana catesbeiana* tadpoles exposed to low temperature in the presence of thyroid hormone. Biochem. Biophys. Res. Commun. 420, 845–850. https://doi.org/10.1016/j.bbrc.2012.03.085

Moeller, L.C., Dumitrescu, A.M., Refetoff, S., 2005. Cytosolic action of thyroid hormone leads to induction of hypoxia-inducible factor-1α and glycolytic genes. Mol. Endocrinol. 19, 2955–2963. https://doi.org/10.1210/me.2004-0542

Monteiro, F.L., Vitorino, R., Wang, J., Cardoso, H., Laranjeira, H., Simões, J., Caldas, M., Henrique, R., Amado, F., Williams, C., Jerónimo, C., Helguero, L.A., 2017. The histone H2A isoform Hist2h2ac is a novel regulator of proliferation and epithelial-mesenchymal transition in mammary epithelial and in breast cancer cells. Cancer Lett. 396, 42–52. https://doi.org/10.1016/j.canlet.2017.03.007

Morris, S.M., Cole, R.D., 1980. Thyroxine stimulation of tadpole liver histone phosphorylation *in vivo*. Dev. Biol. 74, 379–386. https://doi.org/10.1016/0012-1606(80)90439-X

Mukhi, S., Cai, L., Brown, D.D., 2010. Gene switching at *Xenopus laevis* metamorphosis. Dev. Biol. 338, 117–126. https://doi.org/10.1016/j.ydbio.2009.10.041

Munro, A.F., 1953. The ammonia and urea excretion of different species of Amphibia during their development and metamorphosis. Biochem. J. 54, 29–36. https://doi.org/10.1042/bj0540029

Murata, T., Yamauchi, K., 2005. Low-temperature arrest of the triiodothyronine-dependent transcription in *Rana catesbeiana* red blood cells 146, 256–264. https://doi.org/10.1210/en.2004-1090

Nanduri, R., Furusawa, T., Bustin, M., 2020. Biological functions of HMGN chromosomal proteins. Int. J. Mol. Sci. 21, 449. https://doi.org/10.3390/ijms21020449

Narita, T., Higashijima, Y., Kilic, S., Liebner, T., Walter, J., Choudhary, C., 2023. Acetylation of histone H2B marks active enhancers and predicts CBP/p300 target genes. Nat. Genet. 55, 679–692. https://doi.org/10.1038/s41588-023-01348-4

North, J.A., Javaid, S., Ferdinand, M.B., Chatterjee, N., Picking, J.W., Shoffner, M., Nakkula, R.J., Bartholomew, B., Ottesen, J.J., Fishel, R., Poirier, M.G., 2011. Phosphorylation of histone H3(T118) alters nucleosome dynamics and remodeling. Nucleic Acids Res. 39, 6465–6474. https://doi.org/10.1093/nar/gkr304

Nussey, Stephen., Whitehead, S.A., 2001. Endocrinology : an integrated approach. Bios, Oxford.

Ortega-Alarcon, D., Claveria-Gimeno, R., Vega, S., Kalani, L., Jorge-Torres, O.C., Esteller, M., Ausio, J., Abian, O., Velazquez-Campoy, A., 2024. Extending MeCP2 interactome: canonical nucleosomal histones interact with MeCP2. Nucleic Acids Res. 52, 3636–3653. https://doi.org/10.1093/nar/gkae051

Oudet, P., Gross-Bellard, M., Chambon, P., 1975. Electron microscopic and biochemical evidence that chromatin structure is a repeating unit. Cell 4, 281–300. https://doi.org/10.1016/0092-8674(75)90149-X

Paul, B.D., Buchholz, D.R., Fu, L., Shi, Y.-B., 2007. SRC-p300 coactivator complex is required for thyroid hormone-induced amphibian metamorphosis. J. Biol. Chem. 282, 7472–7481. https://doi.org/10.1074/jbc.m607589200

Paul, B.D., Shi, Y.-B., 2003. Distinct expression profiles of transcriptional coactivators for thyroid hormone receptors during *Xenopus laevis* metamorphosis. Cell Res. 13, 459–464. https://doi.org/10.1038/sj.cr.7290188

Postnikov, Y.V., Bustin, M., 2016. Functional interplay between histone H1 and HMG proteins in chromatin. Biochim. Biophys. ACTA-GENE Regul. Mech. 1859, 462–467. https://doi.org/10.1016/j.bbagrm.2015.10.006

Poulson, R., Jackman, S.H., Hansen, M., Helbing, C.C., 2023. Relationship between serum thyroid hormones and their associated metabolites, and gene expression bioindicators in the back skin of *Rana* [*Lithobates*] *catesbeiana* tadpoles and frogs during metamorphosis. Front. Endocrinol. 13, 1103051. https://doi.org/10.3389/fendo.2022.1103051

Præstholm, S.M., Siersbæk, M.S., Nielsen, R., Zhu, X., Hollenberg, A.N., Cheng, S.-Y., Grøntved, L., 2020. Multiple mechanisms regulate H3 acetylation of enhancers in response to thyroid hormone. PLOS Genet. 16, e1008770. https://doi.org/10.1371/journal.pgen.1008770

Reeves, R., 2010. Nuclear functions of the HMG proteins. Biochim. Biophys. Acta Gene Regul. Mech. 1799, 3–14. https://doi.org/10.1016/j.bbagrm.2009.09.001

Reyes, A.A., Marcum, R.D., He, Y., 2021. Structure and function of chromatin remodelers. J. Mol. Biol. 433, 166929–166929. https://doi.org/10.1016/j.jmb.2021.166929

Rivera-Casas, C., Gonzalez-Romero, R., Garduño, R.A., Cheema, M.S., Ausio, J., Eirin-Lopez, J.M., 2017. Molecular and biochemical methods useful for the epigenetic characterization of chromatin-associated proteins in bivalve molluscs. Front. Physiol. 8, 490. https://doi.org/10.3389/fphys.2017.00490

Row, J.R., Donaldson, M.E., Longhi, J.N., Saville, B.J., Murray, D.L., 2016. Tissue-specific transcriptome characterization for developing tadpoles of the northern leopard frog (*Lithobates pipiens*). Genomics 108, 232–240. https://doi.org/10.1016/j.ygeno.2016.10.002

Sachs, L.M., Amano, T., Rouse, N., Shi, Y.-B., 2001a. Involvement of histone deacetylase at two distinct steps in gene regulation during intestinal development in *Xenopus laevis*. Dev. Dyn. 222, 280–291. https://doi.org/10.1002/dvdy.1195

Sachs, L.M., Amano, T., Shi, Y.-B., 2001b. An essential role of histone deacetylases in postembryonic organ transformations in *Xenopus laevis*. Int. J. Mol. Med. 8, 595–601. https://doi.org/10.3892/ijmm.8.6.595

Sachs, L.M., Buchholz, D.R., 2017. Frogs model man: *In vivo* thyroid hormone signaling during development. genesis 55, e23000. https://doi.org/10.1002/dvg.23000

Sachs, L.M., Damjanovski, S., Jones, P.L., Li, Q., Amano, T., Ueda, S., Shi, Y.-B., Ishizuya-Oka, A., 2000. Dual functions of thyroid hormone receptors during *Xenopus* development. Comp. Biochem. Physiol. B Biochem. Mol. Biol. 126, 199–211. https://doi.org/10.1016/S0305-0491(00)00198-X

Sachs, L.M., Jones, P.L., Havis, E., Rouse, N., Demeneix, B.A., Shi, Y.-B., 2002. Nuclear receptor corepressor recruitment by unliganded thyroid hormone

receptor in gene repression during *Xenopus laevis* Development. Mol. Cell. Biol. 22, 8527–8538. https://doi.org/10.1128/MCB.22.24.8527-8538.2002

Sachs, L.M., Shi, Y.-B., 2000. Targeted chromatin binding and histone acetylation in vivo by thyroid hormone receptor during amphibian development. Proc. Natl. Acad. Sci. U. S. A. 97, 13138–13143. https://doi.org/10.1073/pnas.260141297

Shi, Y.-B., 2000. Amphibian metamorphosis: from morphology to molecular biology. Wiley-Liss, New York.

Shi, Y.-B., Brown, D.D., 1993. The earliest changes in gene expression in tadpole intestine induced by thyroid hormone. J. Biol. Chem. 268, 20312–20317.

Shi, Y.-B., Matsuura, K., Fujimoto, K., Wen, L., Fu, L., 2012. Thyroid hormone receptor actions on transcription in amphibia: The roles of histone modification and chromatin disruption. Cell Biosci. 2, 1–10. https://doi.org/10.1186/2045-3701-2-42

Shteynberg, D.D., Deutsch, E.W., Campbell, D.S., Hoopmann, M.R., Kusebauch, U., Lee, D., Mendoza, L., Midha, M.K., Sun, Z., Whetton, A.D., Moritz, R.L., 2019. PTMProphet: Fast and accurate mass modification localization for the Trans-Proteomic pipeline. J. Proteome Res. 18, 4262–4272. https://doi.org/10.1021/acs.jproteome.9b00205

Sidoli, S., Bhanu, N.V., Karch, K.R., Wang, X., Garcia, B.A., 2016. Complete workflow for analysis of histone post-translational modifications using bottom-up mass spectrometry: From histone extraction to data analysis. J. Vis. Exp. e54112. https://doi.org/10.3791/54112

Simonetta, M., De Krijger, I., Serrat, J., Moatti, N., Fortunato, D., Hoekman, L., Bleijerveld, O.B., Altelaar, A.F.M., Jacobs, J.J.L., 2018. H4K20me2 distinguishes

pre-replicative from post-replicative chromatin to appropriately direct DNA repair pathway choice by 53BP1-RIF1-MAD2L2. Cell Cycle 17, 124–136. https://doi.org/10.1080/15384101.2017.1404210

Singh, R., Bassett, E., Chakravarti, A., Parthun, M.R., 2018. Replication-dependent histone isoforms: a new source of complexity in chromatin structure and function. Nucleic Acids Res. 46, 8665–8678. https://doi.org/10.1093/nar/gky768

Starkova, T., Polyanichko, A., Tomilin, A.N., Chikhirzhina, E., 2023. Structure and functions of HMGB2 protein. Int. J. Mol. Sci. 24, 8334. https://doi.org/10.3390/ijms24098334

Starkova, T.Y., Polyanichko, A.M., Artamonova, T.O., Tsimokha, A.S., Tomilin, A.N., Chikhirzhina, E.V., 2023. Structural characteristics of high-mobility group proteins HMGB1 and HMGB2 and their interaction with DNA. Int. J. Mol. Sci. 24, 3577. https://doi.org/10.3390/ijms24043577

Talbert, P.B., Henikoff, S., 2021. Histone variants at a glance. J. Cell Sci. 134, jcs244749. https://doi.org/10.1242/jcs.244749

Talbert, P.B., Henikoff, S., 2017. Histone variants on the move: substrates for chromatin dynamics. Nat. Rev. Mol. Cell Biol. 18, 115–126. https://doi.org/10.1038/nrm.2016.148

Tamori, Y., Wakahara, M., 2000. Conversion of red blood cells (RBCs) from the larval to the adult type during metamorphosis in *Xenopus*: specific removal of mature larval-type RBCs by apoptosis. Int. J. Dev. Biol. 44, 373–380. https://doi.org/10.1387/ijdb.10949046

Tamura, K., Mawaribuchi, S., Yoshimoto, S., Shiba, T., Takamatsu, N., Ito, M., 2010. Tumor necrosis factor–related apoptosis-inducing ligand 1 (TRAIL1) enhances the transition of red blood cells from the larval to adult type during metamorphosis in *Xenopus*. Blood 115, 850–859. https://doi.org/10.1182/blood-2009-04-218966

Tata, J.R., 2006. Amphibian metamorphosis as a model for the developmental actions of thyroid hormone. Mol. Cell. Endocrinol., PROCEEDINGS of the INTERNATIONAL SYMPOSIUM on STEROID HORMONE RECEPTOR SUPERFAMILY & MOLECULAR SIGNALING 246, 10–20. https://doi.org/10.1016/j.mce.2005.11.024

Taylor, A.C., Kollros, J.J., 1946. Stages in the normal development of *Rana pipiens* larvae. Anat. Rec. 94, 7–13.

Thambirajah, A.A., Ausió, J., 2009. A moment's pause: putative nucleosome-based influences on MeCP2 regulation. Biochem. Cell Biol. Biochim. Biol. Cell. 87, 791–798. https://doi.org/10.1139/O09-054

Thambirajah, A.A., Koide, E.M., Imbery, J.J., Helbing, C.C., 2019. Contaminant and environmental influences on thyroid hormone action in amphibian metamorphosis. Front. Endocrinol. 10. https://doi.org/10.3389/fendo.2019.00276

Thambirajah, A.A., Wade, M.G., Verreault, J., Buisine, N., Alves, V.A., Langlois, V.S., Helbing, C.C., 2022. Disruption by stealth - Interference of endocrine disrupting chemicals on hormonal crosstalk with thyroid axis function in humans and other animals. Environ. Res. 203, 111906. https://doi.org/10.1016/j.envres.2021.111906

The, M., MacCoss, M.J., Noble, W.S., Käll, L., 2016. Fast and accurate protein false discovery rates on large-scale proteomics data sets with Percolator 3.0. J. Am. Soc. Mass Spectrom. 27, 1719–1727. https://doi.org/10.1007/s13361-016-1460-7

Tomita, A., Buchholz, D.R., Shi, Y.-B., 2004. Recruitment of N-CoR/SMRT-TBLR1 corepressor complex by unliganded thyroid hormone receptor for gene repression during frog development. Mol. Cell. Biol. 24, 3337–3346. https://doi.org/10.1128/MCB.24.8.3337-3346.2004

Turinetto, V., Giachino, C., 2015. Multiple facets of histone variant H2AX: a DNA double-strand-break marker with several biological functions. Nucleic Acids Res. 43, 2489–2498. https://doi.org/10.1093/nar/gkv061

Veldhoen, N., Skirrow, R.C., Osachoff, H., Wigmore, H., Clapson, D.J., Gunderson, M.P., Van Aggelen, G., Helbing, C.C., 2006. The bactericidal agent triclosan modulates thyroid hormone-associated gene expression and disrupts postembryonic anuran development. Aquat. Toxicol. 80, 217–227. https://doi.org/10.1016/j.aquatox.2006.08.010

Veldhoen, N., Stevenson, M.R., Helbing, C.C., 2015. Comparison of thyroid hormone-dependent gene responses in vivo and in organ culture of the American bullfrog (*Rana (Lithobates) catesbeiana*) lung. Comp. Biochem. Physiol. Part D Genomics Proteomics 16, 99–105. https://doi.org/10.1016/j.cbd.2015.09.001

Viparina, S., Just, J.J., 1975. The life period, growth and differentiation of *Rana catesbeiana* larvae occurring in nature. Copeia 1975, 103–109. https://doi.org/10.2307/1442411

Wakahara, M., Yamaguchi, M., 2001. Erythropoiesis and conversion of RBCs and hemoglobins from larval to adult type during amphibian development. Zoolog. Sci. 18, 891–904. https://doi.org/10.2108/zsj.18.891

Wang, Z., Brown, D.D., 1993. Thyroid hormone-induced gene expression program for amphibian tail resorption. J. Biol. Chem. 268, 16270–16278. https://doi.org/10.1016/S0021-9258(19)85416-9

Weber, R., Blum, B., Müller, P.R., 1991. The switch from larval to adult globin gene expression in Xenopus laevis is mediated by erythroid cells from distinct compartments. Development 112, 1021–1029. https://doi.org/10.1242/dev.112.4.1021

Weber, R., Geiser, M., Müller, P., Sandmeier, E., Wyler, T., 1989. The metamorphic switch in hemoglobin phenotype ofXenopus laevis involves erythroid cell replacement. Rouxs Arch. Dev. Biol. 198, 57–64. https://doi.org/10.1007/BF02447740

Weikum, E.R., Liu, X., Ortlund, E.A., 2018. The nuclear receptor superfamily: A structural perspective. Protein Sci. Publ. Protein Soc. 27, 1876–1892. https://doi.org/10.1002/pro.3496

Weirich, S., Khella, M.S., Jeltsch, A., 2021. Structure, activity and function of the Suv39h1 and Suv39h2 protein lysine methyltransferases. Life 11, 703. https://doi.org/10.3390/life11070703

Wen, L., Fu, L., Shi, Y.-B., 2017. Histone methyltransferase Dot1L is a coactivator for thyroid hormone receptor during *Xenopus* development. FASEB J. 31, 4821–4831. https://doi.org/10.1096/fj.201700131r

West, M.H.P., Bonner, W.M., 1980. Histone 2A, a heteromorphous family of eight protein species. Biochemistry 19, 3238–3245. https://doi.org/10.1021/bi00555a022

Wiśniewski, J.R., Zougman, A., Krüger, S., Mann, M., 2007. Mass spectrometric mapping of linker histone H1 variants reveals multiple acetylations, methylations, and phosphorylation as well as differences between cell culture and tissue. Mol. Cell. Proteomics 6, 72–87. https://doi.org/10.1074/mcp.M600255-MCP200

Wong, J., Li, Q., Levi, B.-Z., Shi, Y.-B., Wolffe, A.P., 1997a. Structural and functional features of a specific nucleosome containing a recognition element for the thyroid hormone receptor. EMBO J. 16, 7130–7145. https://doi.org/10.1093/emboj/16.23.7130

Wong, J., Shi, Y.B., Wolffe, A.P., 1997b. Determinants of chromatin disruption and transcriptional regulation instigated by the thyroid hormone receptor: hormone-regulated chromatin disruption is not sufficient for transcriptional activation. EMBO J. 16, 3158–3171. https://doi.org/10.1093/emboj/16.11.3158

Wong, J., Shi, Y.B., Wolffe, A.P., 1995. A role for nucleosome assembly in both silencing and activation of the Xenopus TR beta A gene by the thyroid hormone receptor. Genes Dev. 9, 2696–2711. https://doi.org/10.1101/gad.9.21.2696

Wright, M.L., Proctor, K.L., Alves, C.D., 1999. Hormonal profiles correlated with season, cold, and starvation in *Rana catesbeiana* (bullfrog) tadpoles. Comp. Biochem. Physiol. C 124, 109–116. https://doi.org/10.1016/S0742-8413(99)00060-2

Yamaguchi, M., Kawaguchi, Y., Minami, S., Matsuda, I., Hirooka, A., Yamakawa, N., Ikoma, A., Ikai, W., Kinoshita, T., 2022. Thyroid hormone-dependent and independent processes of red blood cell transition from larval to adult type during

metamorphosis in *Xenopus laevis*. Dev. Growth Differ. 64, 420–432. https://doi.org/10.1111/dgd.12811

Yamamoto, K., Kanski, D., Frieden, E., 1966. The uptake and excretion of thyroxine, triiodothyronine and iodide in bullfrog tadpoles after immersion or injection at 25° and 6°C. Gen. Comp. Endocrinol. 6, 312–324. https://doi.org/10.1016/S0016-6480(66)80019-9

Yu, F., Haynes, S.E., Teo, G.C., Avtonomov, D.M., Polasky, D.A., Nesvizhskii, A.I., 2020a. Fast quantitative analysis of timsTOF PASEF data with MSFragger and IonQuant. Mol. Cell. Proteomics 19, 1575–1585. https://doi.org/10.1074/mcp.TIR120.002048

Yu, F., Teo, G.C., Kong, A.T., Haynes, S.E., Avtonomov, D.M., Geiszler, D.J., Nesvizhskii, A.I., 2020b. Identification of modified peptides using localization-aware open search. Nat. Commun. 11, 4065. https://doi.org/10.1038/s41467-020-17921-y

Zhang, R., Erler, J., Langowski, J., 2016. Histone acetylation regulates chromatin accessibility: Role of H4K16 in inter-nucleosome interaction. Biophys. J. 112, 450–459. https://doi.org/10.1016/j.bpj.2016.11.015

Zhang, Y., Sun, Z., Jia, J., Du, T., Zhang, N., Tang, Y., Fang, Y., Fang, D., 2021. Overview of histone modification. Springer Singapore, pp. 1–16.

Zoeller, R.T., Tan, S.W., Tyl, R.W., 2007. General background on the hypothalamic-pituitary-thyroid (HPT) axis. Crit. Rev. Toxicol. 37, 11–53. https://doi.org/10.1080/10408440601123446

6. Supplementary Information

6.1. Complete LC-MS/MS details – Chapter 1

The following information was provided in the sample analysis report from the University of Victoria Genome BC Proteomics Centre. All reagents are of HPLC-MS grade.

All samples were rehydrated to 0.5 µg/µL with 2% acetonitrile, 0.1% formic acid. A 2 µg injection was separated by on-line reversed phase liquid chromatography using a Thermo Scientific EASY-nLC 1000 system at a flow rate of 300 nL/minute and an Acclaim PepMap100 C18 reversed-phase pre-column (100 µm I.D., 2 cm length, 5 µm, 100 Å), and an AcclaimPepMap100 C-18 reversed phase nano-analytical column (75 µm I.D., 15 cm length, 3 µm, 100 Å, Thermo Fisher Scientific, San Jose, CA) . The chromatography system was coupled on-line with an Orbitrap Fusion Tribrid mass spectrometer (Thermo Fisher Scientific, San Jose, CA) equipped with a Nanospray Flex NG source (Thermo Fisher Scientific). Solvents were A: 2% acetonitrile, 0.1% formic acid; and B: 90% acetonitrile, 0.1% formic acid. After a 348 bar (~4 µL) pre-column equilibration and 348 bar (~4 µL) nanocolumn equilibration, samples were separated by a 140 min gradient (0 min: 5%B; 100 min: 50%B; 20 min: 70%B; 10 min: 90%B; hold 5 min: 90%B: 1 min:100%B and 4 min 0%B). The Orbitrap Fusion instrument parameters (Fusion Tune 3.4 software) for orbitrap (OT-MS) orbitrap (OT-MS/MS) with high-energy C-trap dissociation (HCD) fragmentation were: Nano-electrospray ion source with spray voltage 2.55 kV, capillary temperature 275^{o}C. The acquired survey MS1 scan range was 350-2000 m/z profile mode, resolution 60,000 FWHM @ 200 m/z one microscan using the Siloxane mass 445.12003 as lock mass for internal calibration. Data-dependent acquisition Orbitrap

survey spectra were scheduled at least every 3 s, with the software determining maximum number of MS/MS acquisitions during this period. The automatic gain control (AGC) target value for FTMS was set to Standard (400,000 counts) and custom 54 ms maximum fill time. The most intense ions charge state 2-7 exceeding 50,000 counts were selected for HCD MS/MS fragmentation in the ion routing multipole. Monoisotopic Precursor Selection (MIPS) was enabled. Dynamic exclusion settings were: repeat count: 1; exclusion duration: 30 s with a 10 ppm mass window. The data dependent (ddMS2) OT HCD scan used a quadrupole isolation window of 1.6 Da; Orbitrap Resolution 50000, mass range normal auto scan, centroid detection, 1 microscan, 200 ms maximum injection time, AGC target (100%) 50,000 counts and custom 200 ms maximum injection time with a fixed HCD collision energy of 30%.

6.2. Complete LC-MS/MS details - Chapter 2

All samples were rehydrated to 0.5 µg/µL with 2% Acetonitrile, 0.1% Formic acid. A 2 µg injection was separated by online reversed phase liquid chromatography using a Thermo Scientific EASY-nLC 1000 system with an Acclaim PepMap100 C18 (100 µm I.D., 2 cm length, 5 µm, 100Å) reversed-phase pre-column, and an AcclaimPepMap100 C-18 (75 µm I.D., 15 cm length, 3 µm, 100Å, Thermo Fisher Scientific, San Jose, CA) reversed phase nano-analytical column at a flow rate of 300 nL/min. The chromatography system was coupled on-line with an Orbitrap Fusion Tribrid mass spectrometer (Thermo Fisher Scientific, San Jose, CA) equipped with a Nanospray Flex NG source (Thermo Fisher Scientific). Solvents were A: 2% Acetonitrile, 0.1% Formic acid; B: 90% Acetonitrile, 0.1% Formic acid. After a 348 bar (~ 4 µL) pre-column equilibration and 348 bar (~ 4 µL) nanocolumn equilibration, samples were separated by

a 140-minute gradient (0 min: 5%B; 100 min: 50%B; 20 min: 70%B; 10 min: 90%B; hold 5min: 90%B: 1min:100%B and 4 min 0%B). The Orbitrap Fusion instrument parameters (Fusion Tune 3.4 software) were as follows for orbitrap (OT-MS) orbitrap (OT- MS/MS) with high-energy C-trap dissociation (HCD) fragmentation: Nano-electrospray ion source with spray voltage 2.55kV, capillary temperature 275°C. The acquired survey MS1 scan range was 350-2000 m/z profile mode, resolution 60,000 FWHM @ 200m/z one microscan using the Siloxane mass 445.12003 as lock mass for internal calibration. Data-dependent acquisition Orbitrap survey spectra were scheduled at least every 3 s, with the software determining maximum number of MS/MS acquisitions during this period. The automatic gain control (AGC) target value for FTMS was set to Standard (400,000 counts) and custom 54ms maximum fill time. The most intense ions charge state 2-7 exceeding 50,000 counts were selected for HCD MSMS fragmentation in the ion routing multipole. Monoisotopic Precursor Selection (MIPS) was enabled and Dynamic exclusion settings were: repeat count: 1; exclusion duration: 30 s with a 10 ppm mass window. The data dependent (ddMS2) OT HCD scan used a quadrupole isolation window of 1.6 Da; Orbitrap Resolution 50000, mass range normal auto scan, centroid detection, 1 microscan, 200 ms maximum injection time, AGC target (100%) 50,000 counts and custom 200 ms maximum injection time with a fixed HCD collision energy of 30%.

6.3. R. catesbeiana protein alignments

Supplemental Figures S1-S20. Alignments of the identified proteins from the *R. catesbeiana* proteome to human histone sequences. The *R. catesbeiana* proteome was generated by *in silico* translation of the version 4 genome (DOI https://doi.org/10.5281/zenodo.8125199). Alignments were performed using Clustal Omega (version 1.2.4). Identical amino acids in the *Ranid* sequences are shaded and the human histone sequence is in bold. N-terminal methionine (M) residues have been trimmed. The NCBI accession numbers are provided in parentheses.

S1. H1.0 alignment (NP_005309.1)

```
H1.0      ------------------------------------------------------------     0
H1.0      DTLGSLVSVLVGVAFAGPSRTQGGRICPLMDLTTGSGMHLHPAGASLLRGPQGPIDRGQN     60

H1.0      ------------------------------------------------------------TE     2
H1.0      GRNVCDFSSSTALFGALPRAVGSPETVRPGKLREQKKFPAAFPRKFSWSEAPTINANMTE     120

H1.0      NSTSAPAAKPKRAKASKKSTDHPKYSDMIVAAIQAEKNRAGSSRQSIQKYIKSHYKVGEN     62
H1.0      NSSAAPAAKPKRSRAAKKSNDHPKYSDMIVAAVQAEKSRSGSSRQSIQKYIKNHYKVGDN     180

H1.0      ADSQIKLSIKRLVTTGVLKQTKGVGASGSFRLAKSDEPKKSVAFKKTKKEIKKVATPKKA     122
H1.0      ADSQIKLSIKRLVTSGTLKQTKGVGASGSFRLAKSDEPKKPT--KKPKKEVKKSATPKKA     238

H1.0      SKPKKAASKAPT-KKPKA---TPVKKAKKKLAATPKKAKKPKTVKAKPVKASKPKKAKPV     178
H1.0      AKPKKAAKSPVKAKKPKVAEKKAKKVAKKKPAPSPKKVKKTKTVKAKPVKVTKVKKAKPS     298

H1.0      KPKAKSSAKRAGKKK     193
H1.0      KPKAKATPKKSGRKK     313
```

S2. H1.3 alignment (NP_005311.1)

```
H1.3          --SETAPLAPTIPAPAEKTPVKKKAKKAGATAGKRKASGPPVSELITKAVAASKERSGVS       58
H1.3(i)       TETESAPAAAPPAEPAAKKKPAKKAAAGGAKKGSKKPSGPSVSELLVKAVAASKERSGVS       60
H1.3(ii)      TETESAPAAAPPAEPAAKKKPAKKAAAGGAKKGSKKPSGPSVSELLVKAVAASKERSGVS       60
H1.3(iii)     TETEIDPAAAPPAEPAAKKKPAKKAAAGGAKKGSKKPSGPSVSELLVKAVAASKERSGVS       60

H1.3          LAALKKALAAAGYDVEKNNSRIKLGLKSLVSKGTLVQTKGTGASGSFKLNKKAASGEGKP       118
H1.3(i)       LSALKKVLAAGGYDVDKNNSRLKIAIRGLVTKGTLVQVKGHGASGSFKINKKQEDKAAGA       120
H1.3(ii)      LSALKKVLSAGGYDVDKNNSRLKIAIRGLVTKGTLVQVKGHGASGSFKINKKQEDKAAGA       120
H1.3(iii)     LAALKKLLAAGGYDVDKNNSRLKIAIRALVTKGSLVQVKGYGASGSFKINKKQEDKAASA       120

H1.3          KAKKAGAAKPRKPAGAAKKPKKVAGAA---TPK----------KSIKKTPKKVKKPAT--       163
H1.3(i)       KKS------TKKPSAAAKSPKKPAAKKPAKSPKKKT--TTKAPTAAKSPKKAAKKPAKKP       172
H1.3(ii)      KKS------TKKPSAAAKSPKKPAAKKPAKSPKKKT--TTKAPTAAKSPKKAAKKPAKKP       172
H1.3(iii)     KKS------TKKPLAAAKSPKKPAAKKKATTKPPTAAKKAAKKKATTKPPTAAKKPAKKP       174

H1.3          -AAGTKKVAKSAKKV-KTPQPKKAAKSPAKAKAPKPKAAKPKSGKPKVTKAKKAAPKKK 220
H1.3(i)       AAAKAKKVTKSPKKPKAAAKPKKVAKSPAKKAAKPKTAAKPK----------KAAPKKK 221
```

```
H1.3(ii)        AAAKAKKVTKSPKKPKAAAKPKKVAKSPAKKAAKPKTAAKPK----------KAAPKKK 221
H1.3(iii)       AAAKAKKVTKSPKKPKAAAKPKKVAKSPAKKAAKPKTAAKPK----------KAAPKKK 223
```

S3. H1.10 alignment (pdb|7XX7|U)

```
H1.10           ------------------------------SMSVELEEALPVTTAEGMAKKV------- 22
H1.10(i)        ANYKDAVKWQVQKVSDNKRSLERVLKEGGAPELSVILQ----QTAREGRLEPREAADIQI 56
H1.10(ii)       --------------------------------SLQLEENVPTTEEEDEEEEEDEDGEA 27

H1.10           ---------TKAGGSAALSPSKKRKNSKKKNQPGKYSQLVVETIRRLGERNGSSLAKIYT 73
H1.10(i)        AMAQPEVAPAASKQAKSAASAAKKSGKKKKNQPGKYSQLVVDSIRKLGERNGSSLAKIYG 116
H1.10(ii)       SEEESDTKSSKKRSKAAGSSSGSKKKNKKKNQPGRYSQLVVDTIRKLAERNGSSLAKIYS 87

H1.10           EAKKVPWFDQQNGRTYLKYSIKALVQNDTLLQVKGTGANGSFKLNRKKLEGGGERRGAPA 133
H1.10(i)        EAKKVSWFDQQNGRTYLKYSGLVAGGKGLI------------------------------ 146
H1.10(ii)       EAKKVSWFDQQNGRTYLKYSVKALVQNDTLVQVKGVGANGSFRLNKKKLEGGTPEKKAA- 146

H1.10           AATAPAPTAHKAKKAAPGAAGSR--RADKKPARGQKPEQRSHKKGAGAKKDKGGKAKKTA 191
H1.10(i)        ------------------------------------------------------------ 146
H1.10(ii)       ----PAPKPAAAAKKAPPKKSPKKAKGKPKPTKTQKPKKSSPKAAAAAP-PAKSTKKKAA 201

H1.10           AAGGKKVKKAAKPSVPKVPKGRK-        214
H1.10(i)        ------------------------        146
H1.10(ii)       GGGGKKVKKAGKPSRAKVHKTRKA        225
```

S4. H2A type 1-A alignment (NP_734466.1)

```
H2A type 1 A    ------------------------------SGRGKQGGKARAKSKSRSSRAGLQFPVGRI 30
H2A type 1 A    PAESWAGEHMYRGMDYHYTGPVQQRFSPYPTPSMEKVQKTAAGKSSRSAKAGLQFPVGRI 60

H2A type 1 A    HRLLRKGNYAERIGAGAPVYLAAVLEYLTAEILELAGNASRDNKKTRIIPRHLQLAIRND 90
H2A type 1 A    HRFLKKGNYAERIGSGAGIYMAATLEYLCAEVLELAGNAARDNKKSRIMPRHIQLAVRND 120

H2A type 1 A    EELNKLLGGVTIAQGGVLPNIQAVLLPKKTESHHHKAQSK-------------------- 130
H2A type 1 A    EELAKLFAGVTIADGGVLPNIQAVLLPKKTLKSSQQSTVAESHDRTTLPSILCAPGWAGW 180

H2A type 1 A    ------------------------------------------------------------ 130
H2A type 1 A    RDTSCVLGDSQLGSWVSMQAARAMAKFRLSLVQLFVSPVKADNLKKASELIKQAAQQGAQ 240

H2A type 1 A    ------------------------------------------------------------ 130
H2A type 1 A    IVALPVHLFNIDVPGKIRFQESETLTPGESFSVFDTPYCKIGVGICYDIRFAELAQIYTK 300

H2A type 1 A    --------  130
H2A type 1 A    KGTSVFVP  308
```

S5. H2A type 2-B alignment (NP_778235.1)

```
H2A type 2-B    --------------------SGRGKQGGKARAKAKSRSSRAGLQFPVGRVHRLLRKGNYA 40
H2A type 2-B    KEGGYRVPFLSKYPDQPVTMSGRGKQGGKVRAKAKTRSSRAGLQFPVGRVHRLLRKGNYA 60

H2A type 2-B    ERVGAGAPVYLAAVLEYLTAEILELAGNAARDNKKTRIIPRHLQLAVRNDEELNKLLGGV 100
H2A type 2-B    ERVGAGAXVYXAAXLEYLTAEIXELAGNAARDNKKTRIIPRHLQLAVRNDEELNKLLGGV 120

H2A type 2-B    TIAQGGVLPNIQAVLLPKKTESHKPGKNK 129
H2A type 2-B    TIAQGGVLPNIQAVLLPKKTESHKAAKSK 149
```

S6. H2A type 2-C alignment (NP_003508.1)

```
H2A type 2-C          SGRGKQGGKARAKAKSRSSRAGLQFPVGRVHRLLRKGNYAERVGAGAPVYMAAVLEYLTA   60
H2A type 2-C(i)       SGRGKQGGKVRAKAKTRSSRAGLQFPVGRVHRLLRKGNYAERVGAGAPVYLAAVLEYLTA   60
H2A type 2-C(ii)      SGRGKQGGKVRAKAKTRSSRAGLQFPVGRVHRLLRKGNYAERVGAGAPVYLVAVLEYLTA   60

H2A type 2-C          EILELAGNAARDNKKTRIIPRHLQLAIRNDEELNKLLGKVTIAQGGVLPNIQAVLLPKKT   120
H2A type 2-C i)       EILELAGNAARDNKKTRIIPRHLQLAVRNDEELNKLLGGVTIAQGGVLPNIQAVLLPKKT   120
H2A type 2-C(ii)      EILELAGNAARDNKKTRIIPRHLQLAVRNDEELNKLLGGVTIAQGGVLPNIQAVLLPKKT   120

H2A type 2-C          ESHKAKSK--      128
H2A type 2-C(i)       ESHKAAAKSK      130
H2A type 2-C(ii)      ESHKAAAKFK      130
```

S7. H2AX alignment (NP_002096.1)

```
H2AX      SGRGK-TGGKARAKAKSRSSRAGLQFPVGRVHRLLRKGHYAERVGAGAPVYLAAVLEYLT      59
H2AX      SGRGKTTAGKTKAKSKTRSSRAGLQFPVGRVHRLLRKGNYAHRVGAGAPVYLAAVLEYLT      60

H2AX      AEILELAGNAARDNKKTRIIPRHLQLAIRNDEELNKLLGGVTIAQGGVLPNIQAVLLPKK      119
H2AX      AEILELAGNAARDNKKTRIIPRHLQLAVRNDEELNRLLGGVTIAQGGVLPNIQAVLLPKK      120

H2AX      TSATVGPKAPS--------GGKKATQASQEY       142
H2AX      SGAAATPTAKSSAKSSAKSPGKKSSQQSQEY       151
```

S8. H2A.Z-2 alignment (pdb|3WAA|C)

```
H2A.Z-2       GSHMAGGKAGKDSGKAKAKAVSRSQRAGLQFPVGRIHRHLKTRTTSHGRVGATAAVYSAA   60
H2A.Z-2       --YIAGGKAGKDSGKAKAKAVSRSQRAGLQFPVGRIHRHLKTRTTSHGRVGATAAVYSAA   58

H2A.Z-2       ILEYLTAE----------------------VLELAGNASKDLKVKRITPRHLQLAIRGDE   98
H2A.Z-2       ILEYLTAEVGYSFNTVRICFCNSLSTEAKSVLELAGNASKDLKVKRITPRHLQLAIRGDE   118

H2A.Z-2       ELDSLIKATIAGGGVIPHIHKSLIGKKGQQKTA  131
H2A.Z-2       ELDSLIKATIAGGGVIPHIHKSLIGKKGQQKTA  151
```

S9. MacroH2A.1 isoform 2 alignment (NP_001035248.1)

```
Macro-H2A.1 isoform 2     SSRGGKKKSTKTSRSAKAGVIFPVGRMLRYIKKGHPKYRIGVGAPVYMAAVLEYLTAEIL   60
Macro-H2A.1 isoform 2     SSRGGKKKTTKTTRSAKAGVIFPVGRMLRYIKKGHPKYRIGVGAPVYMAAVLEYLT----   56

Macro-H2A.1 isoform 2     ELAGNAARDNKKGRVTPRHILLAVANDEELNQLLKGVTIASGGVLPNIHPELLAKKRGSK   120
Macro-H2A.1 isoform 2     -----------------------------------GVTIASGGVLPNIHPELLAKKRGTK   81

Macro-H2A.1 isoform 2     GKLEAIITPPPAKKAKSPSQKKPVSKKAGGKKGARKS-KKQGEVSKAASADSTTEGTPAD   179
Macro-H2A.1 isoform 2     GKLEAIITPPPAKKAKTTSPKKSTSKKPGAKKGVRKSKKKQGEVSKAASADSTTEGAPAN   141

Macro-H2A.1 isoform 2     GFTVLSTKSLFLGQKLNLIHSEISNLAGFEVEAIINPTNADIDLKDDLGNTLEKKGGKEF   239
Macro-H2A.1 isoform 2     GFTILSTKSLFLGQKLNLIHSEISNLAGFEVEAVINPTNADIDLKDDIGSALEKKGGKEF   201

Macro-H2A.1 isoform 2     VEAVLELRKKNGPLEVAGAAVSAGHGLPAKFVIHCNSPVWGADKCEELLEKTVKNCLALA   299
Macro-H2A.1 isoform 2     LEAVIELKKKNGPLDVAGAAVSSGHGLPAKFVIHCNSPSWGSDKCEELLEKTVKNCLALA   261

Macro-H2A.1 isoform 2     DDKKLKSIAFPSIGSGRNGFPKQTAAQLILKAISSYFVSTMSSSIKTVYFVLFDSESIGI   359
Macro-H2A.1 isoform 2     DEKKIKSIAFPSIGSGRNGFPKQTAAQLILRGISNYFVSTMSSSIKTVYFVLFDSESIGI   321

Macro-H2A.1 isoform 2     YVQEMAKLDAN    370
```

```
Macro-H2A.1 isoform 2      YVQEMAKLDAN    332
```

S10. MacroH2A.1 isoform 4 alignment (NP_001387332.1)

```
Macro-H2A.1 isoform 4      SSRGGKKKSTKTSRSAKAGVIFPVGRMLRYIKKGHPKYRIGVGAPVYMAAVLEYLTAEIL  60
Macro-H2A.1 isoform 4      SSRGGKKKTTKTTRSAKAGVIFPVGRMLRYIKKGHPKYRIGVGAPVYMAAVLEYLT----  56

Macro-H2A.1 isoform 4      ELAGNAARDNKKGRVTPRHILLAVANDEELNQLLKGVTIASGGVLPNIHPELLAKKRGSK  120
Macro-H2A.1 isoform 4      ----------------------------------GVTIASGGVLPNIHPELLAKKRGTK  81

Macro-H2A.1 isoform 4      GKLEAIITPPPAKKAKSPSQKKPVSKKAGGKKGARKS-KKQGEVSKAASADSTTEGTPAD  179
Macro-H2A.1 isoform 4      GKLEAIITPPPAKKAKTTSPKKSTSKKPGAKKGVRKSKKKQGEVSKAASADSTTEGAPAN  141

Macro-H2A.1 isoform 4      GFTVLSTKSLFLGQKLQVVQADIASIDSDAVVHPTNTDFYIGGEVGNTLEKKGGKEFVEA  239
Macro-H2A.1 isoform 4      GFTILSTKSLFLGQKLQVVKADIANLESDAVVHPTGSDLYTGGEVGSALEKKGGKEFLEA  201

Macro-H2A.1 isoform 4      VLELRKKNGPLEVAGAAVSAGHGLPAKFVIHCNSPVWGADKCEELLEKTVKNCLALADDK  299
Macro-H2A.1 isoform 4      VIELKKKNGPLDVAGAAVSSGHGLPAKFVIHCNSPSWGSDKCEELLEKTVKNCLALADEK  261

Macro-H2A.1 isoform 4      KLKSIAFPSIGSGRNGFPKQTAAQLILKAISSYFVSTMSSSIKTVYFVLFDSESIGIYVQ  359
Macro-H2A.1 isoform 4      KIKSIAFPSIGSGRNGFPKQTAAQLILRGISNYFVSTMSSSIKTVYFVLFDSESIGIYVQ  321

Macro-H2A.1 isoform 4      EMAKLDAN      367
Macro-H2A.1 isoform 4      EMAKLDAN      329
```

S11. MacroH2A.2 alignment (NP_061119.1)

```
Macro-H2A.2      SGRSGKKKMSKLSRSARAGVIFPVGRLMRYLKKGTFKYRISVGAPVYMAAVIEYLAAEIL        60
Macro-H2A.2      SARGGKKKTTKLSRSSRAGVIFPVGRMMRYLRRGTHKYRIGMGAPVYMAAVIEYLAAEIL        60

Macro-H2A.2      ELAGNAARDNKKARIAPRHILLAVANDEELNQLLKGVTIASGGVLPRIHPELLAKKRGTK        120
Macro-H2A.2      ELAGNAARDNKKGRITPRHILLAVANDEELNQLLRGVTIASGGVLPRIHPELLAKKRGSR        120

Macro-H2A.2      GKSETILSPPPEKRGRKA-TSGKKGGKKSKAAKPRTSKKSKPKDSDKEGTSNSTSEDGPG        179
Macro-H2A.2      GKETILSQ-PVEKKKKKGGKALDKTAKKPKAGKNKLLKK-DKQVDGKEGASSSVSEDGPG        178

Macro-H2A.2      DGFTILSSKSLVLGQKLSLTQSDISHIGSMRVEGIVHPTTAEIDLKEDIGKALEKAGGKE        239
Macro-H2A.2      DGFTILSSKSLLLGQKLSLTQSDLSHIGSMKVEGIIHPTTAEIDLKEDIGNALEKAGGKE        238

Macro-H2A.2      FLETVKELRKSQGPLEVAEAAVSQSSGLAAKFVIHCHIPQWGSDKCEEQLEETIKNCLSA        299
Macro-H2A.2      FLEAVKELRKSHGPLELTGAALSQANGLAAKFVIHCHIPQWGSDKCEEQLEKTIKNCLSV        298

Macro-H2A.2      AEDKKLKSVAFPPFPSGRNCFPKQTAAQVTLKAISAHFDDSSASSLKNVYFLLFDSESIG        359
Macro-H2A.2      AEEKKLKSVAFPSFPSGRNGFPKQTAAQVILRAISNHFGSSSSSTVKNIFFLLFDSESIG        358

Macro-H2A.2      IYVQEMAKLDAK          371
Macro-H2A.2      IYVQEMAKLDTK          370
```

S12. Histone H2B type 1-J (NP_066402.2)

```
H2B type 1-J         ------------------------------------------PEPAKSAPAPKKGSK     15
H2B type 1-J(i)      ------------------------------------IESSNRRVRSQVRPGAPAPKKGSK     24
H2B type 1-J(ii)     TESSNRRVRREETHLHRTPIKSAHEGGSSTHSLHTAEEITLILIMPEPAKSAPAPKKGSK     60

H2B type 1-J         KAVTKAQKKDGKKRKRSRKESYSIYVYKVLKQVHPDTGISSKAMGIMNSFVNDIFERIAG     75
H2B type 1-J(i)      KAVTKSQKKDGKKRRKSRKESYAIYVYKVLKQVHPDTGISSKAMGIMNSFVNDIFERIAG     84
H2B type 1-J(ii)     KAVTKSQKKDGKKRRKSRKESYAIYVYKVLKQVHPDTGISSKAMGIMNSFVNDIFERIAG     120

H2B type 1-J         EASRLAHYNKRSTITSREIQTAVRLLLPGELAKHAVSEGTKAVTKYTSAK      125
H2B type 1-J(i)      ESSRLAHYNKRRTITSREIQTSVRLLLPGELAKHAVSEGTKAVTKYTSAK      134
H2B type 1-J(ii)     EASRLAHYNKRRTITSREIQTAVRLLLPGELAKHAVSEGTKAVTKYTSAK      170
```

S13. H3.2 alignment (NP_001005464.1)

```
H3.2          ARTKQTARKSTGGKAPRKQLATKAARKSAPATGGVKKPHRYRPGTVALREIRRYQKSTEL  60
H3.2(i)       ARTKQTARKSTGGKAPRKQLATKAARKSAPATGGVKKPHRYRPGTVALREIRRYQKSTEL  60
H3.2(ii)      ARTKQTARKSTGGKAPRKQLATKAARKSAPATGGVKKPHRYRPGTVALREIRRYQKSTEL  60

H3.2          LIRKLPFQRLVREIAQDFKTDLRFQSSAVMALQEASEAYLVGLFEDTNLCAIHAKRVTIM  120
H3.2(i)       LIRKLPFQRLVREIAQDFKTDLRFQSSAVMALQEASEAYLVGLFEDTNLCAIHAKRVTIM  120
H3.2(ii)      LIRKLPFQRLVREIAQDFKTDLRFQSSAVMALQEASESYLVGLFEDTNLCAIHAKRVTIM  120

H3.2          PKDIQLARRIRGERA         135
H3.2(i)       PKDIQLARRIRGERA         135
H3.2(ii)      PKDIQLARRIRGERA         135
```

S14. H3.3 alignment (NP_001365972.1)

```
H3.3          ARTKQTARKSTGGKAPRKQLATKAARKSAPSTGGVKKPHRYRPGTVALREIRRYQKSTEL  60
H3.3(i)       TCTKQTARKSTGGKAPRKQLATKAARKSAPSTGGVKKPHRYRPGTVALREIRRYQKSTKL  60
H3.3(ii)      ARTKQTARKSTGGKAPRKQLATKAARKSAPSTGGVKKPHRYRPGTVALREIRRYQKSTEL  60
H3.3(iii)     ------------------------------ELVLMTIIYFSRPGTVALREIRRYQKSTEL  30

H3.3          LIRKLPFQRLVREIAQDFKTDLRFQSAAIGALQEASEAYLVGLFEDTNLCAIHAKRVTIM  120
H3.3(i)       LIRKLPFQRLVREIAQDFKTDLRFQSAAIGALQEASDAYLVGLFEDTNLCAIHAKRVTIM  120
H3.3(ii)      LIRKLPFQRLVREIAQDFKTDLRFQSAAIGALQEASEAYLVGLFEDTNLCAIHAKRVTIM  120
H3.3(iii)     LIRKLPFQRLVREIAQDFKTDLRFQSAAIGALQEASEAYLVGLFEDTNLCAIHAKRVTIM  90

H3.3          PKDIQLARRIRGERA----------       135
H3.3(i)       PKDMQLARRISEERASFFFFSGNSF       145
H3.3(ii)      PKDIQLARRIRGERA----------       135
H3.3(iii)     PKDIQLARRIRGERA----------       105
```

S15. H4 alignment (NP_001029249.1)

```
H4            SGRGKGGKGLGKGGAKRHRKVLRDNIQGITKPAIRRLARRGGVKRISGLIYEETRGVLKV   60
H4(i)         SGRGKGGKGLGKGGAKRHRKVLRDNIQGITKPAIRRLARRGGVKRISGLIYEETRGVLKV   60
H4(ii)        SGRGKGEKGLGKGGAKHHRKVLWENIQGITQKPHLTFGSQRGVKRISRLIYEDTRGVLKV   60
H4(iii)       SVRGKGGKGLGKGSAKRHRKVLRDNIQGITKPAIRRLARRGGVKRISGLIYEETRGVLKV   60
H4(iv)        SGRRKGGKGLGKGGAKRHRKVLWDNIQGITKPAIRRLARRGGVKRISGLIYEETRGVLKV   60
H4(v)         SGRSKGGKGLGKRGAKRHRKVLRDNIQGITKPAIRCLARRGGVKRISGLIYEETRGVLKV   60

H4            FLENVIRDAVTYTEHAKRKTVTAMDVVYALKRQGR----TLYGFGG-----   102
H4(i)         FLENVIRDAVTYTEHAKRKTVTAMDVVYALKRQGR----TLYGFGG-----   102
H4(ii)        FLENIIRNAVTYAEHGKRKTVTAMNRLLLFEISTYQRKALLKAYNSVINMH   111
H4(iii)       FLENVIRDAVTYTEHAKRKTVTAMDVVYALKRQGR----TLYGFGG-----   102
H4(iv)        FLENVIRDAVTYTEHAKRKTVTAMDVIYALKRQGR----TLYGFGG-----   102
H4(v)         FLENVIRDAVTYTEHAKRKTVTAMDVVYALKRQGR----TLYGFGG-----   102
```

S16. H4 (vi) alignment to human H4 (NP_001029249.1) and to human H2B type 1-J (NP_066402.2)

```
H4          SGRGKGGKGLGKGGAKRHRKVLRDNIQGITKPAIRRLARRGGVKRISGLIY---------    51
H4(iii)     SGRGKGGKGLGKGGAKRHRKKGSKKAVTKSQKKDGKKRRKSRKESYAIYVYKVLKQVHPD    60

H4          ----EETRGVLKVFLENVIRD----AVTYTEHAKRKTVTAMDVVYALKR--QGR------    95
H4(iii)     TGISSKAMGIMNSFVNDIFERIAGEASRLAHYNKRRTITSREIQTAVRLLLPGELAKHAV    120

H4          -----TLYGFGG--        102
H4(iii)     SEGTKAVTKYTSAK        134
```

S17. MeCP2 alignment (ADE87882.1)

```
MeCP2       VAGMLGLREEKSEDQDLQGLKDKPLKFKKVKKDKKEEKEGKHEPVQPSAQHSAEPAEAGK   60
MeCP2       AAAPSGEERLEEKTED-LDQKDKSPKLRNVKKDKNNDE-ELSEEAHPSTQQSEEPTEARK   58

MeCP2       AETSE-GSGSAPAVPEASASPKQRRSIIRDRGPMYDDPTLPEGWTRKLKQRKSGRSAGKY   119
MeCP2       AEVPESAEAAAPAVPEASAFPKQRRSVIRDRGPMYDDPTLPEGWTRKLKQRKSGRSAGKY   118

MeCP2       DVYLINPQGKAFRSKVELIAYFEKVGDTSLDPNDFDFTVTGRGSPSRREQKPPKKPKSPK   179
MeCP2       DVYLINPSGKAFRSKVELIAYFQKVGDTSLDPNDFDFTVTGRGSPSRREQKLPKKPKASK   178

MeCP2       APGTGRGRGRPKGSGTTRPKAATSEGVQVKRVLEKSPGKLLVKMPFQTSPGGKAEGGGAT   239
MeCP2       PTGTGRGRGRPKGSGKAKPIV-KLEGVQVKRVVEKTPGKLLVKMPLS----GNKEESDAT   233


MeCP2       TSTQVMVIKRPGRKRKAEADPQAIPKKRGRKPGSVVAAA---------AAEAKKKAVKES   290
MeCP2       TSEQVLVIKRPGRKRKSEIDPSAAPKKRGRKPGSASVAAAAAAAAAAAAEAAKKKAIKES   293

MeCP2       SIRSVQETVLPIKKRKTRETVSIEVKEVVKPLLVSTLGEKSGKGLKTCKSPGRKSKESSP   350
MeCP2       SVKPLLETVLPIKKRKTRETVSLEVKDPEPPEIPSAVTEKSVKVQNPAKSPESKSKESSP   353

MeCP2       KGRSSSASSPP--KKEHHHHHHHHSESPKAPVPLLPPLPPPPPEPESSEDPTSPPEPQDLS   408
MeCP2       KSKSTLPKKEQPHHHHHHHHHHHSESKAST---------TSLEPETSKDSVSVPEPQDLS   404

MeCP2       SSVCKEEKMPRGGSLESDGCPKEPAKTQPAVATAATAAEKYKHRGEGERKDIVSSSMPRP   468
MeCP2       VKICKEDKV-----LESDGCTQEPPKTQPA--------DKCRNRGEGERKDIVSSSIQRP   451

MeCP2       NREEPVDSRTPVTERVS      485
MeCP2       SREEPVDTRTPVTERVS      468
```

S18. HMGN3 alignment (NP_004233.1)

```
HMGN3       MPKRKSPENTEGKDGSKVTKQEPTRRSARLSAKPAPPKPEPKPRKTSAKKEPGAKISRGA   60
HMGN3       MPKRKSPEGAEAKDAGKVTKQEPTRRSARLSAKPASSKPDAKPKKPAAKKEPGTKASKGA   60

HMGN3       KGKKEEKQEAGKEGTAPSENGETKAEEAQKTESVDNEGE    99
HMGN3       KGKKEEKQEAGKEGTAPSENGENRADEEQKTEAADDETE    99
```

S19. HMGB2 alignment (AAV38586.1)

```
HMGB2       GKGDPNKPRGKMSSYAFFVQTCREEHKKKHPDSSVNFAEFSKKCSERWKTMSAKEKSKFE   60
HMGB2       ----------------------------------------------------MSAKEKGKFE    9

HMGB2       DMAKSDKARYDREMKNYVPPKGDKKGK-KKDPNAPKRPPSAFFLFCSEHRPKIKSEHPGL   119
HMGB2       DLAKGDKVRYEREMKTYIPPKGEKGGKRKKDPNAPKRPPSAFFLFCSENRPQIKNDTPGL    69

HMGB2       SIGDTAKKLGEMWSEQSAKDKQPYEQKAAKLKEKYEKDIAAYRAKGKSEAGKKGPGRPTG   179
HMGB2       SIGDTAKKLGELWSEQTPKDKQPFEQKAAKLKEKYEKDVAAYRAKGSSDVGKKIPGRPAS   129

HMGB2       SKKKNEPEDEEEEEEEDEDEEEEDEDEE---     207
HMGB2       SKKKVEPEDDDDEEDEEDEEDEDEEDDDDE     160
```

S20. HMGB3 alignment (XP_047298018.1)

```
HMGB3       MTAADFRGTFFHQEAFDKMEVRMAKGDPKKPKGKMSAYAFFVQTCREEHKKKNPEVPVNF   60
HMGB3       ----------------------MAKGDPKKPKGKMSAYAYFVQTCREEHKKKNPEIPVNF   38

HMGB3       AEFSKKCSERWKTMSGKEKSKFDEMAKADKVRYDREMKDYGPAKGGKKKKDPNAPKRPPS   120
HMGB3       AEFSKKCSERWKTMSAKEKSKFDDMAKADKVRYDREMKDFGPVKGGKKKKDPNAPKRPPS    98

HMGB3       GFFLFCSEFRPKIKSTNPGISIGDVAKKLGEMWNNLNDSEKQPYITKAAKLKEKYEKDVA   180
HMGB3       GFFLFCSEFRPKIKSTNPGISIGDVAKKLGEMWNNLSDGEKQPYNIKAGKLKEKYEKDVA   158

HMGB3       DYKSKGKFDGAKGPAKVARKKVEEEDEEEEEEEEEEEEDE---    222
HMGB3       DYKSKGKVDGAKCAPKLPRKKIEDDDDEEDDEDEEEDDDEEDDE    203
```